Engineering for the ATLAS Inner Detectors and the Route to a High Luminosity Upgrade

Richard French

This thesis is submitted in fulfilment of the requirements for the degree of

Doctor of Philosophy in Applied Physics

The University of Sheffield

Faculty of Science

Department of Physics & Astronomy

March 2017

For my family.

ABSTRACT

This document details the substantial individual contribution made by the author to the research & development of the ATLAS Experiment. Based at CERN, the European Organization for Nuclear Research, the Large Hadron Collider (LHC) is the world's largest and most powerful particle accelerator. ATLAS is one of two general-purpose detectors at the Large Hadron Collider; it investigates a wide range of physics, from the search for the Nobel Prize winning Higgs boson discovery to new extra dimensions and particles that could make up dark matter. At 46m long, 25m high and 25m wide, the 7000-tonne, 100m below ground ATLAS detector is the largest volume particle detector ever constructed. The author's contribution to the construction & integration of the ATLAS Inner Detector (ID) is detailed with focus on the cooling systems.

Following years of operation, the ATLAS ID requires replacement due to radiation damage to electronic components and significant major infrastructure changes are required to operate effectively at higher luminosities. Planned high-luminosity upgrades to the LHC (HL-LHC) require huge increases in power to generate higher energy particle collisions needed for new scientific discoveries. Initial research began in 2005, exploring the possible construction of an ATLAS High-Luminosity Upgrade replacement of the existing ATLAS ID. The author was heavily involved in the construction of this project from the initial conceptual ideas, to the development of radiation hard semi-conductor device qualification, irradiation facility design, construction and operation and cooling system development.

Sharing a number of design philosophies with aerospace, defence and space science, particle detectors require lightweight materials with high strength. Development of modern particle physics detectors to enable new scientific discoveries requires pushing technological boundaries beyond conventional. This document and commentary demonstrate the author's application of these technologies to the ATLAS ID and transference to the industrial domain, predominantly within aerospace and robotics.

Contents

List of Figures

Introduction

This research thesis is divided into three sections describing the contributions made by the author to the ATLAS experiment from 1997 to present day. The sections follow chronological order, as the research work was undertaken.

Chapter 1, highlights the components of the LHC accelerator, which are the essential tools an Applied Physicist requires for the design, prototyping and evaluation of detector components. The evolution of LHC is charted, noting facilities developed, and used by the author for detector performance evaluation.

Chapter 2, documents the development of the authors work for the ATLAS Inner Detector construction, which took place from 1997 to 2009. The author was based at The University of Sheffield, The University of Liverpool and CERN. Contributions were to the design, prototyping, construction, installation, integration and later operation of the Inner Detector (ID) particularly the cooling systems.

Chapter 3, details the authors contributions to the new ATLAS Upgrade detector for the high luminosity LHC (HL-LHC) which is needed for new scientific discoveries using higher energy particle collisions. The route to HL-LHC involves various ATLAS detector upgrades. Detailed is the author's initial research commencing in 2005 to present day for the design and prototyping for the replacement of the existing ATLAS Inner Detector.

Chapter 4, reflects on the experiences and lessons learned by the author during development of the sub-detectors for ATLAS, then implemented in later detector construction. Application of developing Particle Physics technology for wider engineering applications by the author is discussed.

Supporting each chapter are reference publications located in Appendix. A, evidenced with the following thesis commentary highlighting the author's contributions. Combined, these present a coherent body of work for applied physics research activities. Reference publications are subject to the rules of The University of Sheffield PhD by publication [1].

Chapter 1   ATLAS & the Large Hadron Collider

1.1   Introduction

The ATLAS detector has many sub-detectors, detailed in this chapter is the role of the author as a member of the large international ATLAS collaboration comprising of thousands of physicists, engineers and technicians from 172 institutes in 37 countries. Essential accelerator tools required for the design, prototyping and evaluation of detector components are detailed.

The history of the CERN LHC is noted with the author's considerable input to the infrastructure development of the CERN PS "IRRAD" irradiation facility. Further facilities development was made possible through the author's collaborative EU funded projects AIDA and AIDA2020 (Advanced European Infrastructures for Detectors at Accelerators) [2]. Operations for both the ATLAS SCT and ATLAS Upgrade test beam and irradiation activities are later described in Chapter 3.7 and demonstrated in publications [A.5-A.9]. The author's contribution to the CERN PS IRRAD facility, and A10 to A.13 for contributions to the UK-ATLAS irradiation facility sited at The University of Birmingham UK.

1.2   Introduction to ATLAS and the LHC

Based at CERN, the European Organization for Nuclear Research, the Large Hadron Collider (LHC) is the world's largest and most powerful particle accelerator. ATLAS (**A Toroidal LHC ApparatuS**) [A1] is one of two general-purpose detectors using the beam line of the Large Hadron Collider. This general-purpose detector is highly optimised for discovering the Standard Model Higgs Boson, additionally; ATLAS investigates a wide range of new physics such as extra dimensions and particles that could make up dark matter. The ATLAS detector, shown in Figure , is 46 m long, 25 m high and 25 m wide, weighing approximately

7000-tonnes housed in the "Point 1" LHC 100m underground experimental cavern [Fig.2-2]. The ATLAS detector is the largest volume particle detector ever constructed.
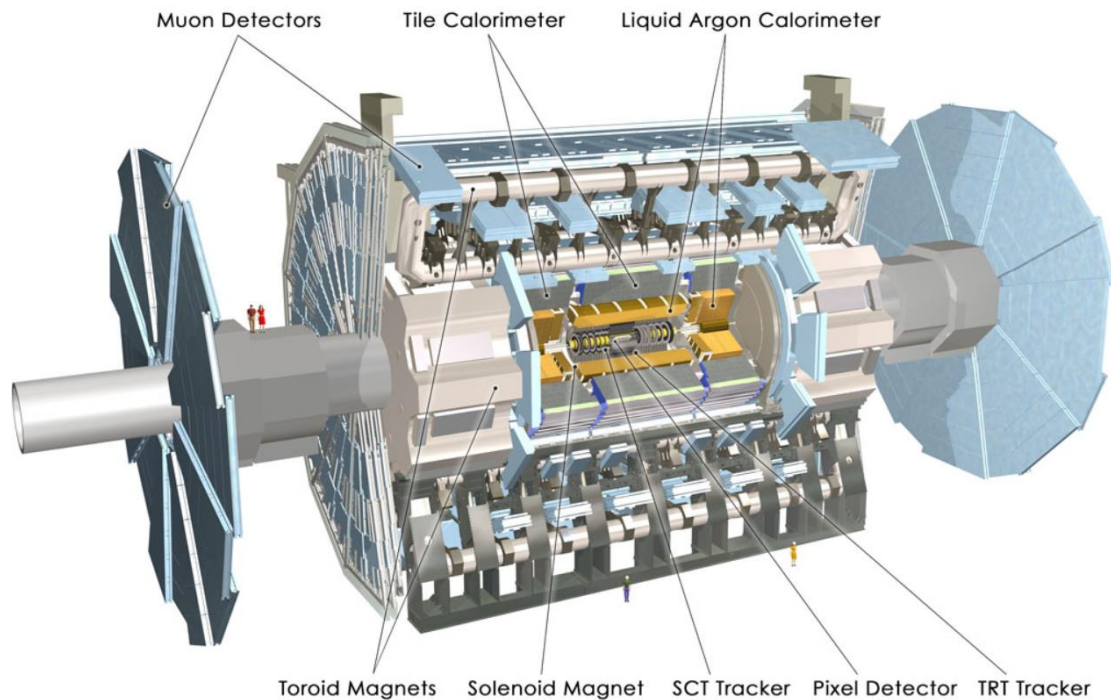
Figure 1-1   3D Rendered Image of the ATLAS Detector [3]

Figure 1-1 shows a cross sectional rendering of the ATLAS detector. The inner detector (ID) is designed to measure charged particle tracks providing excellent pattern recognition. Tracking within a 2 T solenoidal magnetic field is by three ID layers; the PIXEL detector, semiconductor tracker (SCT) and transition radiation tracker (TRT), decreasing in granularity as radii from the interaction point increases. Within the inner detector, tracks left by charged particles, such as, muons, electrons and hadrons, as they are bent by the magnetic field.

The magnet system of ATLAS bends particles around the various layers of detector systems, making it easier to contain the tracks of particles. The main sections of the magnet system are the Central Solenoid magnet, which is surrounded by the Barrel Toroid and End-cap Toroids.

The central solenoid, which is 5.5 tonnes in weight, 2.5 m in diameter and 5.3 m in length, provide an axial magnetic field of 2 T at the centre of the ATLAS tracking volume. As the solenoid coil precedes the barrel liquid-argon (LAr) electromagnetic calorimeter, its thickness must be minimised to achieve maximal calorimeter performance. It contains 9 km of superconducting wire cooled by liquid helium and an electric current of 8000 Amperes.

The Barrel Toroid Magnet system consists of eight-Barrel coils housed in separate cryostats and two End-Cap cryostats housing eight coils each. The End-Cap coils systems are rotated by 22.5˚ with respect to the Barrel Toroids in order to provide radial overlap and to optimise the bending power in the interface regions of both coil systems.

External to the solenoid magnet is the calorimeter system. The liquid argon (LAr) electromagnetic calorimeter measures energy deposits from particle interaction with absorbing and active material or "particle showers" and provides electron and photon identification. The tile-scintillator hadronic calorimeter measures jets and missing transverse energy, which accounts for non-interacting particles with the detector, such as neutrinos.

At the outer sides of ATLAS, the muon spectrometer measures the momenta and charge of a wide range of ρT muons, which are not stopped by previous sub-detectors. In combination with a large magnet system, which dictates the layout of the ATLAS sub-detectors, the general-purpose detector is optimised for a wide physics program.

The LHC accelerator is comprised of a series of huge interconnected superconducting dipole magnets forming a system to bend the path of charged particles around the LHC ring. Using the final focussing quadrupole magnets the charged particles are brought together to produce collision in the very centre of the ATLAS detector.

These particle interactions within the ATLAS sub-detectors create a monumental flow of data. To understand this data, the ATLAS experiment uses an advanced "Trigger" system to communicate with the detector instructing which events to record and ignore. Complex data-acquisition (DAQ) and computing systems analyse the collision events recorded.

1.3   CERN Large Hadron Collider (LHC)

Manipulating particles to collide exactly within the central point or interaction point (IP) of ATLAS or any LHC based experiment is a non-trivial operation. The LHC [Fig.1-2] is the world's most powerful tool to investigate a question of the standard model, the generation of mass. Sub-atomic or particle physics investigation requires more than just a magnifying glass, requiring higher resolution than possible with Nuclear magnetic resonance (NMR). The size of equipment needed for sub-atomic particle detection at high resolution comprises of a 27-kilometre ring of superconducting electro-magnets buried 175m underground forming the LHC accelerator.
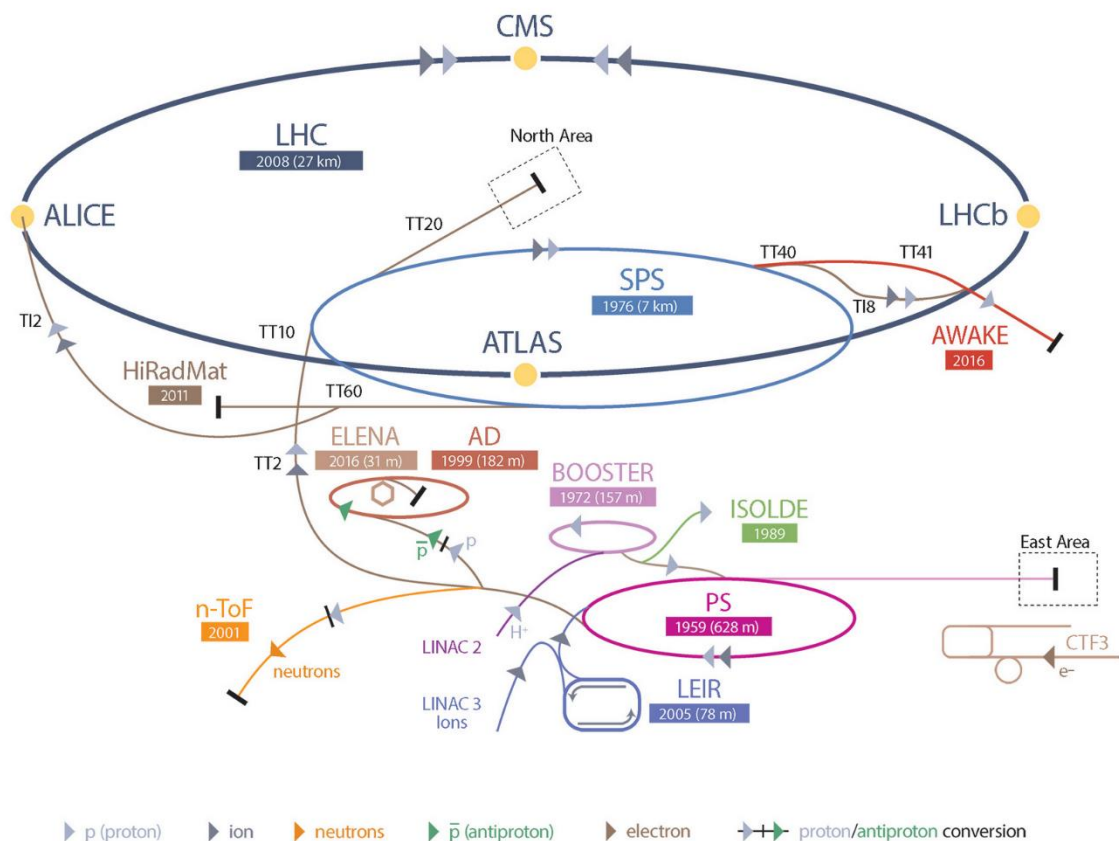
Figure 1-2   Graphical Representation of the CERN Accelerator Complex [4]

Internally the LHC accelerator ring has two separate beam pipes containing high-energy particles travelling in opposite rotational directions. Each beam pipe carries these high-energy protons, which over the course of operation span three centre of mass energies with 3, 7 and 13 TeV of energy and a bunch frequency of 40MHz [5] accelerated near to the speed of light. Before a forced collision, the speed of the protons is precisely maintained in an ultrahigh vacuum within each beam pipe. The particles produced are steered around the accelerator ring by a strong magnetic field maintained by the superconducting (dipole) electromagnets.

These 1232 dipole magnets form the LHC ring, built from coils of superconducting electrical cable, are designed to efficiently conduct electricity without resistance or loss of energy. To achieve a state of superconductivity and provide an operational magnetic field of 8.3 T the dipole magnets require cryogenic cooling by means of Helium (He) to 1.9 K.

Figure 1-3   Image of LHC Superconducting Magnets [6]

Many of the interesting physics questions at the LHC require high luminosity, and so the primary goal is to operate at 14 TeV centre of mass energy at a luminosity of $10^{34}\text{cm}^{-2}\text{s}^{-1}$ to provide the detectors with as many signatures as possible, using electron, photon, muon, jet, and missing transverse energy measurements, as well as b-quark tagging. This variety of signatures are considered important in the high-rate environment of the LHC in order to achieve robust and redundant physics measurements with the capability for internal crosschecks.

1.4   Proton Synchrotron (PS) Accelerator

Proton injection into the LHC accelerator reveals some of the geographical and technical history of the CERN site sourced from the early study of elementary or sub-atomic particles. This unique history provides the necessary infrastructure for ATLAS detector development alongside quality assurance and control required to achieve a long service life.

The Proton Synchrotron (PS)[Fig.1-4] plays a vital role in the entire accelerator complex by providing the particles required directly to experiments or to the more powerful accelerators such as the LHC. There are two modes of standard running, both relevant to ATLAS, usual operation accelerates either protons delivered by the PS Booster or heavy ions from the Low Energy Ion Ring (LEIR). In addition to its operation of proton acceleration for ATLAS, other CERN experiments can utilise accelerated antiprotons, electrons, and positrons [5].

From its initial first operation on 24th November 1959, PS became the world's highest energy particle accelerator and CERN's flagship. As the desire to study particles at increased energies or luminosity grew, the 1970s brought the construction of new accelerators at CERN. The PS became the supply machine at the heart of the LHC, supplying particles to the new machines. With a circumference of 628 metres, the PS accelerator operates at up to 25 GeV. To achieve this power it has 277 conventional (ambient temperature) electromagnets, including 100 dipoles to direct the beams round the smaller accelerator circuit [5].

Figure 1-4   Image of the Proton Synchrotron [7]

1.5   PS Booster Accelerator

Performance enhancements to the CERN accelerator complex in 1972 were achieved by the addition of the Proton Synchrotron Booster to the PS accelerator. Prior to the installation of the Booster, the original PS design injected protons directly from the Linac into the PS, and accelerated to 26 GeV. The low injection energy of 50 MeV limited the number of protons the PS could accept. The PS Booster comprises of four synchrotron rings that receive beams of protons from the linear accelerator Linac 2 at 50 MeV and accelerates them to 1.4 GeV for injection into the Proton Synchrotron (PS). Current day operation of the Booster now allows the PS to accept over 100 times more protons. The acceleration process uses protons, injected

from the small linear accelerator then boosted into the PS (Proton Synchrotron) and accelerated to 26 GeV [8].

1.6   SPS Booster Accelerator

From the PS and Booster, the acceleration of protons injected into the Super Proton Synchrotron (SPS) are increased to 450 GeV. These protons are injected into what is now the modern day flagship of CERN, the LHC. Protons produced from the LHC accelerator collide with high precision at the centres of the experimental caverns sited on the LHC ring. The resulting collision debris is in the form of new particles, which distribute from the collision point in all directions, in this case, the heart of ATLAS.

1.7   Overview of the PS Accelerator Complex

From the PS and Booster, the acceleration of protons injected into the SPS (Super Proton Synchrotron) is increased to 450 GeV [6]. These protons, injected from the PS complex [Fig.1-5] provide ATLAS and the other LHC based experiments with high-energy particle collisions. The CERN PS complex is essential for providing the correct environmental conditions for particle physics detector development, along with identification of new fundamental physics. A number of bespoke facilities for detector development and evaluation are constructed on this complex.
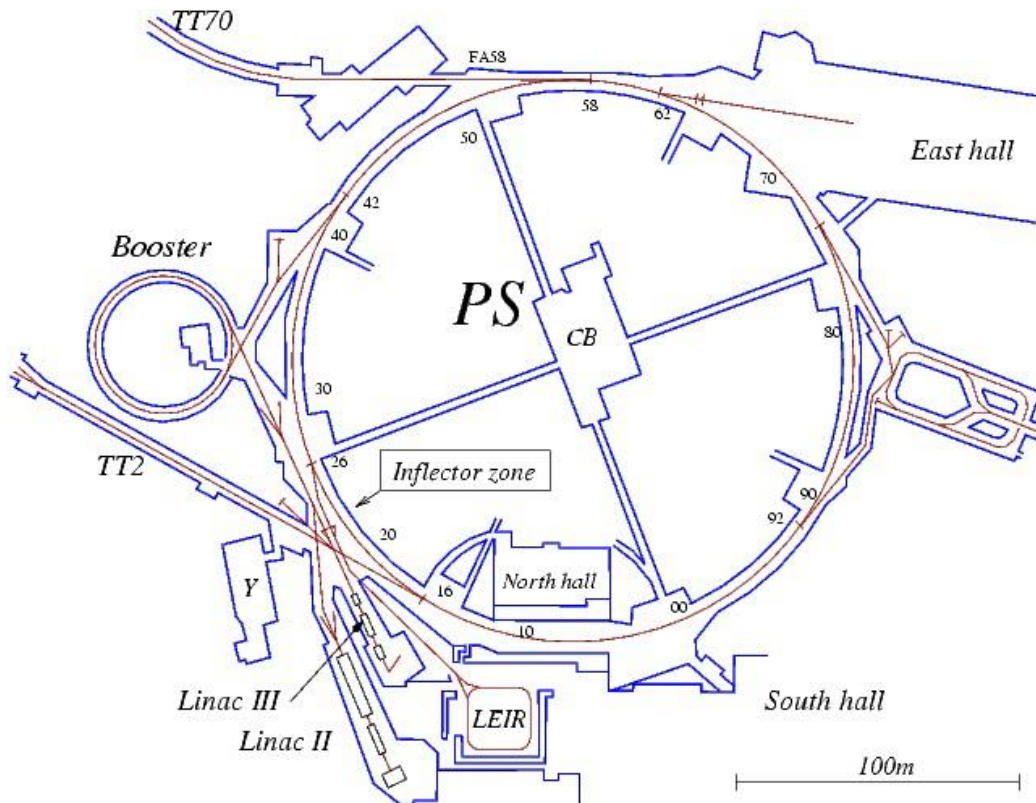
Figure 1-5   Drawing of the Proton Synchrotron Complex [9]

1.8   IRRAD Facility

The IRRAD proton facility [Fig.1-6] is located on the T8 beam-line at the CERN PS East Hall (building 157) where the primary 24GeV/c proton beam is extracted from the PS ring. Irradiation testing in the PS East-Hall is divided between two facilities. The IRRAD proton facility is located upstream of the beam while the CHARM mixed-field facility is located downstream of the beam [8].

The majority of the protons pass through the IRRAD facility without interacting, the mixed-field facility benefits from the same protons used by IRRAD. The author has provided considerable infrastructure development of these facilities during the EU projects AIDA and AIDA2020 (Advanced European Infrastructures for Detectors at Accelerators) [2] and operations for both the ATLAS SCT and ATLAS Upgrade test beam activities later described in Chapter 3.5, demonstrated in publications [A.5 to A.13].
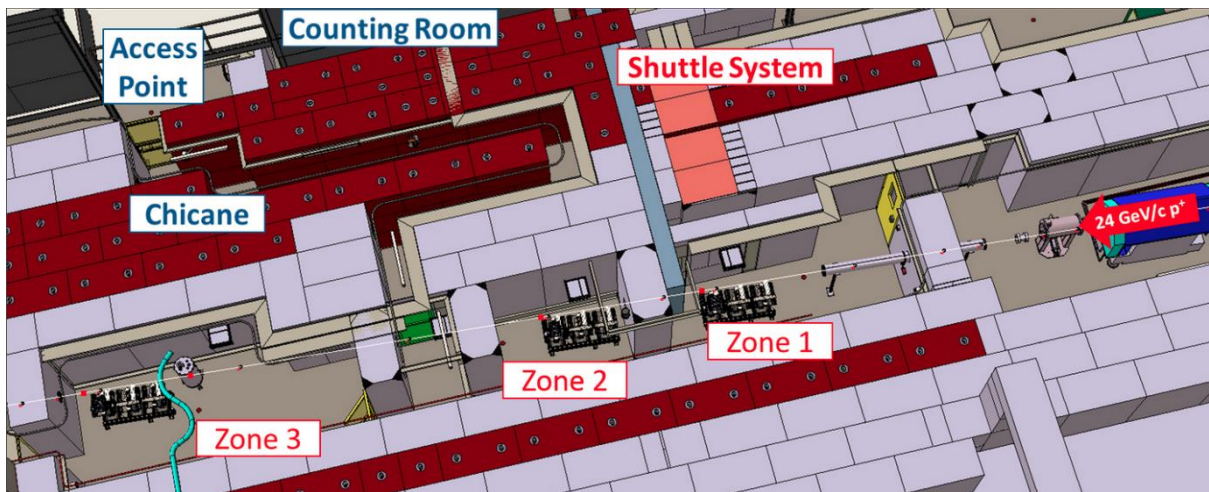
Figure 1-6   Detailed CAD Rendering of IRRAD layout [10]

Chapter 2   The Engineering of the ATLAS SCT

2.1   Introduction

Focusing on the author's substantial R&D involvement with the construction of ATLAS SCT EC-C, chapter two demonstrates the author's main contributions to the following when based at Liverpool University UK; the SCT EC-C Macro-Assembly; the evaluation of EC transportation system design; the EC-C detector integration with SCT TRT-C in the SR1 surface building at CERN. When the author when based at CERN he contributed to the completion of successful combined testing of the integrated STC detectors in SR1, and was heavily involved in the installation of EC-C & EC-A inside ATLAS.

The author contributed heavily to the ATLAS ID cooling system providing both design, production, installation and testing contributions to the SCT ECs and Barrel Detectors. The author contributed to the commissioning and the first operations of the ATLAS Inner Detector (ID) and the subsequent operation of the Inner Detector cooling system during physics data taking. The outcome of this work was the first event recorded by ATLAS, giving indication of success, confirmed by discovery of the Higgs Boson.

Reference publications used in the section are:

[A.1] Engineering for the ATLAS SemiConductor Tracker (SCT) End-cap

[A.2] The evaporative cooling system for the ATLAS inner detector

[A.3] The integration and engineering of the ATLAS Semi-Conductor Tracker Barrel

[A.4] Combined performance tests before installation of the ATLAS Semiconductor and Transition Radiation Tracking Detectors

2.2   Inner Detector Overview

The ATLAS Inner Detector or Semi-Conductor Tracker [A.1, A.3] or SCT as shown in Figure 2-1, is essentially a vertex tracking detector designed to provide high momentum resolution combined with high primary and secondary vertex positional measurements. The SCT has an active silicon surface area of $61m^2$ or 6 million operational channels.
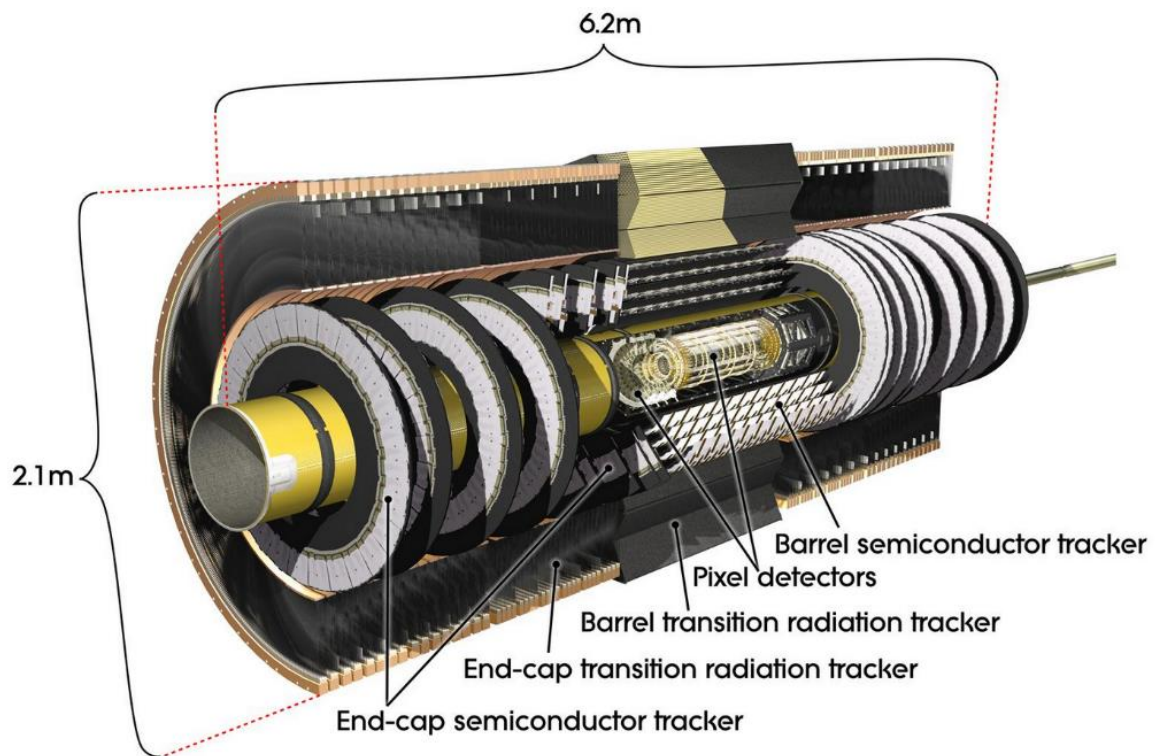
Figure 2-1   Image of the ATLAS Inner Detector [11]

The LHC offers a large range of physics opportunities, among which the origin of mass at the electroweak scale is a major focus of interest for ATLAS. The guiding of detector optimisation and design is by physics performance goals such as sensitivity to the largest possible Higgs mass range. The Standard Model proposes the Higgs field, and by interacting with this field, particles acquire their masses. Particles that interact strongly with the Higgs field are heavy, while those that interact weakly are light.

Other important targets are the searches for heavy W- and Z-like objects, for supersymmetric particles, for compositeness of the fundamental fermions, as well as the investigation of CP violation in B-decays, and detailed studies of the top quark.

Optimisation of sub-detector design is based on the relative position of the detector to the interaction point (IP) enabling the recording of particle paths, momentum, and energy, allowing individual identification. The ATLAS machine is effectively a giant cylindrical object; the sections below describe the layout from the innermost layer to outer following the natural trajectory of particle collision from the IP. In engineering design terms the LHC beam dictates the plane of Z (the beam pipe), the IP dictates the central datum of the entire ATLAS experiment X,Y,Z= 0.
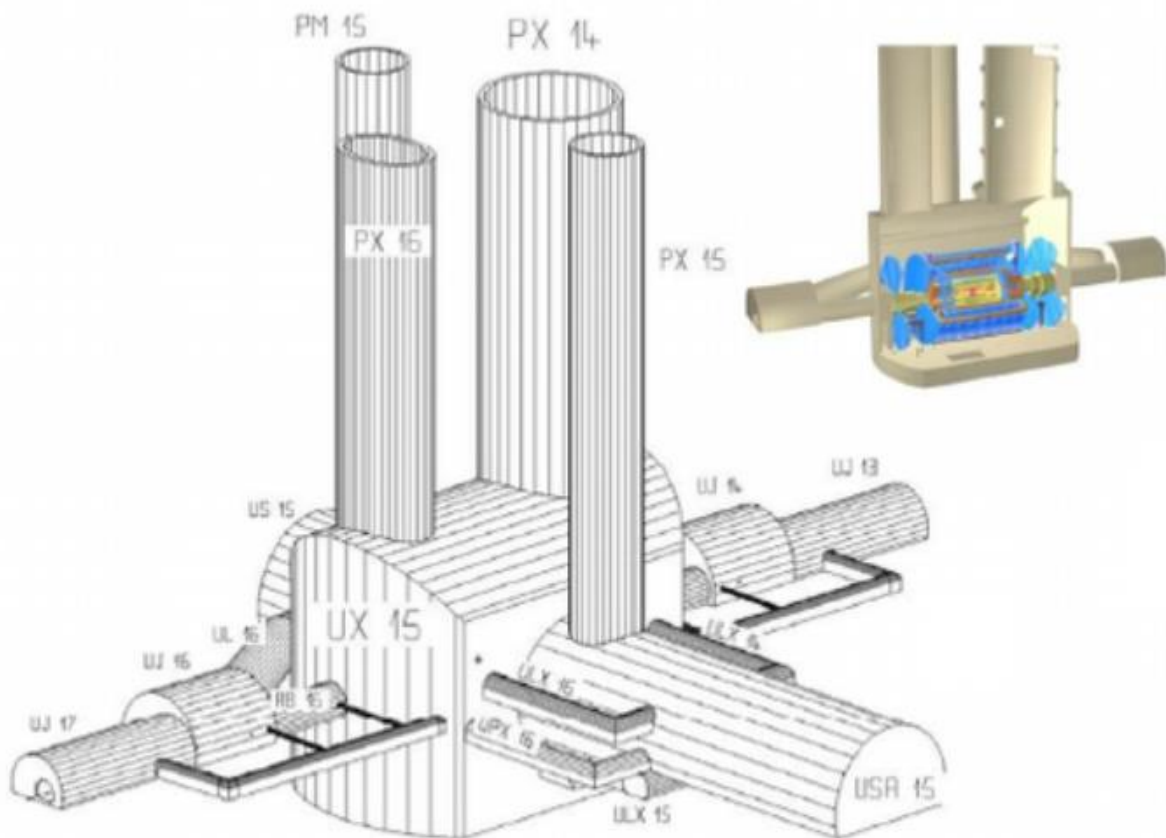
Figure 2-2   ATLAS Point 1 Underground Installation Schematic [12]

Determination of the geometric positon of the ATLAS sub-detectors and associated services within the experimental cavern is simply stated as + or – from the IP datum in the

relevant plain. This simple nomenclature is essential for understanding and measurement of both the positional accuracy and alignment of the ATLAS sub-detectors but also its services, cable mappings and access where the author provided considerable contribution of work ref A1, A2, A3, A4.

Positional location of the detectors within the ATLAS experimental cavern sited at Point 1 on the LHC complex is determined by the detector cavern layout itself shown in [Fig 2-2]. Named UX15, the ATLAS service caverns USA15 and US15 contain the essential services for ATLAS. Surface installation shafts are PX16 and PX14 [13]. The UX15 experimental cavern is effectively split in two halves either side of the LHC beam line referred to by the adjacent service cavern "sides" USA and US respectively. The entire ATLAS detector is split in two longitudinal halves to the LHC beam direction (z) named Side A (+z) and Side C (-z), shown in [Fig 2-3]. In addition, the cavern is separated transversely due to detector access and entry points.
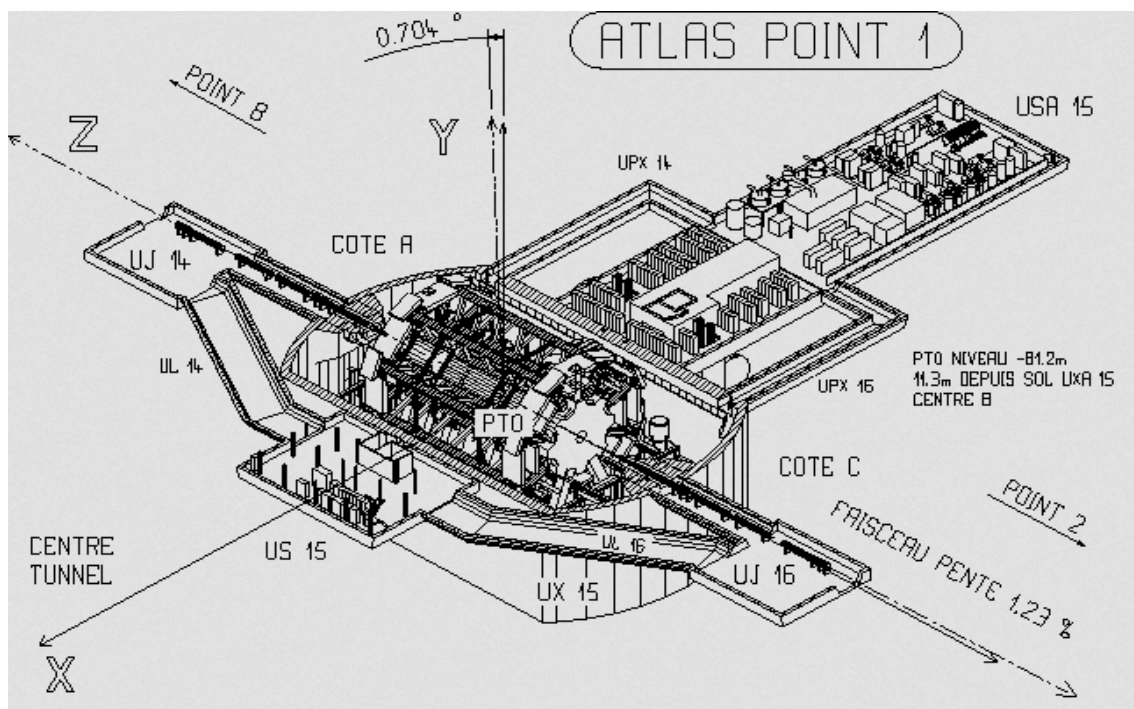
Figure 2-3   Right-handed XYZ coordinate schematic of the ATLAS Point 1 cavern [12]

The ATLAS Inner Detector [Fig.2-1] consists of the three integrated sub-detectors, which underwent final construction and testing, in the CERN SR-1 surface building prior to installation inside the Point 1 cavern. The Inner sub-detectors are described as the path of

particle collisions would follow, from closest to the LHC beam line outwards. The author specifically has worked on the design, construction, installation, commissioning and operation of the Inner Detectors [A.1, A.3, A.4].

The main Inner Detector diameter is 2300mm and 7000mm long. Charged particle momenta analysis is provided by a uniform 2 Tesla magnetic field from the superconducting central solenoid. This is integrated within the liquid argon cryostat of the electromagnetic calorimeter shown as a quadrant view of the ID in [Fig.2-4].
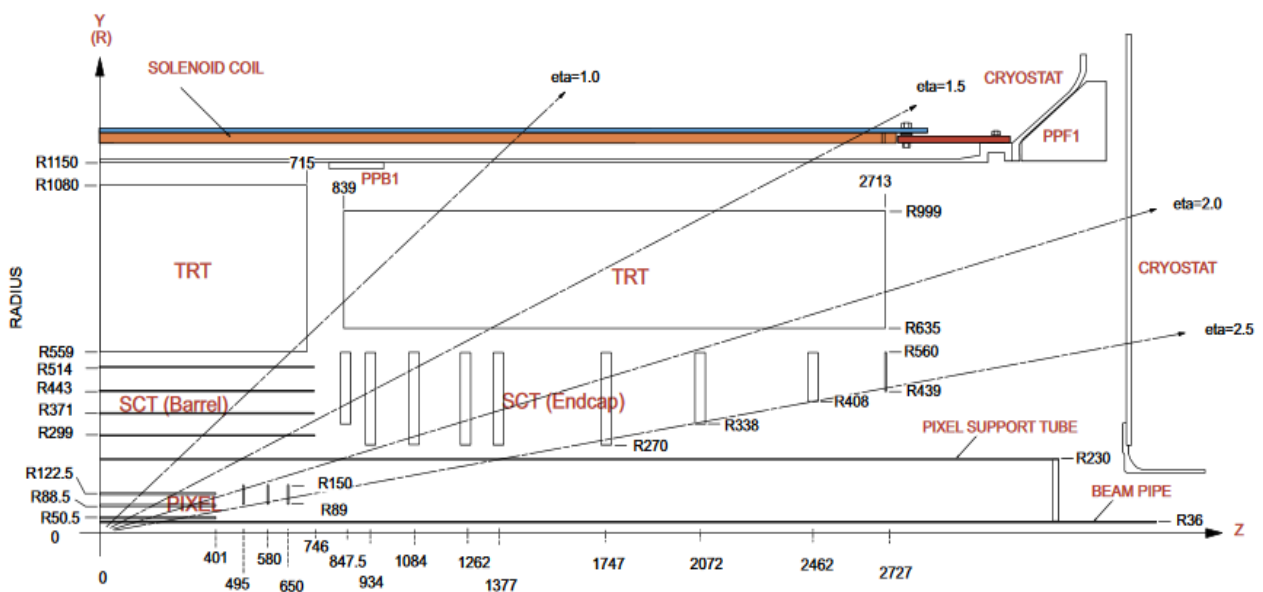
Figure 2-4   View of a ID quadrant with the central solenoid inside liquid argon electromagnetic calorimeter cryostat [14]

One interaction generates a phenomenal amount of particles and therefore a single crossing of the proton bunches generates multiple interactions. This physics motivation drives the ATLAS Inner Detector design requirements e.g. the tracking of numerous charged particles with high precision, bunch crossing identification, electron identification, high radiation dose tolerance or hardness and low mass – high strength construction.

2.3   ATLAS PIXEL Detector

The ATLAS PIXEL Detector [Fig.2-5] is comprised of 1744 modules, which equates to approximately 80 million channels in a cylindrical support structure of 1.4m long, 0.5m in diameter encapsulating the LHC beam pipe directly at the interaction point.
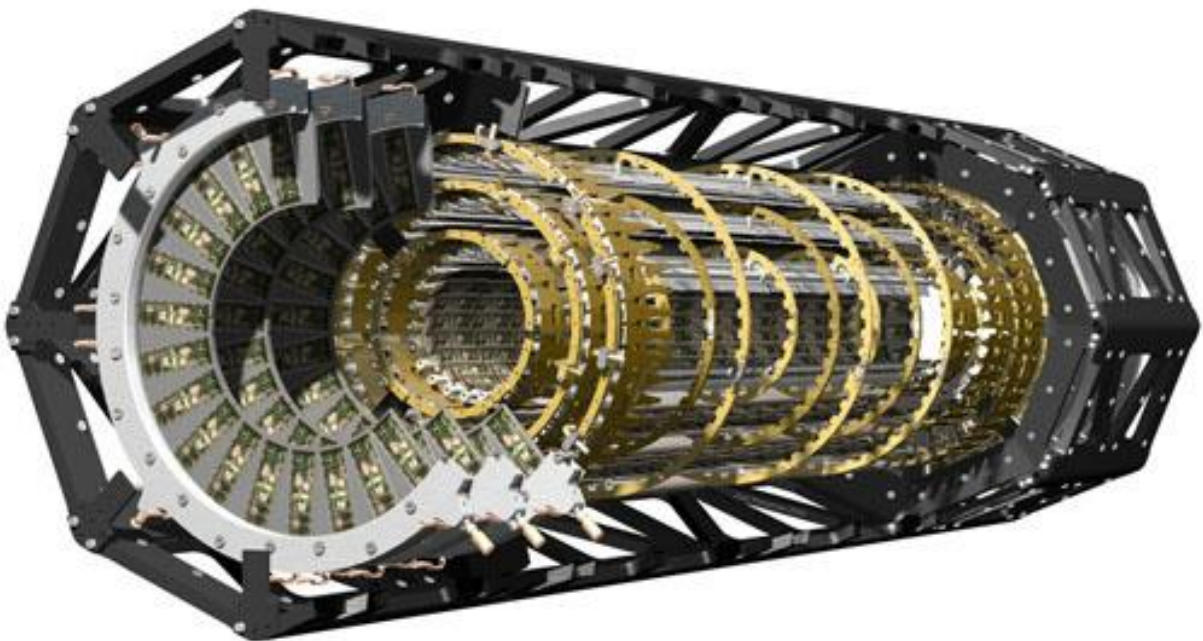
Figure 2-5   Rendered Image of the PIXEL Detector [15]

These pixels cover an area of 1.7 m^2. The PIXEL Barrel detector consists of 3 cylindrical layers positioned radially at R=50.5 mm, R=88.5 mm and R=122.5 mm respectively, identical Stave barrel layers are inclined with azimuthal angle of 20 degrees. Within each radial layer, there are 22, 38 and 52 Staves respectively holding 13 pixel modules [16].

Each PIXEL module comprises of 16 front-end (FE) chips plus one Module Control Chip (MCC). Each single FE chip contains 160 rows and 18 columns of pixel cells equating to 2889 pixels per FE chip and 46080 pixels per module. The readout chips ionising radiation tolerance requirement is over 300 kGy, $5x10^{14}$ neutrons per cm^2 with a service life of ten years operation. Forward region coverage is provided by three PIXEL disks, one disk sector is made up with 6 PIXEL modules with 8 sectors in total.
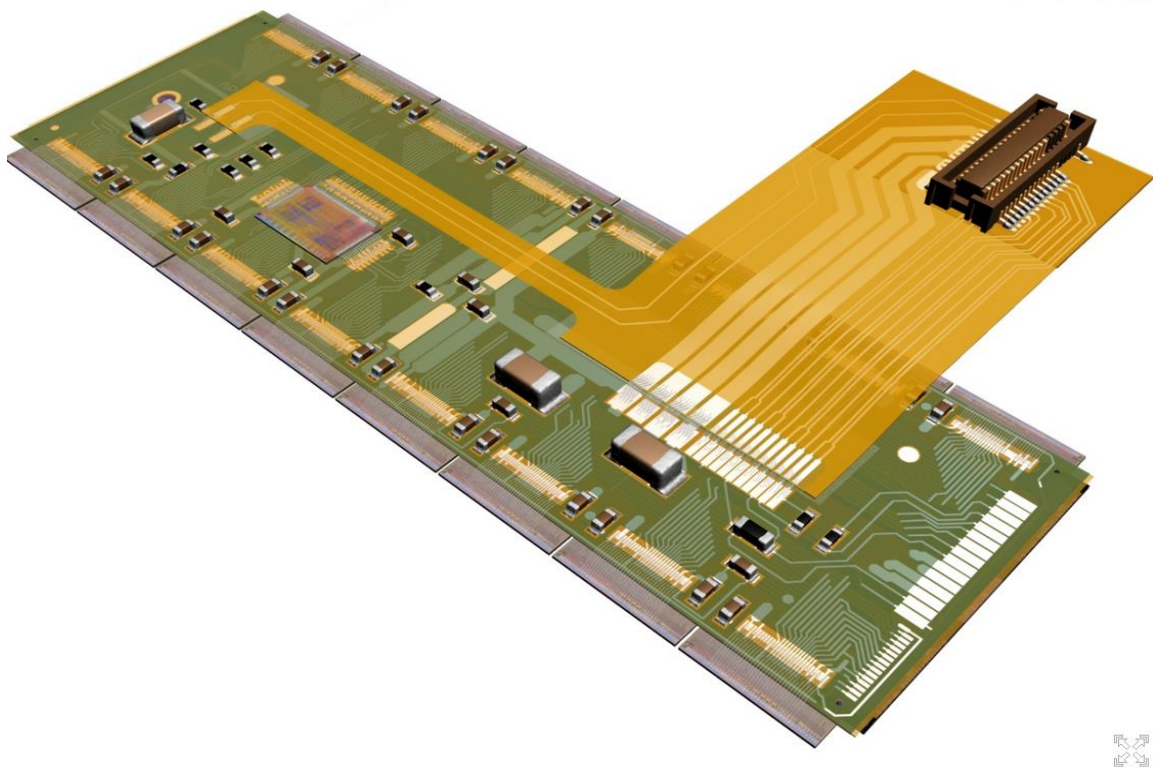
Figure 2-6   Rendered Image of ATLAS PIXEL Module [17]

The ATLAS PIXEL Detector utilises a Pixel sensor of 16.4 x 60.8 mm silicon wafer with 46,080 pixels, 50 x 400 microns each. Construction of an un-packaged flip-chip assembly Pixel module [Fig 2-6] comprises of 16 front-end chips bump bonded to a sensor substrate. PIXEL Disk modules mirror the barrel modules but have different connectivity due to geometry. The main heat source is the front-end chips ($0.8W/cm^2$) dissipating more than 15kW into the detector volume. Integrated cooling channels remove the electronics heat load through

thermal conduction in the detector support elements: Staves in the barrel region and Sectors in the forward region

One crucial design feature of the PIXEL detector is it allows independent installation with other components of the ID. In the starting phase, only two of the three layers planned were installed allowing for parallel installation in the liquid argon cryostat with the ATLAS SCT. The author was heavily involved with the commissioning, testing [A.4] and subsequent operation of the PIXEL detector cooling system as part of the IDE (Inner Detector Expert) on-call shifts. This work centred on the optimisation and testing of the Detector Control System (DCS) for ATLAS described in section 2.5 and links to the submitted reference publication A.3.

2.4   ATLAS Barrel Semi-Conductor Tracker

The design aim of the ATLAS SCT (Semi-Conductor Tracker) Barrel [Fig.2-7] is to provide precision particle tracking measurements. The SCT Barrel is vital for the measurement of particle momentum and vertex position.
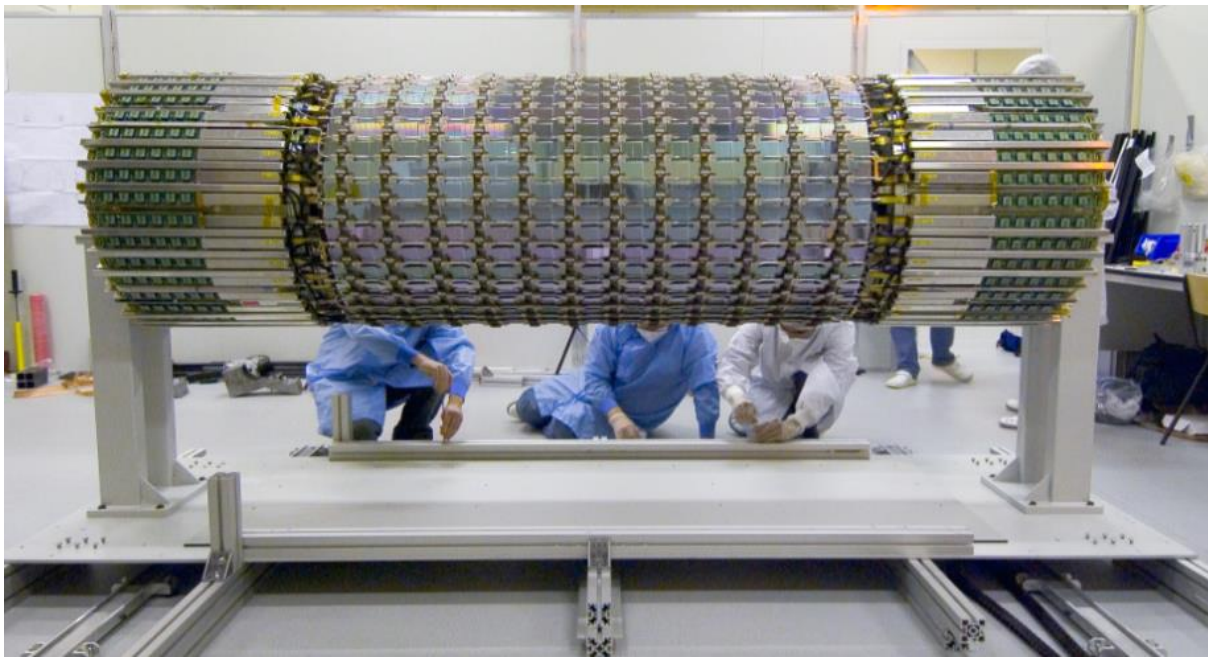
Figure 2-7   Photograph of the 3rd ATLAS SCT Barrel [18]

Construction of the SCT Barrel is around the 2112 silicon detector modules. Each module is 6.36 x 6.40 cm^2 with 780 readout strips of 80µm pitch. The barrel modules are mounted to four separate carbon-fibre support cylinders with radii (R) of 30.0, 37.3, 44.7, and 52.0 cm. These four concentric barrels of length 1.6m and up to 1m diameter. Comprising of eight layers of silicon micro-strip detectors, the SCT Barrel provides precision point measurement in the r-ϕ and z coordinates using small angle stereo to obtain the z-measurement [19].
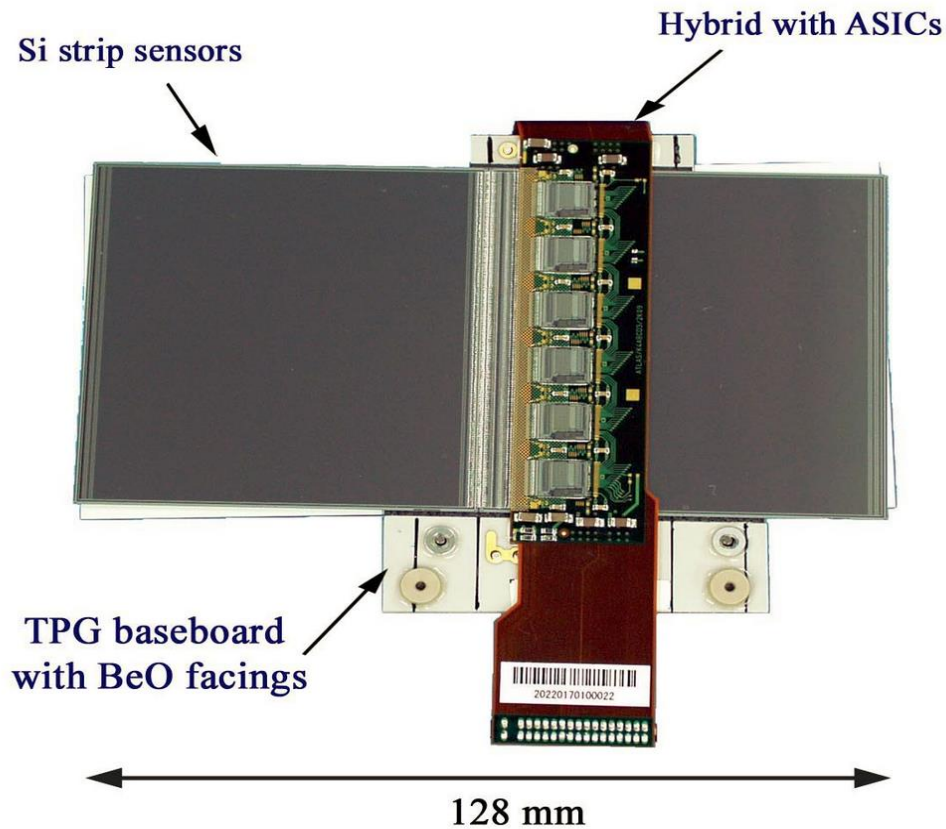
Figure 2-8   Image of ATLAS SCT Barrel Module [19]

The SCT barrel modules [Fig2-8, 2-9] are connected to the binary signal readout chips located on the hybrid. The polyimide hybrid contains 12 (6 per side) identical 128 channel ASICs (chips) and forms a bridge over the silicon sensor. To achieve desired stereo rotation, these four silicon sensors are positioned in opposing pairs with a rotation angle of 40 mrad. A 380μm thick sensor mounting base board is made of thermal pyrolitic graphite (TPG). TPG has excellent thermal conductivity and gives mechanical strength to the module structure.

SCT barrel module cooling is provided by the SCT barrel cooling stave structure. The modules are fixed to Aluminium cooling blocks using thermal grease and are capacitively shielded with a copper-polyimide shunt. These block structures are soldered to the barrel stave cooling tube. Heat dissipated from the silicon sensor utilises a cold finger arrangement, via the hybrid, through the TPG base board, to the beryllium facing connected to the aluminium cooling blocks.
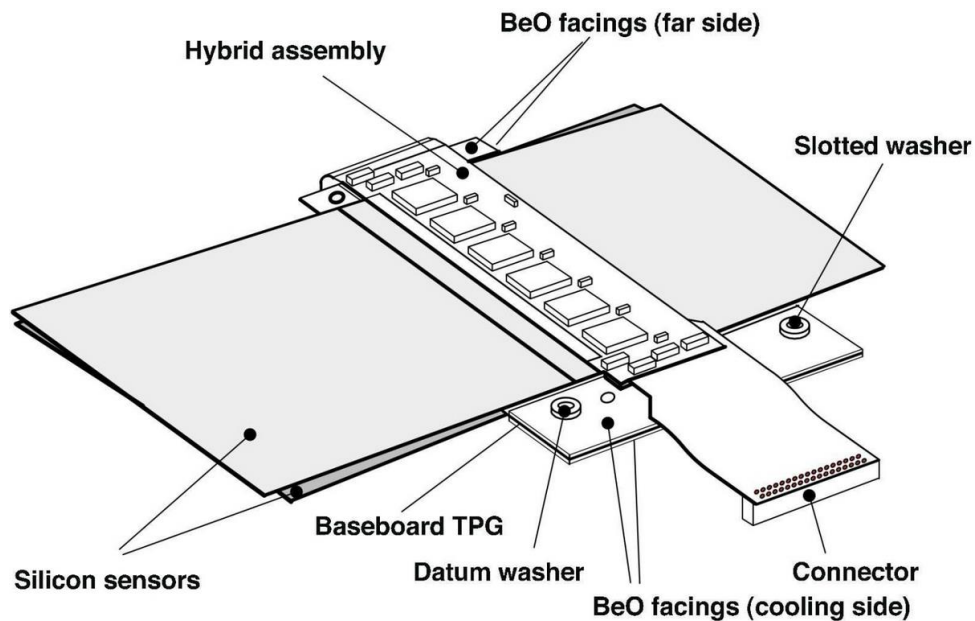
Figure 2-9   Drawing of SCT Barrel Module [19]

Prior to the SCT Barrel installation in the ATLAS cavern, the author established combined noise acceptance tests for the Barrel using cosmic rays in the SR1 surface building. These ID surface commissioning noise tests validated operational efficiencies of the integrated SCT barrel modules with the TRT barrel [A.3, A.4]. The SCT and the TRT barrels were integrated together in February to May 2006 and the top right (TR) and bottom left (BR) sector of both detectors was prepared for cosmic testing [20].

The everyday above ground environment on the Earth's surface is bombarded with Muons created indirectly as decay or by-products of cosmic ray collisions with molecules in the upper atmosphere. Resulting from this absorption of deflection by other atoms, the slow decay of a cosmic muon has an approximate energy of ~2 GeV at sea level [21]. Testing, using

large area scintillators to measure this natural energy, verifies the absence of cross-talk in the integrated TRT/SCT Barrel detector [21]

Few muons pass through the interaction point to ATLAS, multiple scattering events occur from muon interaction with material. This allows the testing of the full detector reconstruction chain and provides accurate detector alignment information before the detector becomes inaccessible when installed in the ATLAS cavern. This combined TRT/SCT test measured noise without signal and allowed a full test of the SCT DAQ (Data Acquisition) system giving indication of stable operation [Fig.2-10]. Approximately 167000 cosmic events recorded showed no influence on noise occupancy observed from TRT/SCT activities [A.4].
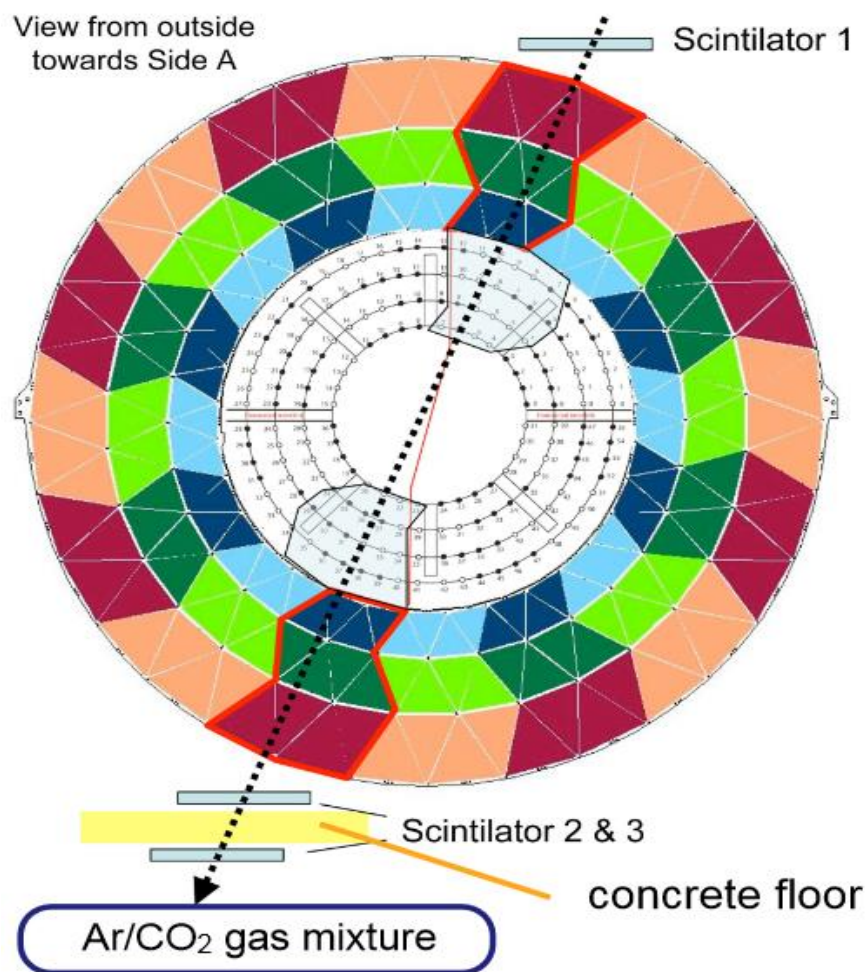
Figure 2-10 TRT & SCT Opposite Sector Cosmic Test Setup in SR1 Drawing [20]

The SCT TR & BL sectors consist of 468 modules, this is the capacity of one ROD data acquisition (DAQ) readout system. The TRT TR & BL sectors consisted of 12 TRT modules, totalling of 3284 straws. Three external scintillators were mounted by the author, one above and below the SCT/TRT detector with an additional scintillator under the SR1 building 20cm thick concrete floor [Fig.2-10]. The trigger used two scintillators closest to the SCT/TRT while the sub floor scintillator, was used offline to select higher momentum tracks (above about 300 MeV).

Positional accuracy of the sub floor scintillator was better than 10mm, the concrete acted to remove low energy particles. The two 1440× 400×25 mm scintillators nearest the SCT were positioned to an accuracy of better than 4mm. The light emitted by all three scintillators was collected by a photo-multiplier tube (PMT) mounted at opposite ends. The pulse height and arrival time information from all PMTs was readout and stored by means of a constant fraction discriminator (CFD) which synchronises the timing signal trigger with the PMT output signal.

The signal from the middle scintillator was delayed to make it arrive last, this determines the muon trigger time is always the exact time which the cosmic ray crosses the middle scintillator. In these tests, an internal ATLAS trigger is not used as in the final experiment this would be provided by the muon trigger chambers or hadronic calorimeter.

This work was essential, prior to final installation in the ATLAS experimental cavern, the cabling procedure; the connectivity and integrity of the cooling; the calibration to adjust readout settings and test communication to the detector. Successful verification of both detectors in their final, as built condition, before installation in the ATLAS cavern was made. The full operation chain: data acquisition, detector control and safety system, monitoring and offline reconstruction, alignment and analysis chains were successfully evaluated along with detector performance efficiency, resolution and construction tolerance using real cosmic events [22].

The author was involved in the regular collation and recording of the Barrel cooling system performance data known as "the long run". Using a representative prototype mock-up structure to evaluate the ATLAS ID design [Fig 2-11], a quadrant of cooling circuits were operated to provide reference data to verify detector performance [Fig 2-12].
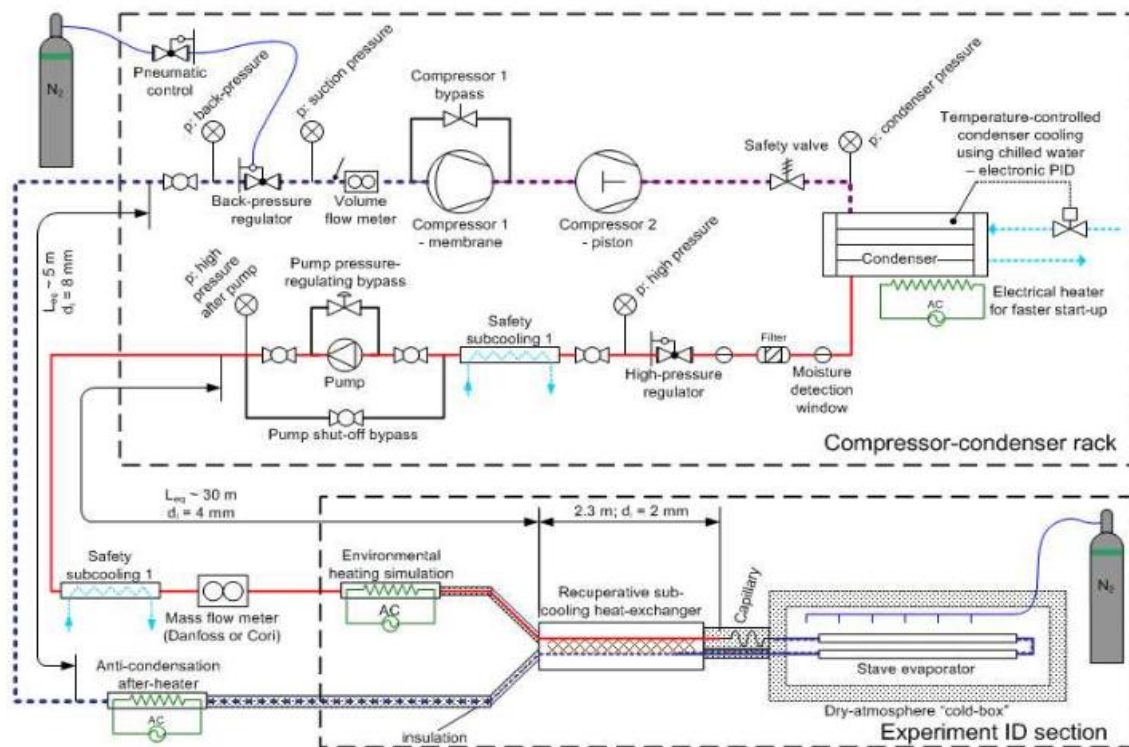
Figure 2-11   Schematic of evaporative cooling test system [A.3]

The "long run" series test results, before the Barrel installation in ATLAS, demonstrated that the modules of the SCT Barrel would not receive adequate cooling power from the chosen C_3F_8 fluorocarbon refrigerant indicating that the silicon module would reach thermal runaway. Thermal runaway occurs if the power dissipated in the silicon semi-conductor contributes to an increase in the temperature of the sensor, reducing performance and service life.

The author began investigations during the Barrel cooling system [A3] testing and first operation for the SCT Barrel during system pre-qualification tests using a "loop back" circuit arrangement. These works are detailed in the reference publications A3 & A4 with a commentary linking these works included in section 2.8.

The integrated SCT Barrel would be the first ID element installed in the ATLAS liquid argon electromagnetic calorimeter cryostat. These initial system tests and further integration [A.3, A.4] with the ATLAS fluorocarbon evaporative cooling system [Fig.2-17] highlighted serious limitations in performance of the cooling circuits of the entire cooling system jeopardising the ATLAS installation schedule and operational schedule [Fig.3-1].

Figure 2-12   ATLAS SCT Barrel Mock-Up in BAT180 [23]

Results from the "long run" data when combined with the "loop back" test results, the calculations and values for operational scenarios, values for the predicted luminosity, depletion voltage and leakage current based on the thermal runway limits proved that it was not possible to guarantee the inner detector's thermal stability with the coolant's evaporation temperature below or at -15∘C.

For ATLAS, such a substantial amount of the cooling system was constructed preventing any significant cooling system redesign or replacement. Investigations to select a

new fluorocarbon or fluorocarbon blend began. The new refrigerant had to achieve the target operational temperature on the detector structure of -25°C with the total cooling capacity of 70kW. This later investigation [24] corrected the detector structure cooling problems and a summary conclusion is found in 2.9.

2.5   ATLAS End-Cap Semi-Conductor Tracker

The ATLAS SCT (Semi-Conductor Tracker) End Caps (EC) are mounted at each end of the Barrel detector region in line with the main LHC beam line on side A (EC-A) and side C (EC-C). Each SCT EC [Fig.2-13] comprises of 988 modules supported by a series of 9 carbon fibre discs in one main outer supporting structure. The ATLAS SCT ECs are specifically designed to provide precision particle tracking measurements in the forward region of ATLAS. The SCT EC is vital for the measurement of particle momentum, impact parameter and vertex position [25].
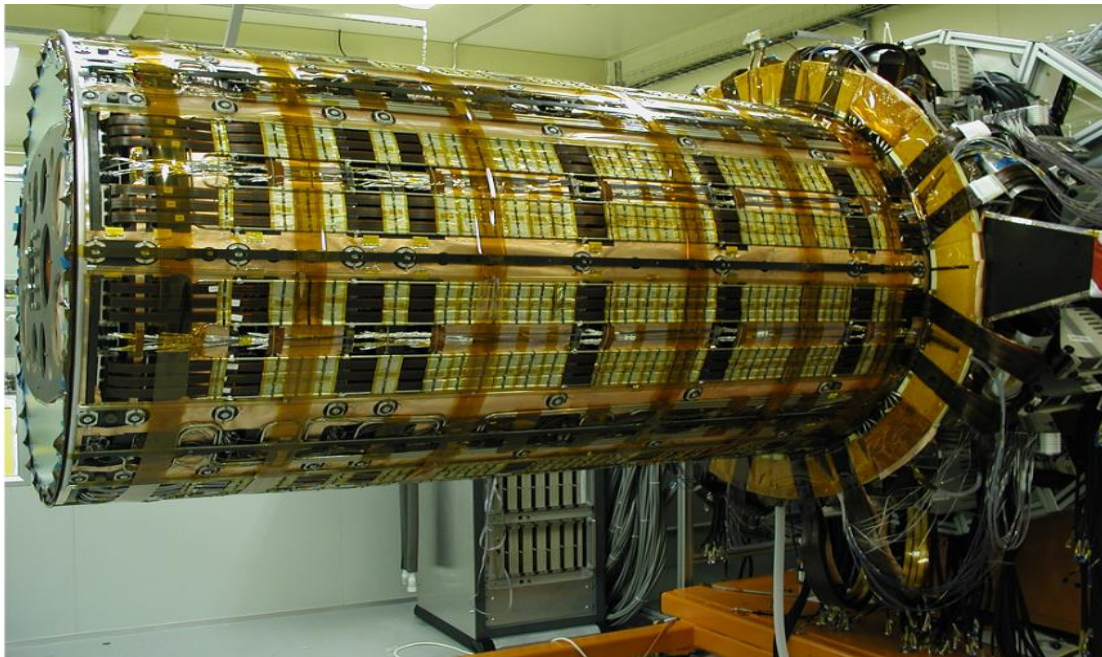
Figure 2-13   Photo of SCT EC-C before final assembly at CERN [26]

The main design requirements of the ATLAS SCT ECs were to provide 4 space-points within |η| < 2.5 to withstand hadron fluence of 2×10E14cm −21 MeV neutron equivalent with minimal magnetic materials (Fe,Ni), and minimise use of potential activation materials (Ag). Electrical noise pick-up from external sources and emissions is addressed by a complex grounding and shielding system [12].

The author made considerable contributions towards the design, construction, transportation, integration and installation of SCT EC-C from 2003 to 2008. These works are detailed in the reference publications: A.1 with the commentary linking these works below.
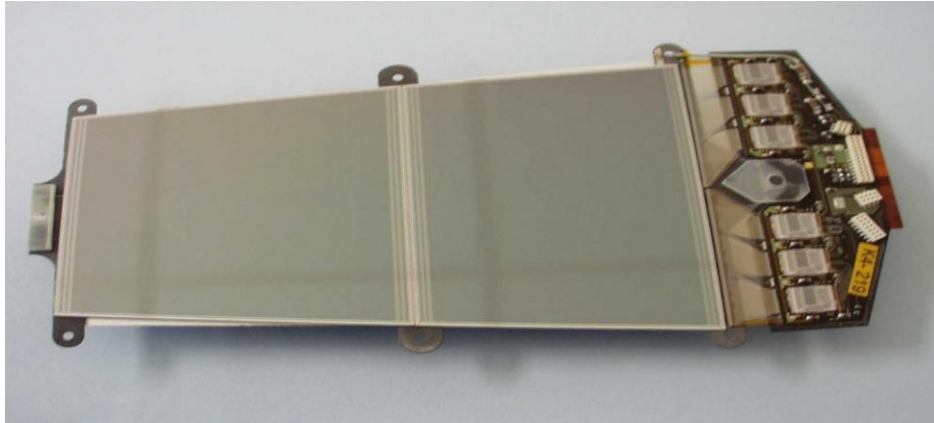
Figure 2-14   Image of an ATLAS SCT Endcap Wedge Shaped Module [25]

Each silicon detector is wedge shaped using similar construction to that of the SCT Barrel with 780 readout strips of 80-µm pitch aligned radially and mounted to a carbon-fibre support disc with a comparable thermal pathway. The Endcap wedge shaped modules, shown in [Fig.2-14 & 2-15], are designed to optimise the size of silicon detectors cut from circular wafers, reducing wafer scrappage and cost.
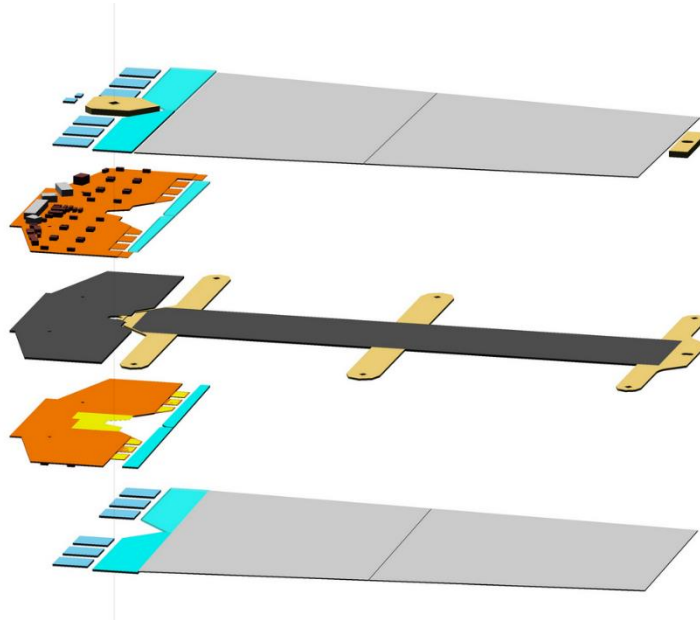
Figure 2-15   CAD Rendering of ATLAS SCT Module [24]

Production of the SCT Endcap wedge modules began in 2003 at production sites located in the UK, Germany, the Netherlands, Switzerland, Spain and Australia. Distribution of the 1976 modules was to NIKHEF and Liverpool for final assembly onto discs and testing before installation in the support structure. The first SCT EC disc was completed in 2003 [Fig.2-16]
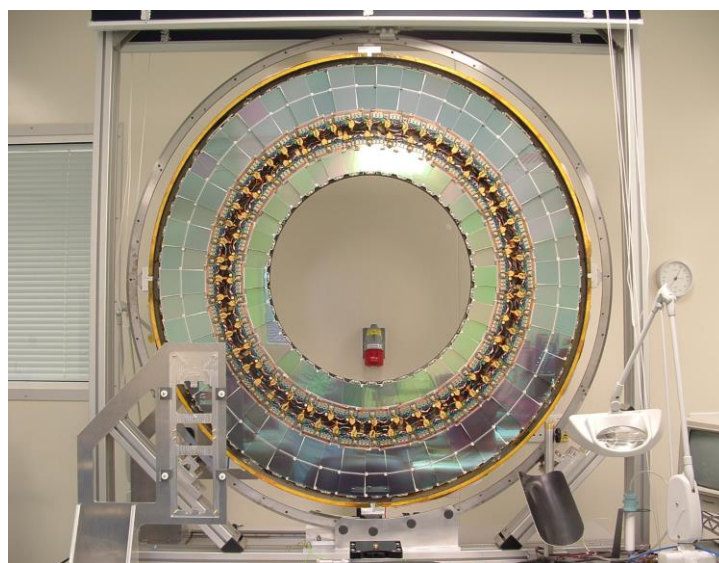
Figure 2-16   ATLAS EC-C Disc photograph [27]

The SCT Endcap discs has up to three rings of silicon modules: outer, middle and inner shown in Figure 2-15. Each ring of Silicon sensors overlap in radius front to back on each disk which prevents tracking gaps in azimuth [A.1]. EC discs are numbered from Disc 1 (closest to the interaction point) to Disc 9 shown in [Fig.2-16]. However, EC assembly into the outer supporting cylinder is in reverse order 9 to 1. A geometric error observed during the first SCT Barrel services construction and cryostat installation reduced installation area within the ATLAS cryostat for both EC-A and EC-C.

Reduction of the support cylinder size and retention of service connections resulted in disc 9 for both ECs being installed in the support cylinder back to front. This allowed for service patch panel connections and creation of a services aperture in the support cylinder.
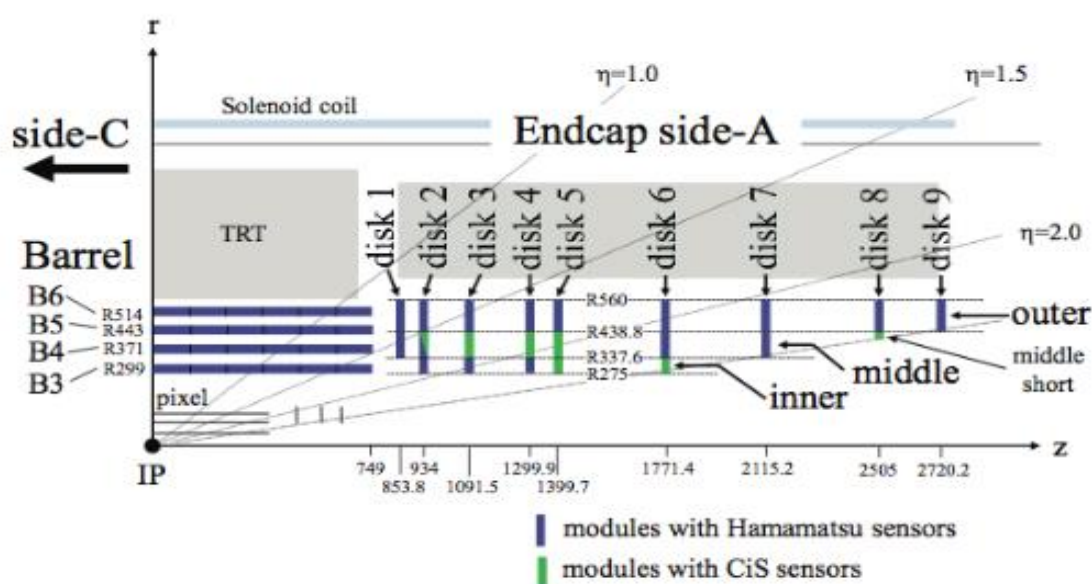
Figure 2-17   Drawing of a quarter section of the ATLAS SCT [A.1]

Disc 9 reversal presented initial problems; effectively it became a mirror of disc 8, requiring a special wiring harness to allow connectivity of the four modules affected by the flip. Geometric regions of space are used to provide areas of services connectivity within the ATLAS SCT defined as patch panels. On-detector patch panel connections are referred to as PP0 and connections on the cryostat flange are PP1. On-disc wiggly power tapes and the PPF0 to PPF1 services Low Mass power tapes (LMT) all required the tracks reversing. This required

additional one-off manufacture of special LMTs as opposed to the standard production of D1 to D8 LMTs. Poor alignment of the original aluminium LMT due to disc 9 reversal is shown in [Fig.2-18]
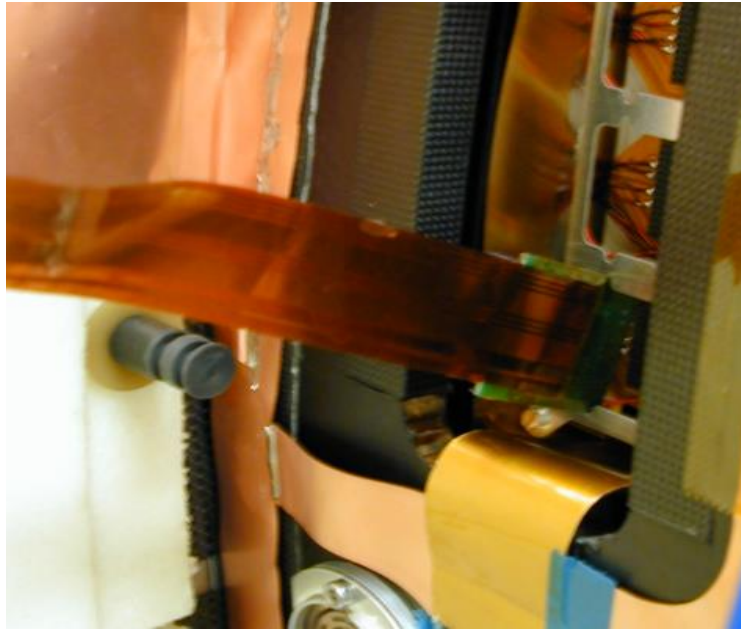
Figure 2-18   Image of distortion to LMT from D9 reversal [28]

Little documentation of initial failures of the original endcap design exist as mainly technical notes aiding the evolution of the final detector. Poor materials selection through lack of experience and prototyping time produced common modes of failure. In the design phase, Aluminium was the material of choice for both the cooling tubes and the power tapes or LMT's due to its low radiation length, the primary driver for material selection. Corrosion evident in the prototype Al cooling tubes resulted in a materials change to a more robust CuNi material; however, this increased the detector material mass and therefore radiation length in the tracker volume.

Pre-installation of the services on the SCT ECs was made possible by using a folding services arrangement. With the exception of the cooling connections all services were folded or coiled on a temporary frame [Fig.2-19] which would allow the installation of the detector thermal enclosures prior to integration with the TRT-EC. This temporary frame also provided the insulation needed for the temporary thermal enclosures for cold testing of the endcaps.

This flexible nature of the services, whilst shortening installation and testing times, did incur other penalties. Critical failure of the aluminium low mass tapes carrying clock, high voltage and slow controls from the endcap modules (LVDS, Temp) resulted in the author providing significant fault analysis to reveal a delaminated area of aluminium in the Polyamide-Aluminium laminated structure as shown in [Fig.2-20].
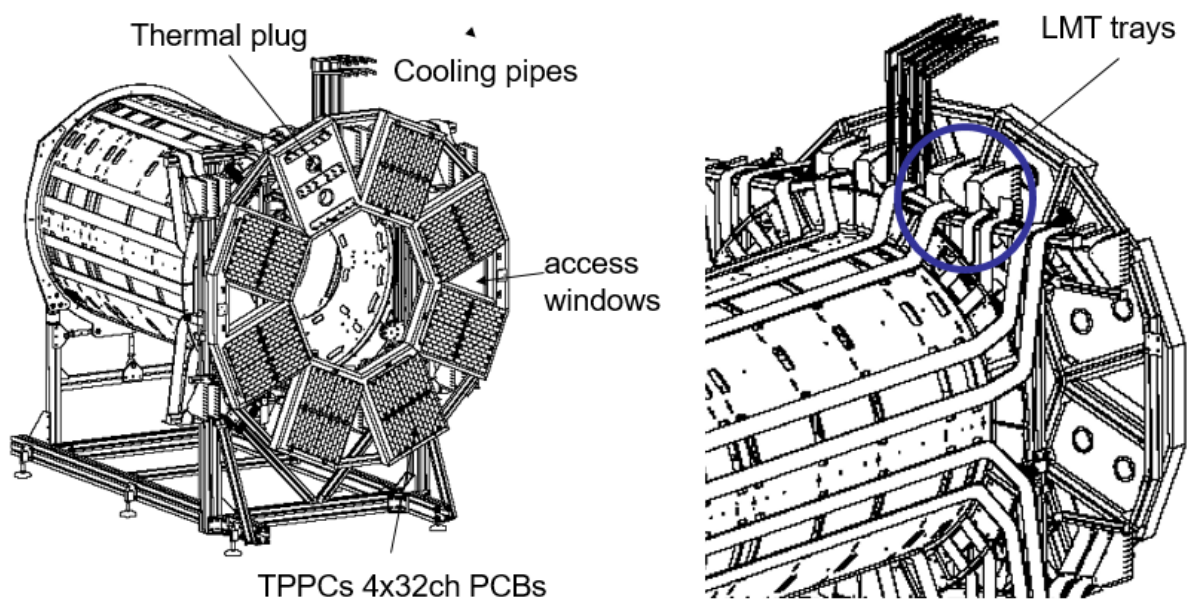
Figure 2-19   Drawing of EC temporary services frame TPPF1 [29]

The author contributed substantial R&D to correcting this problem, which occurred during multiple flexing of the LMT in non-laminated regions. During EC-C services assembly the first quadrant laid on the cylinder was top right, which required minimal handling of the LMT harnesses. Two failed LMT traces were found after the harnesses installation on the cylinder, both on the HV line near PPF0 (on-detector patch panel) indicated by incorrect module temperature signals. A crack was identified on one harnesses 5mm from the edge [Fig.2-20 (R)]

During a simple simulation of the how the LMTs would move in the ATLAS cavern, the LMT trays [Fig.2-19] were removed from the tray-holders and the harnesses moved radially outwards and then moved back into position. After this test, additional fails were found at PPF1 and PPF0. The author observed failures on HV and HV return near PPF1 were under Kapton self-adhesive tape and in a non-laminated region without galvanic plating.

Results of these tests required complete remanufacture of the LMTs. Subsequently the outer laminated Polyamine (Kapton®) layer was retained with a change of internal signal carrying material from aluminium to copper, marginally increasing radiation length of the ECs. The author designed and constructed an automated manipulation test equipment to rapidly assess the robustness of the new copper LMTs, which were re-manufactured in Taiwan and Glasgow.

Figure 2-20   Photo of LMT testing (left) and failure (right) [30]

SCT end-caps design and components, such as the modules, support structures and services were made in collaboration across a number of institutes; Sheffield, Liverpool, Glasgow, Manchester, Oxford, Rutherford Appleton Laboratory, NIKHEF and Valencia. The EC construction was split between two main assembly sites, EC-C was assembled in the UK

by the universities of Glasgow, Lancaster, Liverpool, Manchester, Oxford, Sheffield and the Rutherford Appleton Laboratory (RAL). EC-A was assembled at NIKHEF (Amsterdam, The Netherlands).

Installation of the SCT EC on-detector cooling involved the author in numerous on the fly investigations and subsequent modifications. Cooling connections to PPF0 (Forward patch panel on-detector) on the EC discs leaked when fully assembled. Investigations as to the torque applied to the fixings and the potential damage to the surface quality of the seals began. Fears of corrosion led to the requirement for qualification of copper Delta form Helicolfex seals to replace the original round form seal manufactured in Aluminium [Fig.2-21].
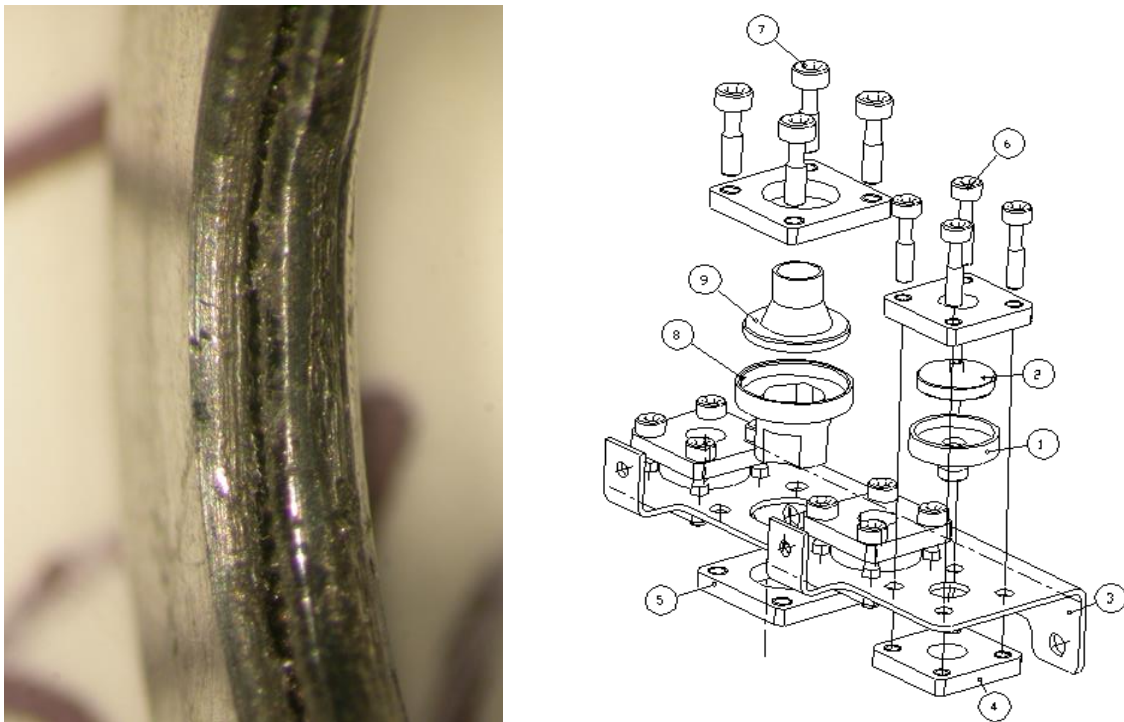
Figure 2-21   Photo of Garlock Al Helicoflex seal [31] (L) and drawing of EC connector assembly (R) [32]

A series of component sealing face tolerance measurements revealed a + 0.1mm error above maximum tolerance in the depth of the fitting, with these corrected the copper seals still did not perform well. Trials conducted in collaboration with RAL staff using digital laser metrology equipment revealed that the compressive force of the aluminium seals was actually correct but the copper seals did not perform as the manufacturer, Garlock, intended [Fig.2-22].

The aluminium seal under maximum applied torque compressed sufficiently to force the seal into full contact with the EC housing face. This rendered the seal difficult to remove but not through means of corrosion. The copper delta section peak required to form the seal failed to compress sufficiently to provide full-face contact. This was possible with the softer aluminium seal, which has a flat face after compression.
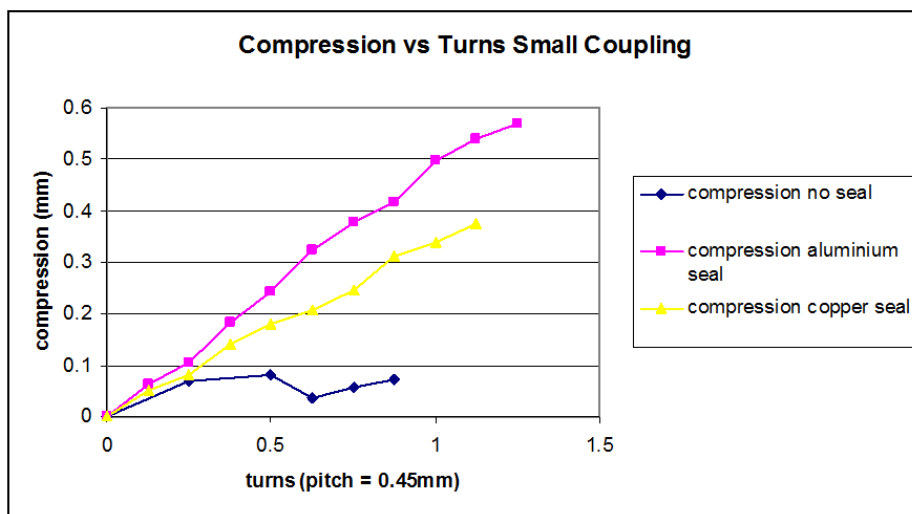
Figure 2-22   Helicoflex seal compression test plot [33]
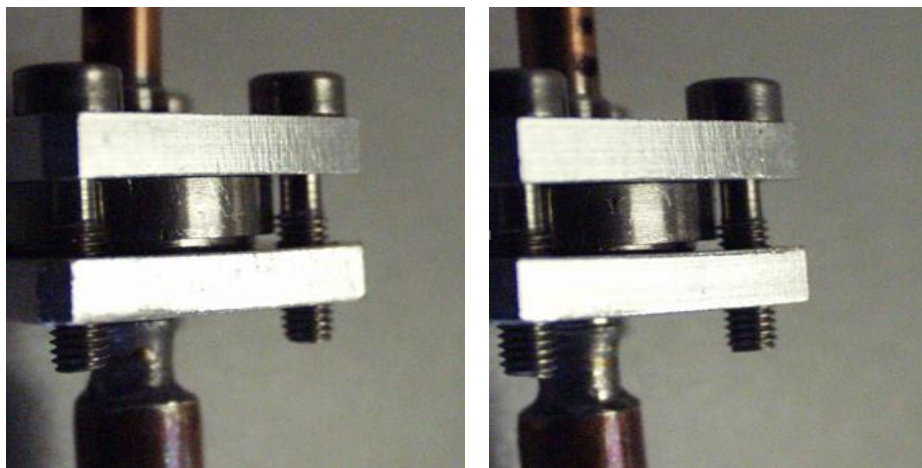
Figure 2-23   EC PPF0 Cooling connector with Ti bolts (L) and 316L SS bolts (R) [34]

Solving compression issues showed that the aluminium seals were functioning as intended. However leak tests on EC Disc 9-C showed a gradual leak over time. Further measurements of the fixing bolts thread pitch by the author showed that over time the titanium screws stretched or suffered from creep, a common performance of Ti material under tensile stress [Fig.2-23]. Whilst not ideal for the materials mass budget of the EC's, a change to stainless steel screws allowed the ECs to pass the helium pressure test of 25bar and a leak rate of 10^{-7} torrl/s.

The author was heavily involved with the engineering design and entire construction of the SCT end-caps, predominantly EC-C constructed in Liverpool. This activity, known as the macro-assembly of the EC, involved work on the mechanical support, detector alignment [Fig.2-24] & [A.3], testing then installation, redesign of supply services and final assembly in Liverpool. This work is detailed in [A.1, A.3, A.4] [Fig.2-25].

The author was involved in all elements of ATLAS SCT EC-C construction and the eventual transportation to CERN via road. When based at CERN, the author provided substantial contributions to the integration with the TRT EC and design, construction and manufacture of the environmental test chambers to verify inner detector performance prior to
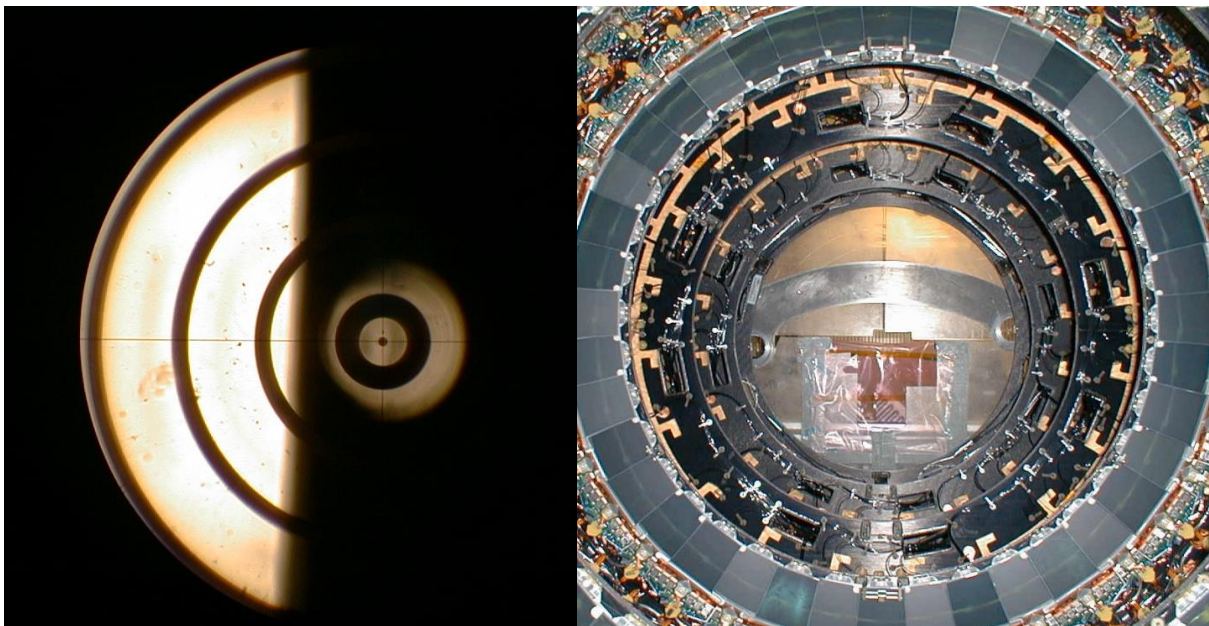
Figure 2-24   Image of Disc alignment target and EC-C discs in cylinder [35]

installation. He then continued with the detector installation in the ATLAS Cryostat and its subsequent completion, testing and operation.

Completion of the macro-assembly in Liverpool (UK) was achieved in 2005 ready for shipping to CERN. Alignment checks made by the author [Fig.2-24] confirmed that the module placement and position on the carbon fibre support discs was to 70um (Inner Module) or 220µm (Outer Module). Disc to cylinder positional accuracy of better than 100µm (x, y) and 1000µm (z) was achieved [A.2]. These accurate conventional optical measurement technique results were verified by the CERN EN Photogrammetry team. Using this reference data confirmed the SCT would achieve its design goal of a pseudo-rapidity η, coverage up to 2.5 [36].
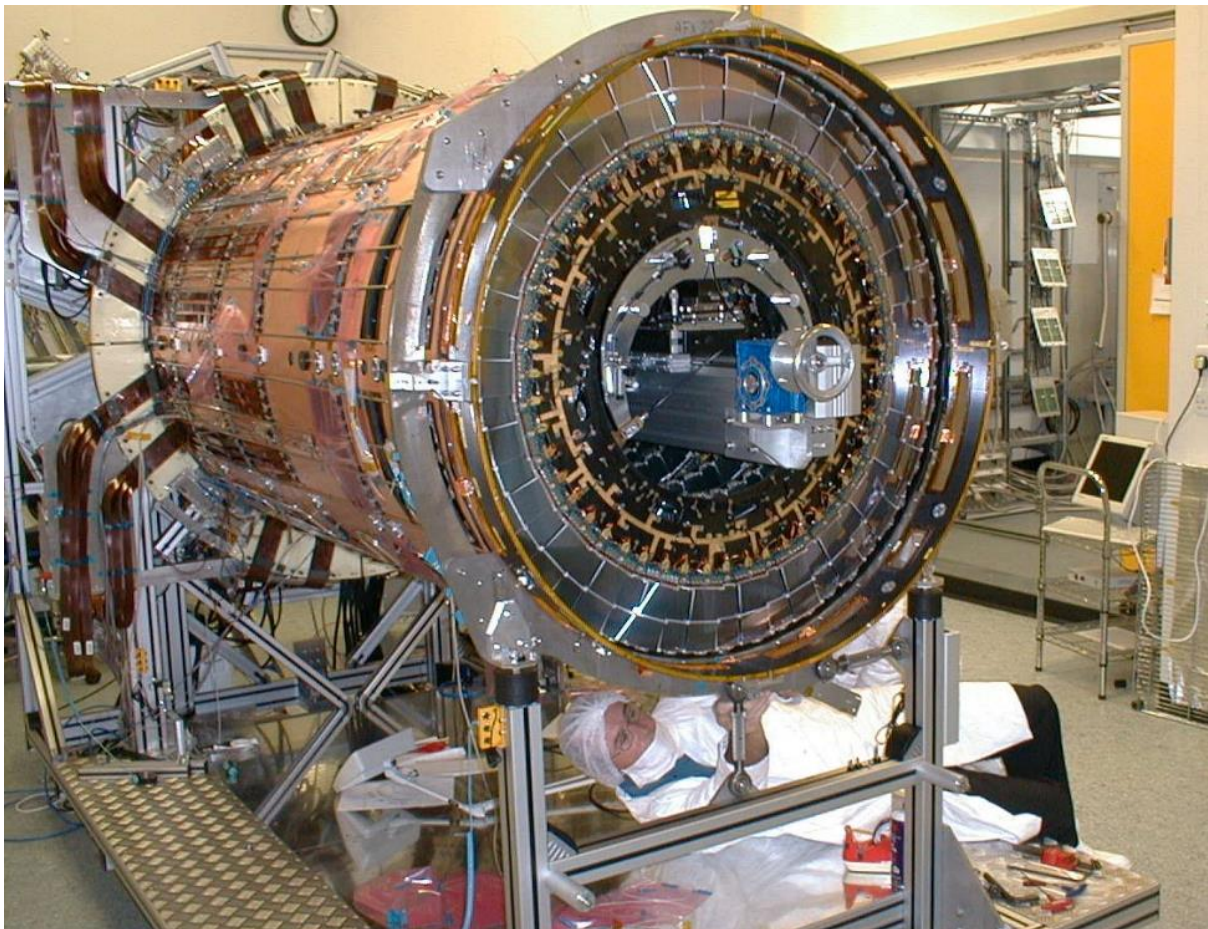
Figure 2-25   ATLAS SCT EC-C under construction at Liverpool UK [37]

2.6   ATLAS Transition Radiation Tracker

The ATLAS Transition Radiation Tracker (TRT) Fig.2-26 consists of a central barrel section and two end-caps. These all are of a larger diameter than the SCT barrel and ECs, which are installed inside the TRT.
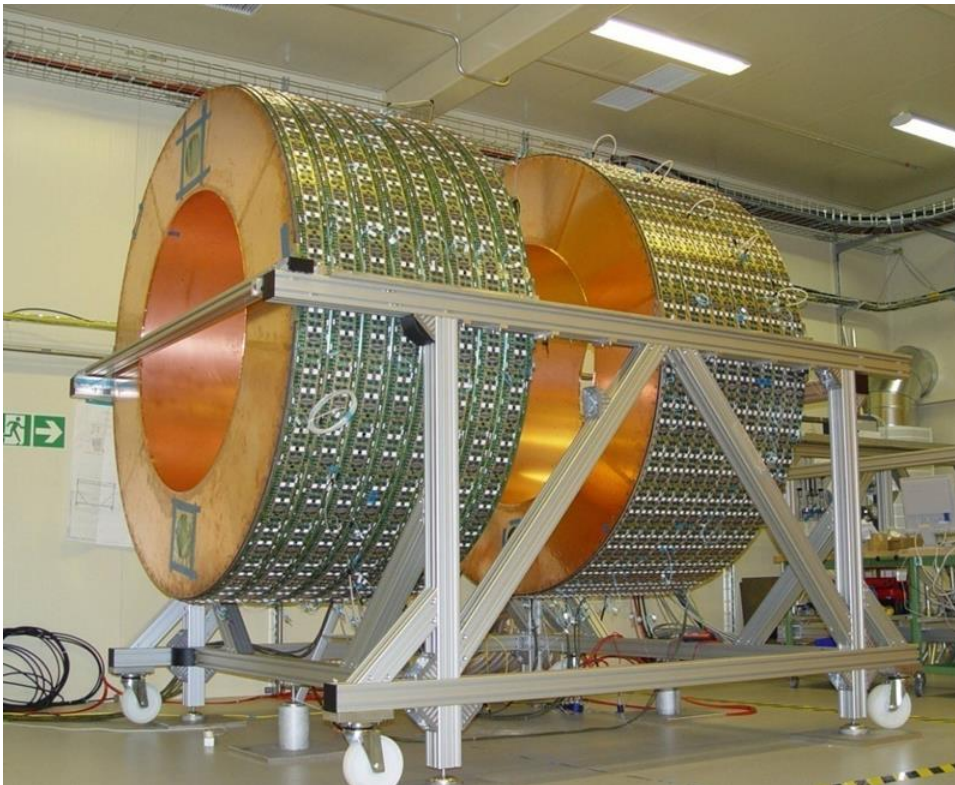
Figure 2-26   Image of TRT prior to integration with SCT Barrel [38]

Technology used for particle detection on the TRT is based on a straw tube detector. Utilising a simple 4 mm inner diameter tubes filled with a $Xe/CO_2/O_2$ gas mixture with a central Anode wire. The barrel region of the TRT contains 50000 straws oriented longitudinally with the beam. The TRT end-cap region has 20 end-cap wheels per side containing 320000 straws aimed transversely to the beam line [38].

The TRT tracker geometry is angled so it guarantees that approximately 40 straw tubes are crossed by each charged particle. Precision tracking is now made possible at large radii regions of the ATLAS inner detector enhancing pattern recognition.

Ionization occurs in the gas mixture when charged particles pass through the TRT straw tubes [Fig.2-27]. Electrons drift to the Anode (central wire) which is divided in two halves and read out every 75 ns at each end providing the information about the drift time. The distance from the wire to the track is determined by converting the drift time into the distance. In the TRT straw tube tracks position measurement accuracy is ≈170μm. The transition radiation measurement in the TRT is based on use of the polypropylene radiator material which fills the space between the straw tubes
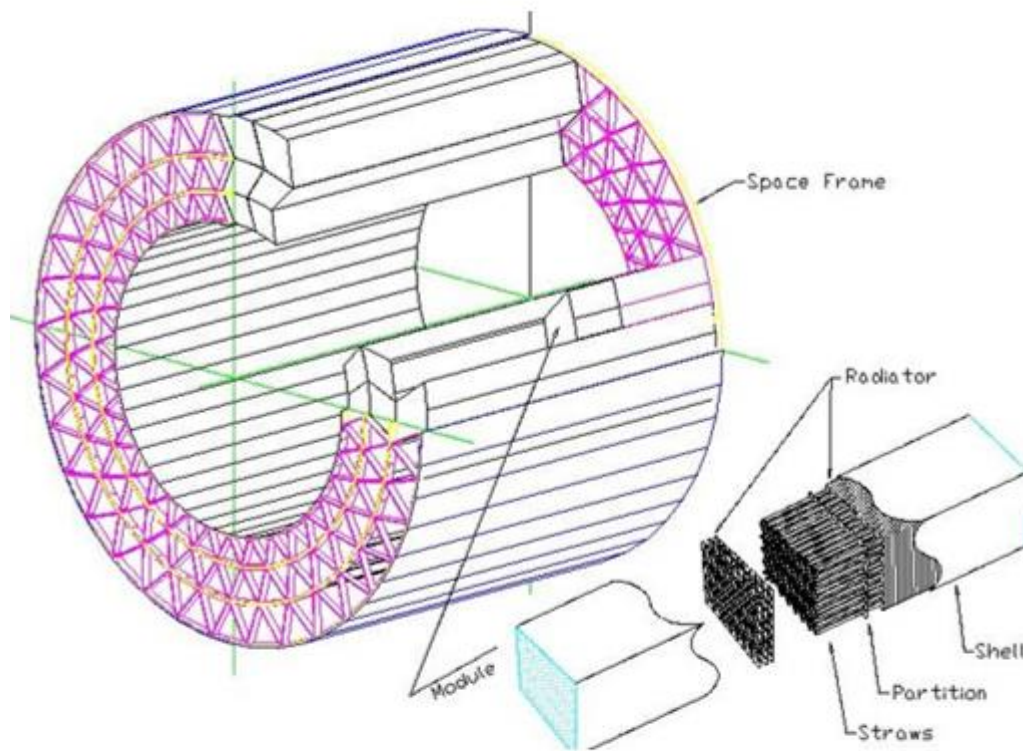
Figure 2-27   Drawing of TRT and axial straw module [39]

Transition radiation (X-rays) are produced when charged particles pass between the two materials having different dielectric constants. Transition radiation is dependent on the Lorentz factor (γ), mass and momentum of the particle. The straws containing the gas mixture absorb X-rays and produce significant amounts of charge [39]. The TRT readout thresholds

provide electron identification. Ionization detection triggers the low threshold, X-Ray detection triggers the high threshold.

Heat is dissipated along each tube (maintained at 10˚C) which uses the module shells produced from a high thermally conductive, 400μm thick carbon fibre support structure acting as a radiator. Mono-phase C6F14 refrigerant cooling removes the heat via two cooling pipes located in the corners of each module shell dissipating to the CO_2 gas envelope surrounding the TRT structure [A.2]. The same principle applies to both the TRT barrel and end-caps [Fig 2-28].

Figure 2-28   Image of TRT being integrated into the SCT Barrel [40]

During integration with the ATLAS SCT with the TRT the author was involved with this entire process [A.4], predominantly acceptance testing of the SCT to ensure that, once integrated, no inaccessible faults would occur or need rework. Following integration the author was involved with the cosmic testing of both TRT Barrel and End Cap systems as previously described in section 2.5 and reference publication A.4.

2.7 ATLAS Detector Control System

The ATLAS Inner Sub-Detectors need to function as one integrated unit. The ATLAS Detector Control System (DCS) is the overriding control system, which determines function and safe operation of the ATLAS machine. DCS is the global interface to all sub-detectors and infrastructure of the ATLAS experiment.
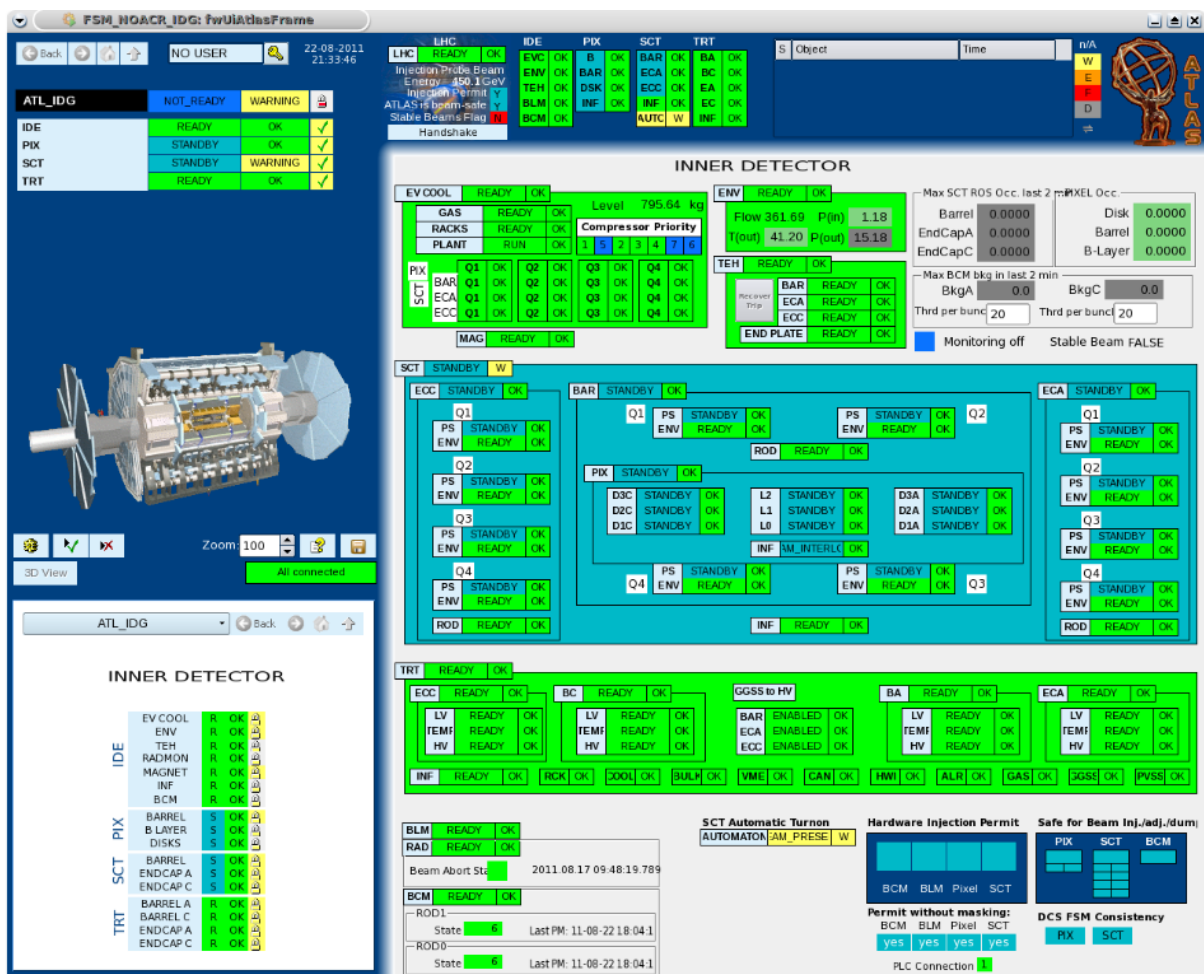
Figure 2-29   Image of the ATALS DCS FSM Control Display [41]

The DCS primary design is to bring the detector into an operational state and continuously monitor operations, recording this data. It then is required to indicate any abnormal behaviour to the operators in the ATLAS control room, allowing implementation of either manual or automatic intervention action [Fig.2-29].

Contributions from the author involved later detector operations as an on-call "expert" as part of the Inner Detector Expert team responsible for global control of ATLAS during physics running and early stages of full ATLAS detector characterisation [A.2, A.4]

Synchronisation of detector state and physics data requires communication between the DCS and the ATLAS run control. The LHC accelerator, the LHC magnets and the Detector Safety System (DSS) are managed by the DCS system. During physics data taking or long-term operation, overall control of ATLAS is managed by the more complex Trigger and Data-Acquisition (TDAQ) control system [42].

What is essential for the ATLAS operation is the distribution of event driven control across a large number of computers. ATLAS DCS is essentially an industrial standard Supervisory Controls and Data Acquisition (SCADA) system. CERN uses PVSS II [Fig.2-36] to connect to hardware and software interface using a Finite State Machine (FSM) shown in [Fig.2-30], which uses the acquired data for system operation.
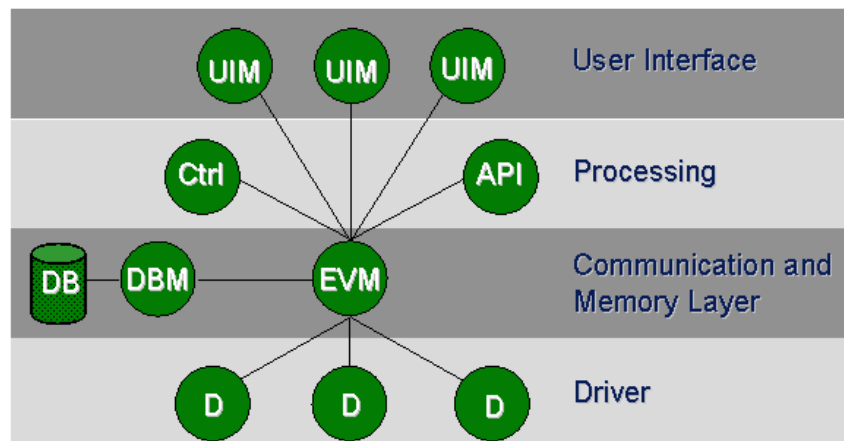
Figure 2-30   Diagram of PVSS Architecture [42]

Essential to the ATLAS Inner Detector cooling system control (described in section 2.8) is a general purpose I/O and processing unit called Embedded Local Monitor Board (ELMB) [43]. The bespoke ELMB, designed to operate in high magnetic fields under ionizing radiation in

the ATLAS cavern, can either be embedded in detector electronics, or stand alone and directly read out.

The Back-End (BE) of the ATLAS DCS comprises of more than 150 PC in a networked system. The PVSS handles inter-process communication using the LAN (local area network). The BE operator to interface hierarchy through to individual devices control is represented by the FSM, a distributed Finite State Machine.
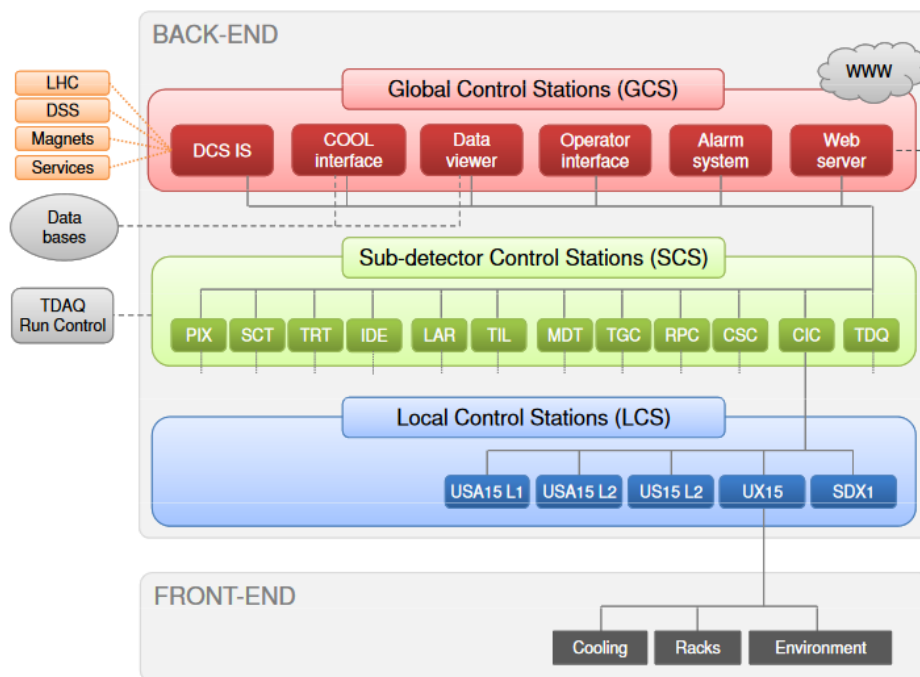
Figure 2-31   ATLAS GCS System Layout [42]

FSM allows standard operations and error handling in each functional layer of the LCS (Local Control Stations). The SCS (Sub-detector Control Stations) maintain a high-level sub-detector control during stand-alone operation. The GCS (Global Control Stations) utilises server applications interfaced in the ATLAS control room providing overall operational control of ATLAS [Fig.2-31].

The Embedded Local Monitor Board (ELMB) [42] device has an on-board CAN-interface and is in-system programmable. There are 18 general-purpose I/O lines, 8 digital inputs and 8 digital outputs. Optionally a 16-bit ADC and multiplexing for 64 on-board analogue inputs is provided [Fig2-32].
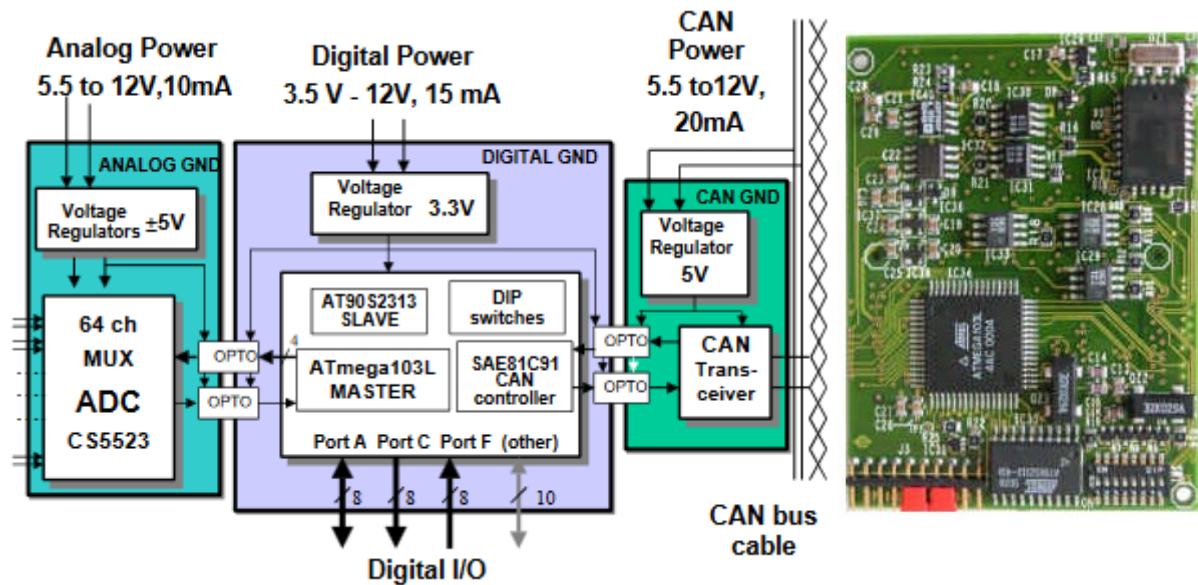
Figure 2-32   Diagram & Photograph of ATLAS ELMB [43]

The author used the DCS system to assist in the monitoring of the SCT ID cooling "loop-back tests" [A.2]. The addition of pressure and temperature sensors provided a full test of two cooling lines and measurements of the evaporation pressure generating a full temperature profile of all remaining lines. This temperature profile was used to provide a crude calculation of the C_3F_8 fluid pressure before and after the heater. Connection with the final DCS cables plus the connection of additional cables to the loop-back NTC temperature sensors was carried out.

Additional low-pressure sensors to measure the evaporation pressure before and after the heaters with the supporting new PVSS codes were implemented. Some later instances of mapping SCT ID DCS sensors required a PVSS project running on a locally mounted laptop with its own ELMB.

2.8   ATLAS SCT Cooling System

The SCT and Pixel cooling system is required to have enough capacity for cooling or removal of heat generated from the on-detector electronics. The majority of the heat load generated is removed by means of heat transfer from the detector modules. Stable silicon module temperatures must be maintained at or below $-7°C$ for the SCT (during active run data it was found to improve performance running warmer) and a marginally warmer $0°C$ for the Pixel [A.3].

Cold temperatures are required to prevent reverse annealing of the silicon detectors [A.2 & A.3] requiring an exhaust vapour temperature of -25°C. Radiation damage induced in silicon detectors is shown when measuring change in the doping region of the semiconductor as a function of time. In the case of the SCT semiconductor module, calculations performed take into account the time needed to accumulate the required fluence and the time elapsed after exposure to radiation is halted e.g. detector shut down. These effects, known as reverse annealing, are accelerated by increasing sensor temperature but is slowed by cooling or reduction of sensor temperature. Specific semiconductor properties are specified to perform well under exposure to radiation [A.6, A.7. A.8, A.9].

The cooling system faces a fundamental design challenge, the avoidance of mass build up high in the detector volume. With a 70kW total heat load removal and a target temperature on the detector structure of -5°C the refrigerant's total mass flow rate was specified at 1130 gs^{-1} [A.2].

Mass, especially from materials with high atomic number (Fe) are avoided in order to minimize the production of secondary particles which is measured in radiation length. This philosophy is generally applied throughout the inner detector. Restrictions on the physical size of the cooling system embedded within the central structure of ATLAS requires the dimensions of tubes, pipes and components used in the cooling system to be as small as possible.

The author began investigations on the cooling system [A.3] for the SCT Barrel, when initial operation of the ATLAS silicon tracker fluorocarbon evaporative cooling system highlighted serious limitations in performance of the cooling circuits of the barrel. Leaks found on the Barrel Heat Exchangers required the author to analyse and design a repair method [Fig.2-33] that would last for the service life of the ID.

SCT HEX problem of Autumn/Fall 2007 taken from 124th ATLAS EB notes 30/11/2007

"A new problem has been observed: at the transition from a 3mm pipe to 5 mm of a heat exchanger (HEX) a leak had occurred. Further investigations revealed that for 70% of the HEX the soldering at this point is faulty and that all HEX have to be reworked. By now 60% of the HEX have been repaired and re-installed. This has however further impact on the schedule, which foresees now to seal the end-caps before Christmas." "Because of all these problems much work is being carried out in parallel. The teams work 2 shifts per day and over the weekend, but the schedule is still extremely tight and requires much interleaving of installation and commissioning work."

Figure 2-33   SCT HEX fault notes from ATLAS EB meeting in 2007 [44]
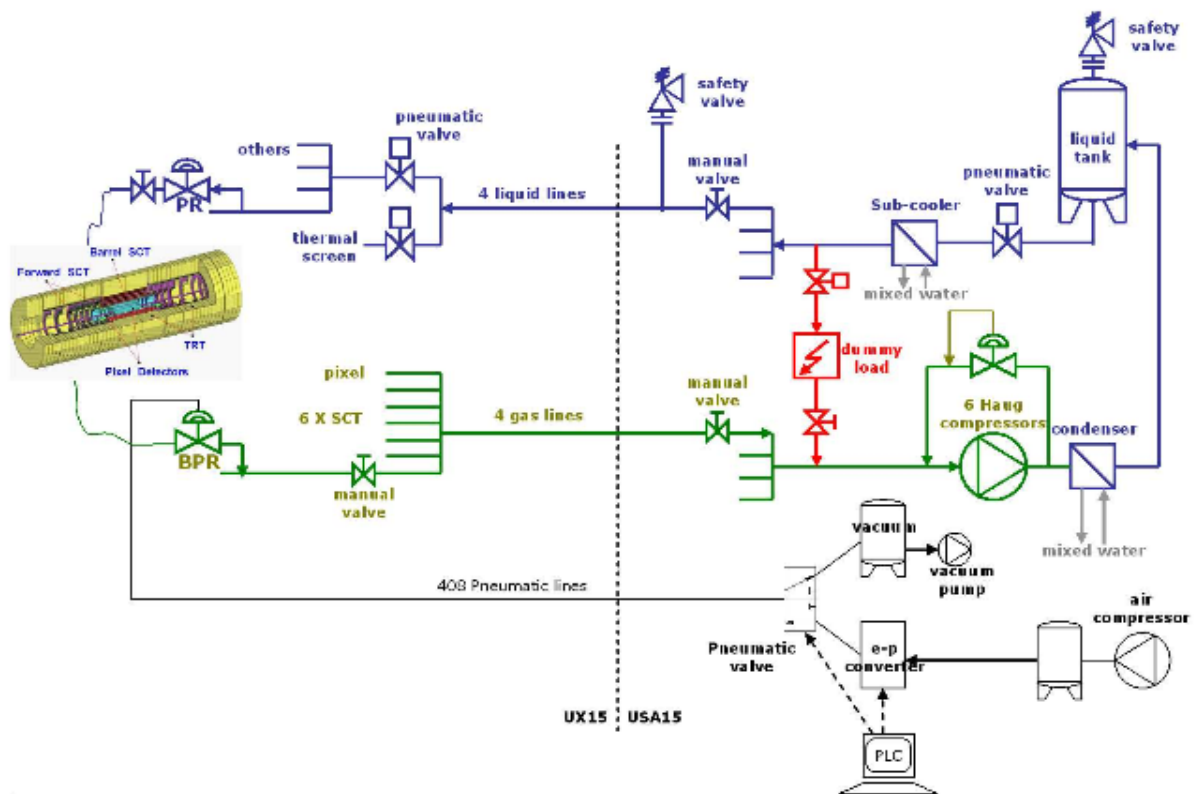
Figure 2-34   SCT evaporative cooling system main plant schematic [A.2, 23]

Later problems with the induction heaters boiling exhaust fluid affected not only the SCT Barrel but also the SCT End cap cooling design. The author was involved with the full tests of the SCT cooling system, which were cut short due to the need to maintain the installation schedule of the SCT Barrel. Following installation of the Barrel in the ATLAS cryostat, the author was involved with the integration, re-design, testing, manufacture and performance testing of a modified SCT cooling system [Fig.2-34] and the overall integration of the SCT Barrel with the SCT EC and Inner Detector completion [A.2, A.3, A.4]

In July 2006 the SCT heater system designed to warm the C3F8 refrigerant and prevent ice forming on the exhaust pipes into the main ATLAS cavern failed. Initially thought to be anomalous behaviour, investigation was terminated due to the closure of the cryostat and the mapping of the magnetic field in order to keep to detector installation schedules.

Testing revealed a small number of the 200 induction type heaters, contained in a 700mm long 25mm diameter stainless steel jacket, showed cold spots. Using the heater sensors and DCS system used to control the heaters, these cold temperatures could not increase irrespective of the amount of electrical power input used to boil the fluid. The author began the modifications required for a revised cooling system and layout of the heaters in a way that was not anticipated in the original experiment design. Relocation of the entire heater system, heat exchange system (HEX) and cooling transfer lines was required [Fig.2-35].
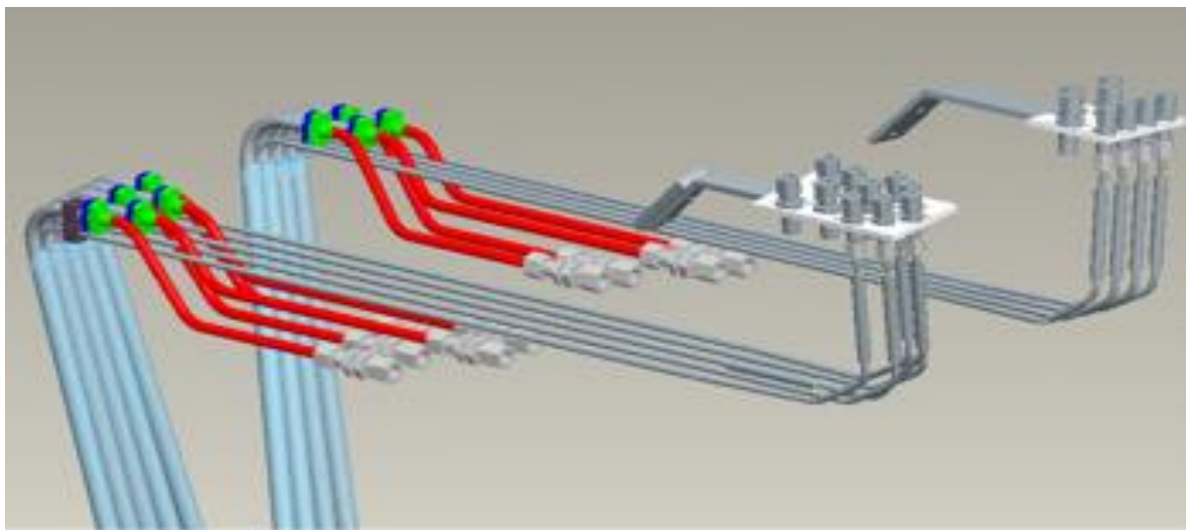
Figure 2-35   CAD Rendering of EC HEX Heater Modification [45]

The author was responsible for the remanufacture of the SCT HEX system and its integration with a relocated electrical heater to allow access should it fail in the future. The relocated system was known as the "Far Heater Solution". He developed the entire testing procedure for the HEX heater system of the SCT, qualifying each unit to leak rate (down to 10^{-7} torrl/s) and pressure-tested (24 bar$_a$) to determine acceptance for installation in ATLAS. The Far Heater solution relocated all potential components which would require future intervention to the more accessible cryostat flange [Fig.2-36]. The cryostat flange due to the radial increase in size is less densely populated with services as opposed to other areas of the cryostat.
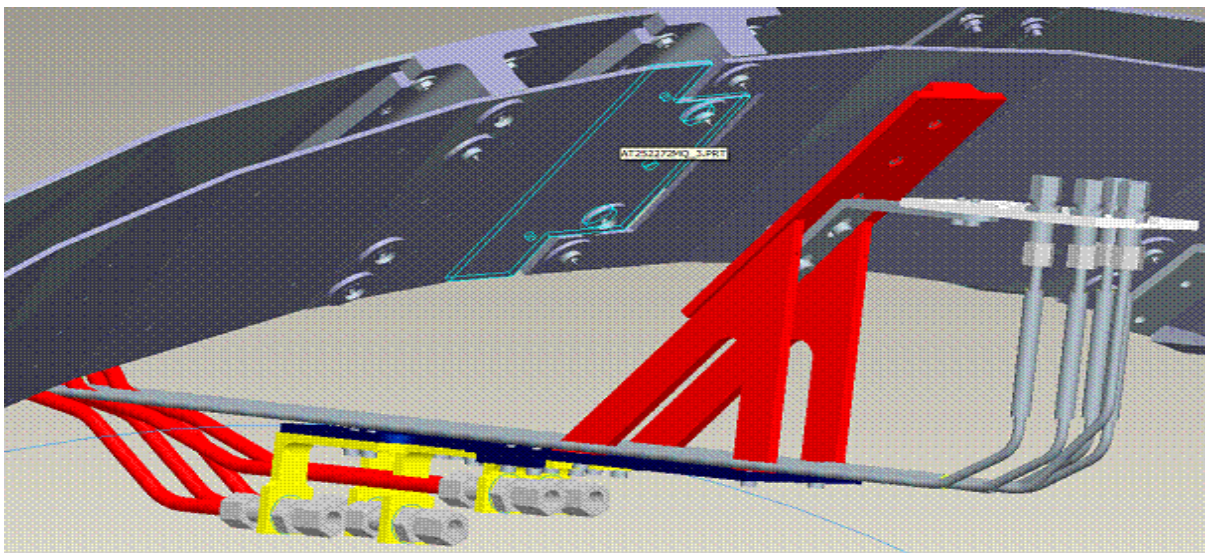
Figure 2-36 CAD Rendering of Cryostat Flange Heater Location [45]

Investigations were incomplete, a second mode of failure was found with the heaters for the SCT cooling system producing erratic results. During a cooling test run in ATLAS the heater on cooling circuit 130 failed to respond to automatic DCS signals and was switched-off. When at room temperature, the refrigerant gas C3F8 is in a liquid state at high pressure (13 bar), it then flows to the SCT. Coolant flow rate is controlled and set by the capillaries on-detector. The backpressure regulators (BPR) set control of the evaporation pressure. Reduction of BPR pressure produces colder running of the SCT cooling system [Fig 2-37].
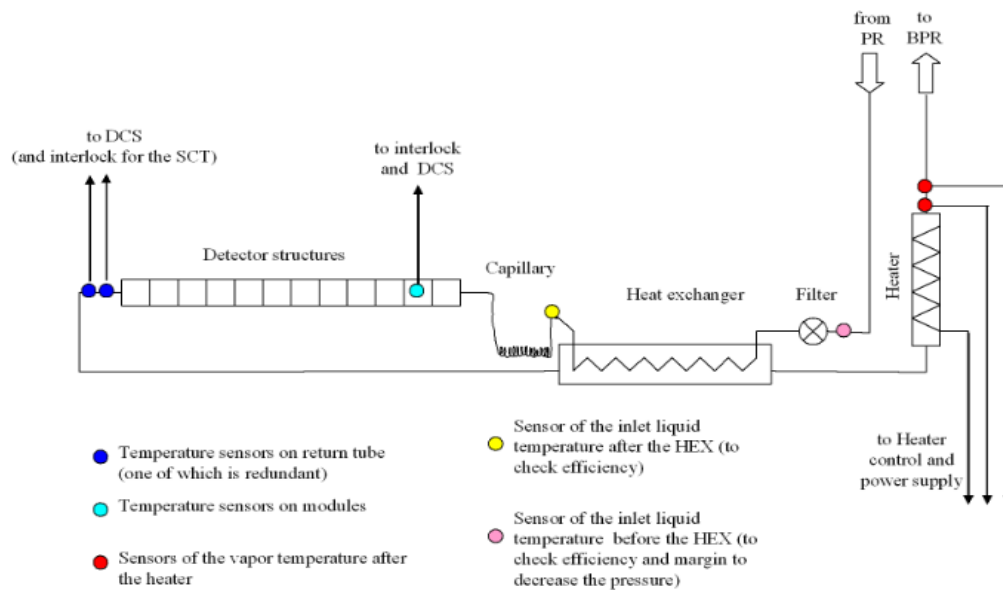
Figure 2-37   On-Detector cooling circuit schematic [A.2]

The heater main function is to boil off any remaining liquid C_3F_8, preventing cooling in the exhaust lines outside the inner detector volume. The heater design [Fig.2-38 & 2.39] utilised two thermocouples with interlock control located inside the stainless steel heater body, one for control of the heater power, and one as an interlock to prevent overheating.

Figure 2-38   Image of a SCT cooling heater [46]

During initial cooling system tests, the control function was not operating with the thermocouple in the existing location. Thermal imaging of the heater indicated that potential remaining liquid failed to evaporate from the end of the tube (thermocouple side). Further operation and investigations revealed the interlock function did not function correctly in some states; some of this was attributed to poor thermal conductivity of the heater body material.
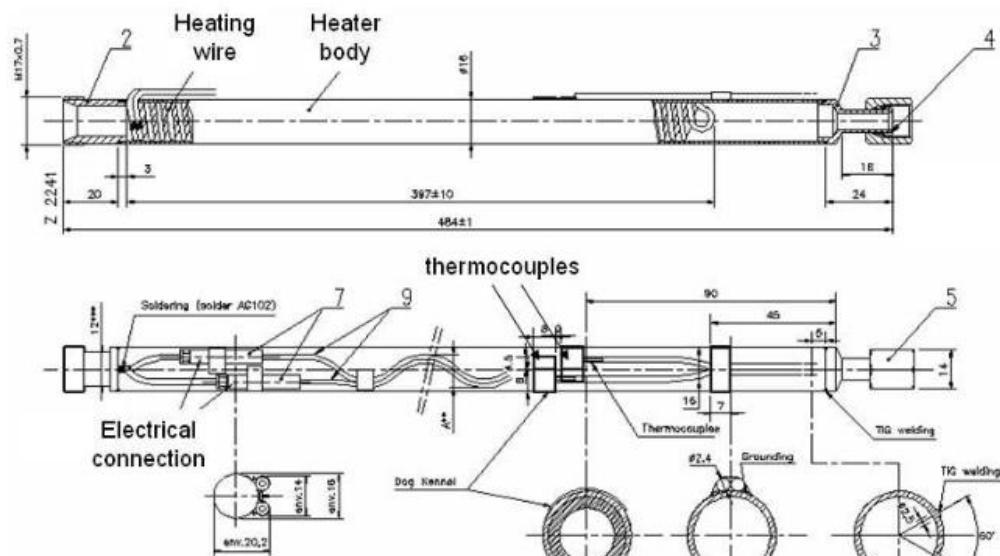
Figure 2-39   Thermocoax SCT heater drawing [46]

Problems observed when running warm C_3F_8 were caused by debris found in the system. From further investigations small pieces of copper waste were trapped in the BPR, which would cause a sudden drop in temperature during stable running. The effect was to block the BPR open, which reduced the backpressure and therefore the temperature. Additional filters called micro-sieves were installed in the SCT cooling system before the BPR to prevent this problem, along with the swapping of the BPR membranes which became too hard (from cold temperature exposure) to achieve a low enough operation pressure.

Catastrophic failure was again observed in heater 130 during system running. No existing modes of failure could be connected with the erratic behaviour of the control system or heater. A further 21 heaters demonstrated the same characteristics when later tested. Leaks in the heaters close to the internal thermocouples were found. Internal inspection with an endoscope, revealed evidence of corrosion. Detailed analysis indicated the flux used to braze

the thermocouple internal 0.1mm stainless steel sleeve into the 1mm thick heater body caused aggressive corrosion through lack of correct cleaning [Fig.2-40].
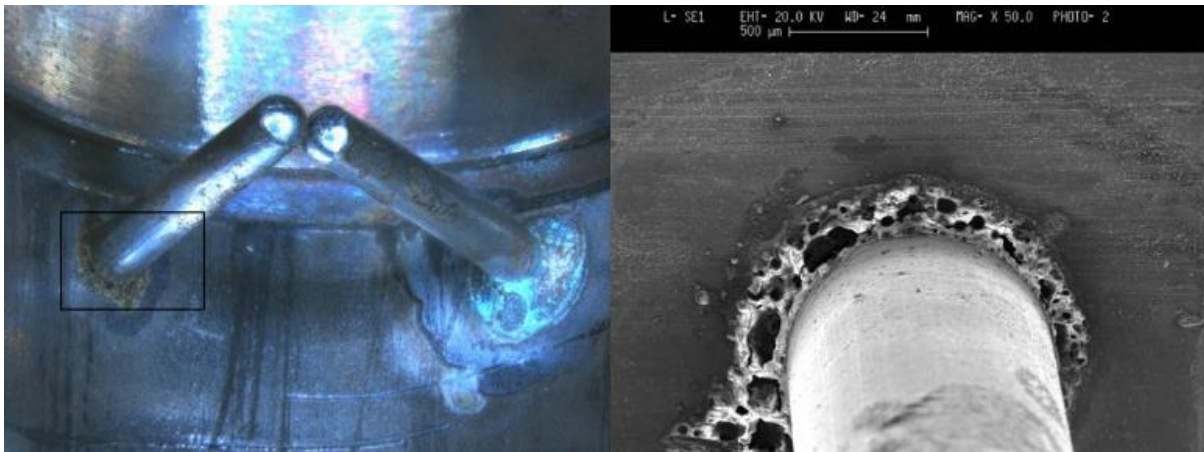
Figure 2-40   Endoscope (L) and SEM (R) image of SCT Heater corrosion [47]

Further fine-tuning was made to the ID cooling system by altering the C_3F_8 concentration [24] with a blended refrigerant gas. Greater pressure drops found in inaccessible areas of the cooling system were recorded. This affected the minimum achievable evaporation temperatures of the fluorocarbon refrigerant-based cooling system [A.3]. A blend of C_3F_8 Octafluoro-propane and C_2F_6 Hexafluoro-ethane gas was used in the entire SCT cooling system with the exception of the mono-phase TRT detector. The critical problem faced by the detector was the factor of safety allowed to prevent thermal runaway once the detector modules radiation dose increased to achieve a level expected during their 10-year service life within ATLAS.

The author provided initial test data for the ATLAS SCT Barrel and End-Cap cooling system and was responsible for the entire ATLAS Endcap cooling system installation. On final testing using helium leak detection equipment, two leaks were detected in the evaporative cooling circuits on EC-Disc 9C. One circuit had a leak of 25 mbar/hr at 7bar of Helium [Fig.2-41]. This is marginally outside the upper leak rate tolerance given for the SCT cooling system, and could be recoverable if access were permitted [A.4]. The second circuit "Loop 186" has a leak rate of 1 mbar/s which would create a huge loss of C3F8 and is potentially irreparable without strip down of the endcap. These faults can be viewed using the SCT DCS system IDEEVCOOL panel [Fig.2-29].
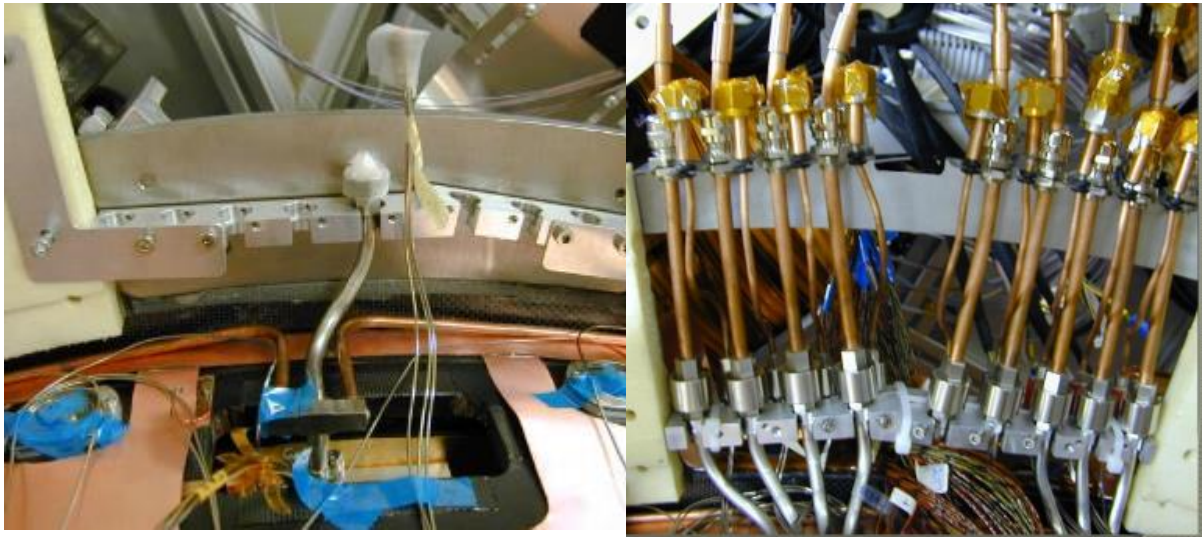
Figure 2-41   Image of STFC D9C "186" connection (L) and fully installed (R) [48]

The exact locations of these leaks have been a matter of age old debate [Fig.2-41], using helium leak detection equipment with helium pressurising the lines and "sniffing" outside the detector cooling lines the author determined the leak to be in the region of the STFT (services thermal feed-through). The ATLAS schedule prevented any further investigation and repair of these circuits and sealing of the enclosures commenced [A.2].

2.9　　　First events in ATLAS

Two decades of hard work by an interdisciplinary, international team who worked towards one common goal: the successful operation of ATLAS and new physics discovery. On the 10th September 2008 at 10:25 CET, the LHC circulated its proton beam around the 27 km ring. ATLAS tracked this event [Fig.2-42] seen as a cross-section of the beam-pipe in which one dot was the injection in, and the second dot was the beam returning, to the LHC accelerator ring [49] [A.4].
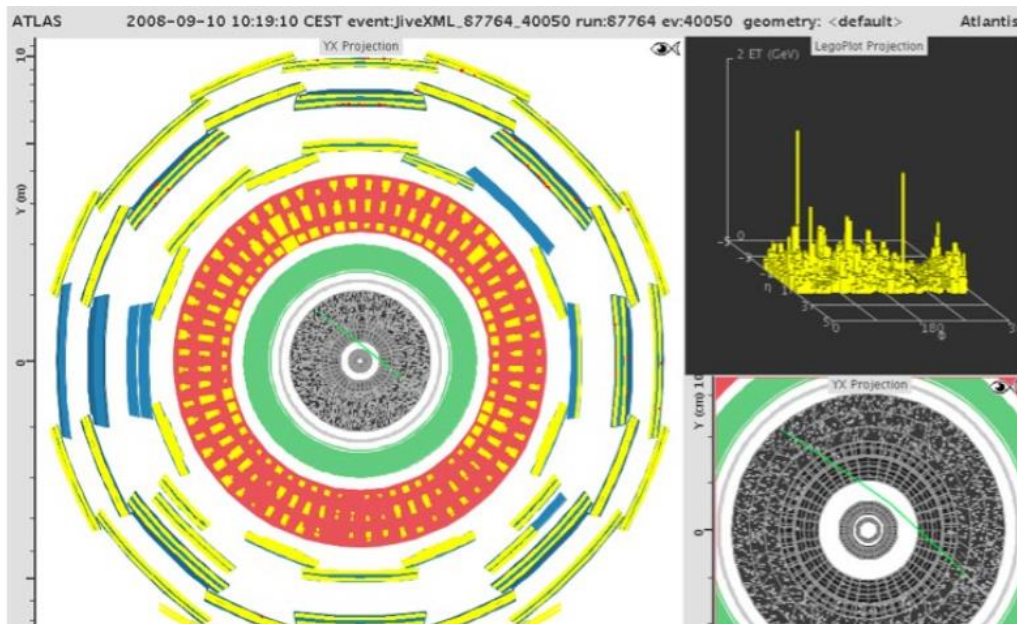
Figure 2-42　　First event ever seen in ATLAS [49]

2.10   ATLAS Insertable B-Layer (IBL)

The B-Layer is the current innermost layer of the PIXEL detector (fourth PIXEL layer) and is critical to the performance of full realization of the physics capabilities of the ATLAS experiment. This detector consists of 14, carbon-fibre reinforced plastic Staves, 20mm wide, 64mm long, and tilted by $14°$ in φ surrounding the beam-pipe at a radius of 33 mm [16]. Good vertexing and b tagging performance must be maintained ensuring LHC Phase I 14TeV upgrade physics program success. Event pileup and eventual problems in the present B-layer and other Pixel layers were to be addressed with this additional detector layer inside the B-layer [50].

Figure 2-43   Image of Side-C IBL Installation [51]

Originally, the Insertible B-Layer (IBL) detector [Fig.2-43] installation, intended for the 2016 LHC shutdown was to prepare ATLAS to enter the HL-LHC phase (High Luminosity). The IBL detector was designed to squeeze in the gap between the main LHC beam pipe and the SCT PIXEL [Fig.2-44]. The new detector insertion gap between the Inner

Supporting Tube and the IBL detector is 0.2 mm and 1.9mm between the supporting tube and the PIXEL detector is 1.9 mm.
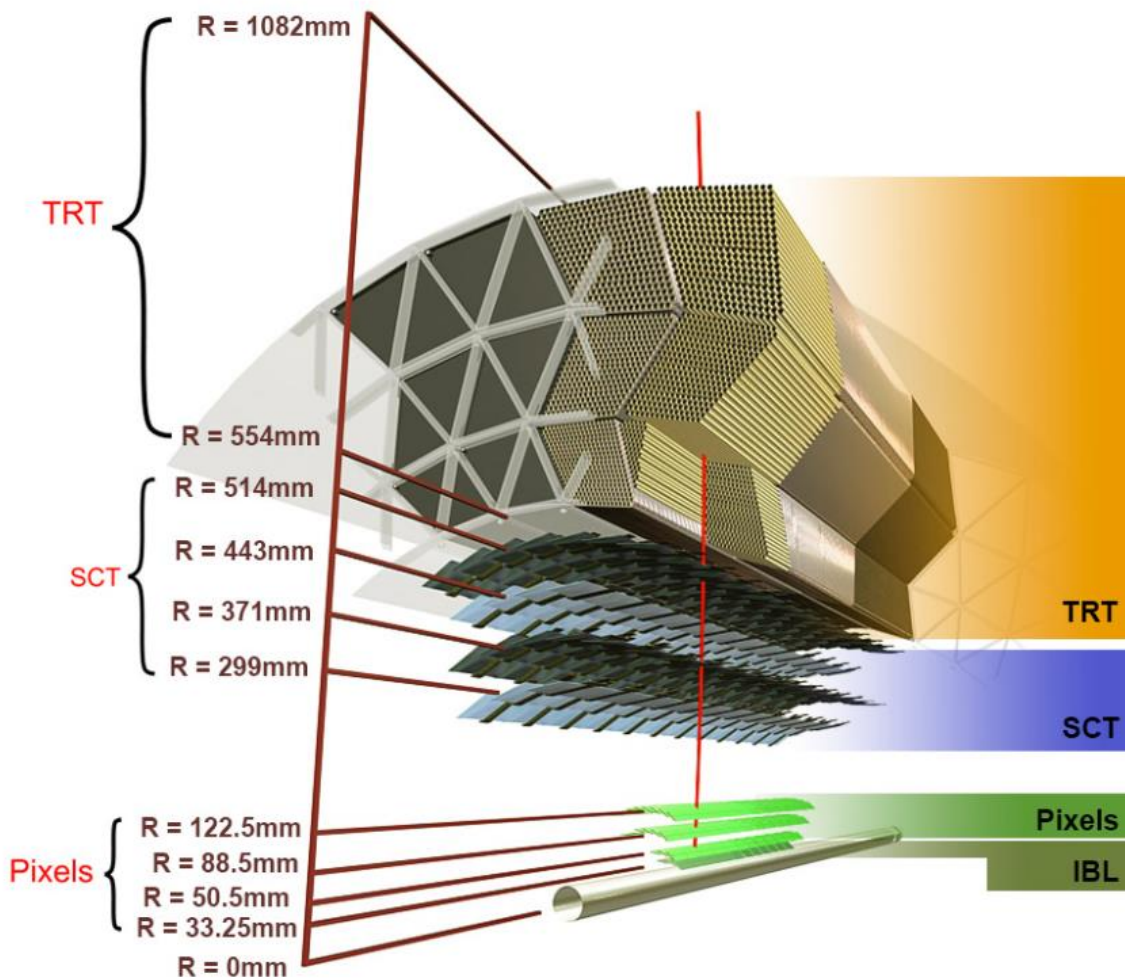
Figure 2-44   Rendering of IBL position in the ATLAS ID [52]

The aim was to provide improved tracking and robustness before the LHC exceeds nominal peak luminosity, before the large LHC Phase-I data set is collected. Radiation tolerance design requirements of the IBL are to withstand 250 MRad of total ionizing dose (5×10^{15}neq/cm2 non-ionizing radiation dose). This achieves a factor of safety of 40% with respect to the expected total integrated luminosity in 2020 [50].

Arising from the IBL Technical Design Review (TDR) the original extractable design (for hot swaps during LHC shutdowns) was determined no longer possible due the mechanical design changes of the Inner Detector during installation and its rework schedule. The now Insertable, but not extractable B-Layer (IBL) along with an entirely new section of smaller radius LHC beam pipe "should maintain robust tracking despite effects arising from luminosity, hardware lifetime, and radiation" [56].

Although both the radiation tolerance of the IBL and the total integrated luminosity for HL-LHC Phase II were uncertain, it was expected that the integrated luminosity could approach or exceed the radiation tolerance of the B-layer before the end of Run I. The IBL ultimate design is to mitigate the effects of radiation-induced loss of efficiency in the innermost PIXEL SCT layers.
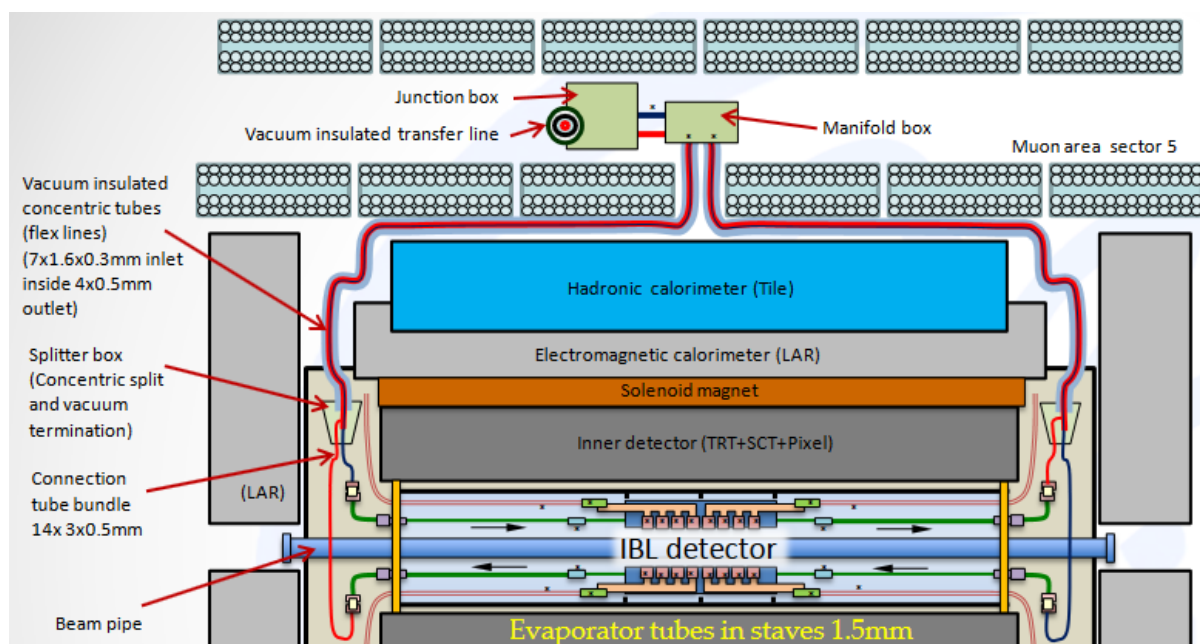
Figure 2-45   Schematic of ATLAS IBL Cooling System [53]

One novel element of the IBL that differs to the main ATLAS SCT was the shift away from using the fluorocarbon based refrigerant gas cooling systems, to using an IBL specific CO_2 high pressure two phase accumulator loop controlled cooling system [Fig.2-45]. The author was responsible for reviewing the final stages of the IBL cooling system [53], before production could proceed.

The use of evaporative CO_2 is the first of its kind in ATLAS, designed for lower temperature operation ($< -35^{\circ}C$) than previously developed CO_2 cooling systems in High Energy Physics experiments such as LHCb [53]. Protection of the IBL sensors to withstand the expected high radiation doses received at the maximum design integrated luminosity of 550 fb1 is achieved by the additional cooling power of CO_2 [50].

Serious potential impact to the existing ATLAS detector operation was perceived and required mitigation. Cooling system specific issues were the perceptions of force translating into movement exerted from bends, elbows, azimuthal service doglegs and rotation. This could have impact on a tracking detector structure required to maintain position (order of 5-10 microns), with very high pressure cycling (~60 bar to 12 bar, CO_2 evaporation pressures at $20°C$ and $-40°C$) [52].

These first CO_2 cooling systems provided prototype design and operational data to influence later detector construction. The IBL Stave design [Fig.2-46] and sensor technology were the benchmark development platform for future detector upgrades to both ATLAS and LHCb, which are now under design for the Phase-II upgrade detectors described in Chapter 3 hence inclusion in this document.
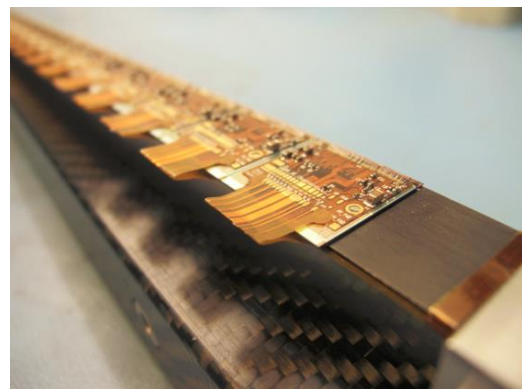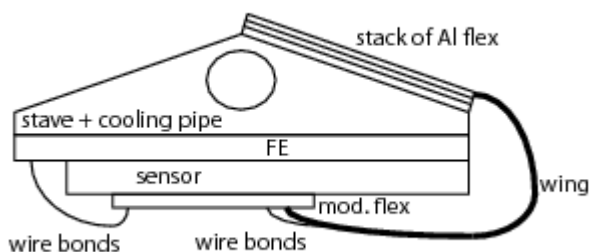
Figure 2-46   Cross-sectional drawing & image of IBL Stave [51]

Semi-conductor advancement, not available to the original ATLAS designers in the late 1990's, introduced the use of both planar technology as used for the current PIXEL detector and new 3D CMOS sensor technology used for the first time in any LHC experiment. Advancements to improve radiation hardness and to reduce inactive area were achieved in this detector design [16].
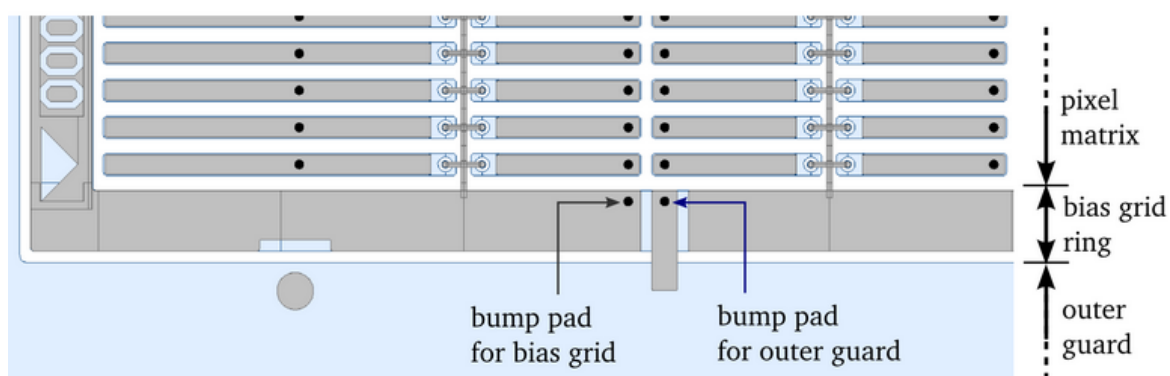
Figure 2-47   IBL planar sensor design [54]

The IBL Stave construction using an embedded cooling tube within a carbon foam [56] core is now the methodology applied by the ATLAS Upgrade Stave described in Chaper 3.3. This robust Stave construction has reduced cost, increased speed of manufacture, improved thermal conductivity from the sensor heat load and provides better particle tracking resolution. This concept was based on a proposal for CDF in the Tevatron Run IIb [55].
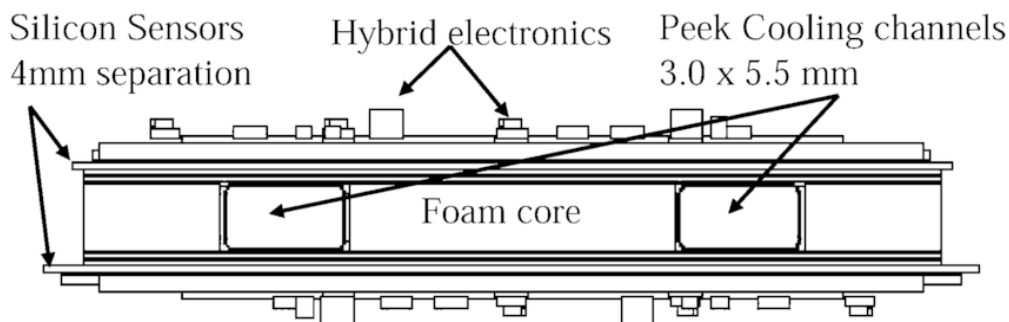
Figure 2-48   CDF Run IIb Stave design [55]

The IBL planar sensors are built in n-in-n technology [54], 200µm thick, 40×20mm wide. Novel slim edge technology reduces the overall inactive region of the sensor to only 200µm by moving the 13 guard rings underneath the active region from the edge Fig2-47.

3D, 130nm technology uses the innovative concept of an electrode passing through the bulk region, increasing measurement surface area into silicon sensor as well as using the outer faces. Lower bias voltages are possible with respect to the planar technology and improves sensor irradiation performance [54].
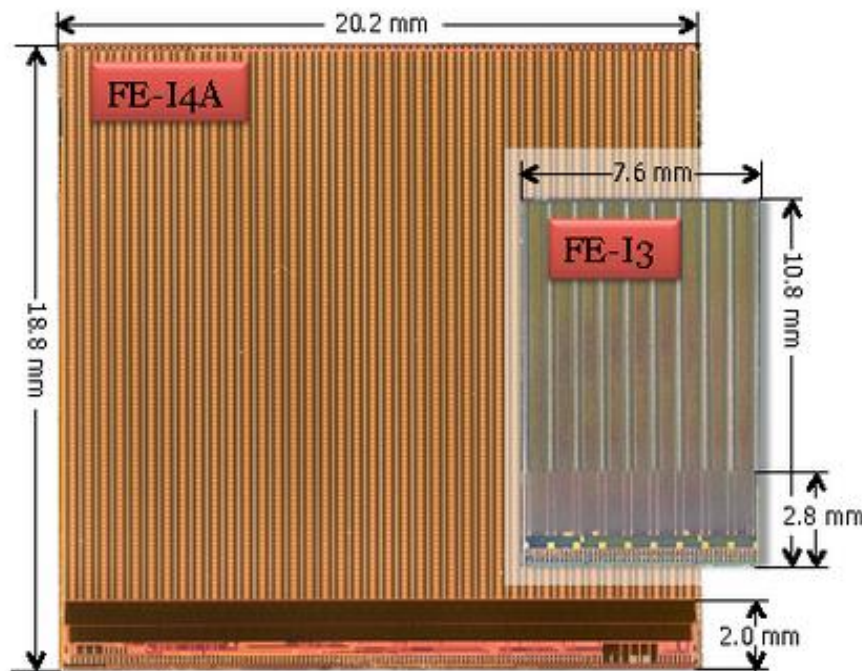
Figure 2-49   Image of both IBL FE-I4 & PIXEL FE-I3 Sensors [54]

The existing FE-I3 sensor as used in the current ATLAS PIXEL detector [Fig 2-49] differs considerably in both size and pitch from the IBL sensor as shown in [Fig 2-47]. 3D technology used on the IBL is an n-in-p type silicon sensor. The dimensions are, 230µm thick and 20×19mm wide Fig2-10.

During 2012, a potential installation gap in the LHC maintenance shut down schedule was identified and the IBL production schedule accelerated to align for a late 2013 installation [52]. This installation activity was to take place during the winter shut down of the LHC for completion in 2014 ready for data taking as part of ATLAS. Successful installation of the ATLAS IBL was completed by the end of May 2014. From spring 2015, the detector is successfully taking data within ATLAS.

Chapter 3   ATLAS High-Luminosity Upgrade

3.1   Introduction

Chapter 3 details the author's significant contributions to R&D for new detector technologies in the ATLAS Upgrade. Subsequent studies made by both the ATLAS and CMS experiments have found the Higgs boson, which widened the search for new physics and the desire for high luminosity running of the LHC.

The author made substantial contributions to the development of initial conceptual ideas in 2005, the research and development of the ITk to present day ITk Strip Tracker pre-production. Additional contributions made by the author are the development & testing of adhesives for the ITk Module Hybrid to Silicon sensor, development of the Silicon sensors through irradiation facility design, construction and operation. Finally, the authors development of novel technologies for ITk cooling system R&D is detailed along with successful transference into the industrial domain, predominantly aerospace and robotics industries is referenced.

Reference publications used in the section are:

[A.5] Progress with the single-sided module prototypes for the ATLAS tracker upgrade stave. [A.6] Testing of bulk radiation damage of n-in-p silicon sensors for very high radiation environments. [A.7] Development of n-on-p silicon sensors for very high radiation environments. [A.8] A double-sided, shield-less stave prototype for the ATLAS Upgrade Strip Tracker for the High-Luminosity LHC. [A.9] Development of n+-in-p large-area silicon microstrip sensors for very high radiation environments – ATLAS12 design and initial results. [A.10] The Birmingham Irradiation Facility. [A.11] Detailed Studies of Full-Size ATLAS12 Sensor. [A.12] Upgrade to the Birmingham Irradiation Facility. [A.13]   Pre-configured XY-axis Cartesian Robot System for a new ATLAS scanning facility

3.2 The ATLAS & LHC Upgrades

ATLAS, running successfully at CERN on the LHC for many years now has made the Nobel Prize winning discovery, the Higgs Boson. Inevitably the LHC future energy range will reach an upper limit and the LHC magnets will require upgrading to achieve higher energy operation or High Luminosity LHC (HL-LHC) needed for new physics discovery [57].

Serious challenges presented to the ATLAS detector when operating at future high luminosity in the HL-LHC will be from the extra proton – proton (P-P) luminosities, reaching an integrated luminosity of around 3000 - 4000 fb throughout its ten-year operation, reaching a peak luminosity of 3300 fb with a fluence of $10^{34} \text{cm}^{-2}\text{s}^{-1}$ [58]. Current LHC P-P performance in the same bunch crossing is now exceeding the ATLAS design specifications. HL-LHC allows for further extension of the search for indication of new physics phenomena plus existing mechanisms far into the multi-TeV region.

Period	Year	Luminosity [$10^{34}\text{cm}^{-2}\text{s}^{-1}$]	Integrated luminosity [fb^{-1}]	Pile-up [events/BX]
Run-I	2009-2013	0.75	7 TeV 5.1	9.1
			8 TeV 21.3	20.7
Run-II	2015-2018	1	50-100	23
Run-III	2020-2023	2.2	300-400	55
HL-LHC	2026-2035	5-7.5	3000	140-200

Figure 3-1   HL-LHC upgrade programme [57]
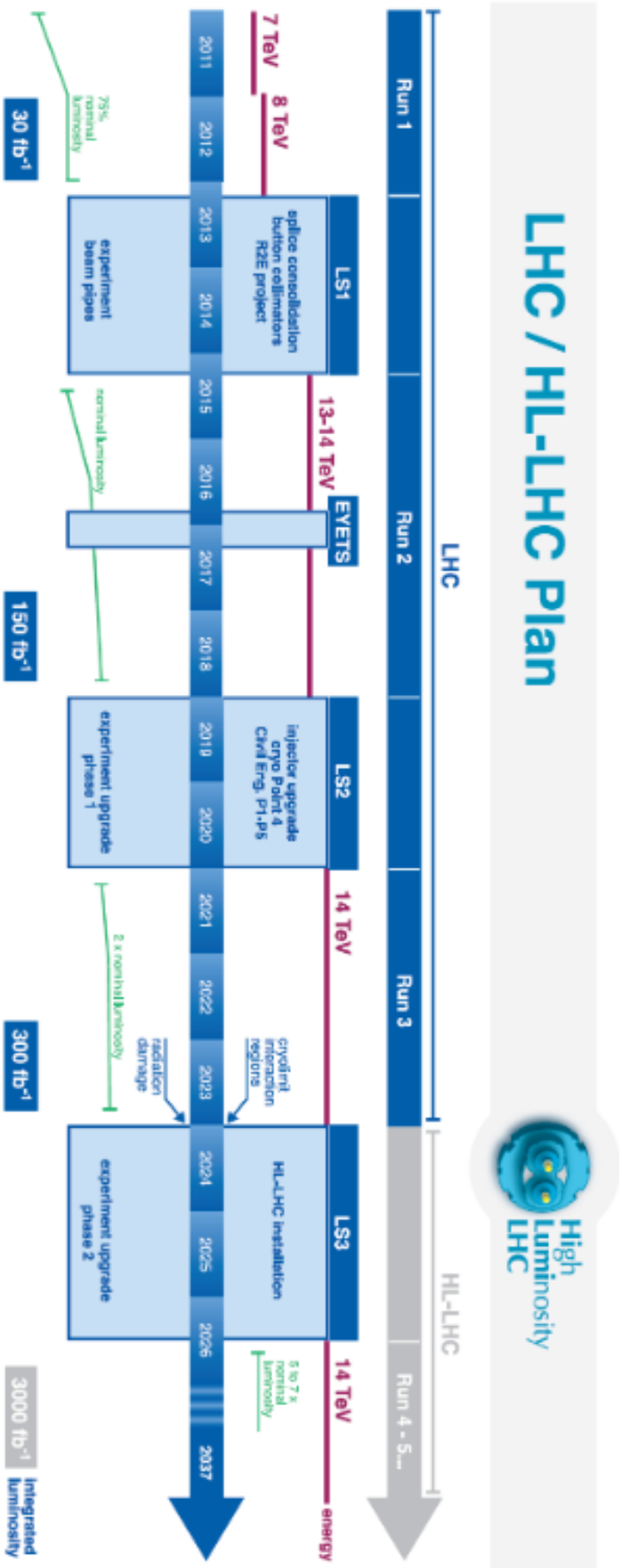
Figure 3-2   2016 CERN HL-LHC Future Schedule 2016-2020

[58]

3.3   ATLAS Inner Tracker Upgrade

LHC Run-II nears a close at the time of writing [Fig.3.1] the ATLAS community is nearing production of the upgraded ATLAS inner detector, the "ATLAS Inner Tracker" (ITk). The second long-shut down of the LHC, known as LS2 is likely to begin in 2019/2020 opening a two-year window for essential work to the LHC in preparation for HL-LHC run-III Fig.3-2.
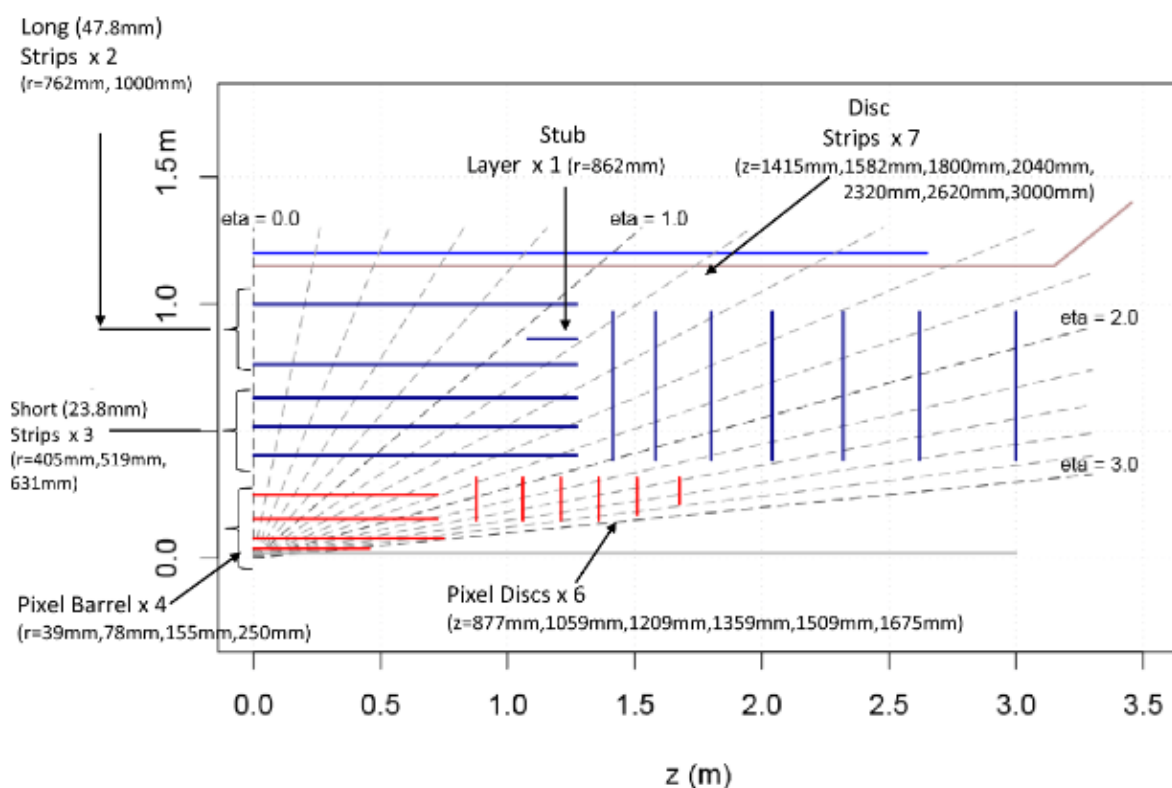
Figure 3-3   Image of pre 2016 proposed ITk LoI Layout [58]

The ITk, like is predecessor, will identify and reconstruct electrons, photons, muons, tau leptons; b-jet tagging and hadronic decays. The author has worked to understand these physics design requirements for the new ITk. His work translating these requirements into the development of new detector technologies for ITk construction, capable of operation in Run-III and HL-LHC, is detailed in this chapter [A5, A6, A7,A8, A9].

Upgrading ATLAS requires the detector to cope with increased P-P collisions and increases of the accumulated radiation damage. Expected radiation levels within the current

Inner Detector render it unsuitable for future operation in HL-LHC. From 2006, the author was involved in the research and development for the construction of a new silicon tracker to replace the existing ATLAS Inner Detector in 2019, the Phase II Upgrade [Fig.3-3] start.

The ATLAS Inner Tracker Upgrade or ITk, is designed as an all silicon tracker which will allow it to perform in the HL-LHC high occupancy environment with good tracking performance. Originally, the assumed schedule had a Technical Design Report (TDR) in April 2010 with ID installation during the long shutdown foreseen in early 2016 [52]. As ITk delays lengthened, the LS1 2016 period saw installation of the IBL detailed in the previous sections.

High luminosity operation requires the new ITk to withstand a factor of ten increase in radiation fluence than the existing SCT. Physics requirements for the ITk will allow it to; measure transverse momentum and direction of isolated particles (in particular electrons) and muons; have vertex identification from pile up event reconstruction; secondary vertices identification in b-jets with high efficiency to measure high energy jet core tracks; good double-track resolution; identification of tau lepton decay and converted photon track reconstruction [57].

The ITk will operate within a magnetic field from a 2 Tesla solenoid. The outline Inner Tracker layout follows a similar design principle to the ATLAS SCT, which it replaces. Closest to the LHC beam is a hybrid silicon pixel detector, with silicon micro-strip modules at larger radii. Dimensions are an active length of 6m, occupying the entire cryostat area with an outer radius of 1m, which is currently occupied by the TRT.

The physics requirements translate into a series of technology developments to ensure reliable system operation in the highly radioactive environment. Design requirements should optimise materials mass to improve tracking and tolerate operation within a radiation fluence. A baseline layout design [Fig.3-3] is based on the use of silicon detector modules mounted on strips (low z) and discs (high z) with number of different detector technologies covering low to high eta [58].

The proposed barrel detector will have four layers of a pixel type sensor with five strip layers, three shorter strips and two long strips. To optimise performance in the area between

the end of the barrel and the largest radius of the end-cap, a short-stub barrel (R=862 mm) will be installed in the remaining space (z) Additionally there will be a Forward PIXEL detector with a total of six pixel discs and seven strip discs [58].

ITk design balances Phase-II physics tracking performance against the construction cost. The LoI layout of the detector is shown in Fig.3-3. With relevance to chapter 2, ITk design utilises the new technologies developed since the existing ATLAS ID construction. Performance enhancements found from lower mass construction reduces multiple scattering effects, photon conversions and hadronic interactions.

Lower mass is achieved by efficient multiplexed powering schemes; high cooling power using evaporative CO_2 technology allows the use of smaller diameter cooling tubes. The combining of better performing carbon composites used to construct high strength, high thermal conductivity structures with co-cured electro-mechanical assemblies lead to substantial improvements.

This design optimisation of the ITk lends well to the use and development of new materials or novel application. The author's role in developing these new advances in low mass technologies, particularly cooling materials development and qualification, is described in the following sections.

3.4   ITk Strip Tracker

Constraints provided by the HL-LHC schedule [Fig.3-2] require the ITk design to have the capability of rapid installation and later access, which mitigates the need to work within the highly activated environment found close to the interaction point. During 2006, two clear concepts evolved for a new strip tracker design or Barrel replacement. The "Stave" and alternative "Super Module" both could meet the design requirements, however the sheer cost of construction required only one solution be investigated.
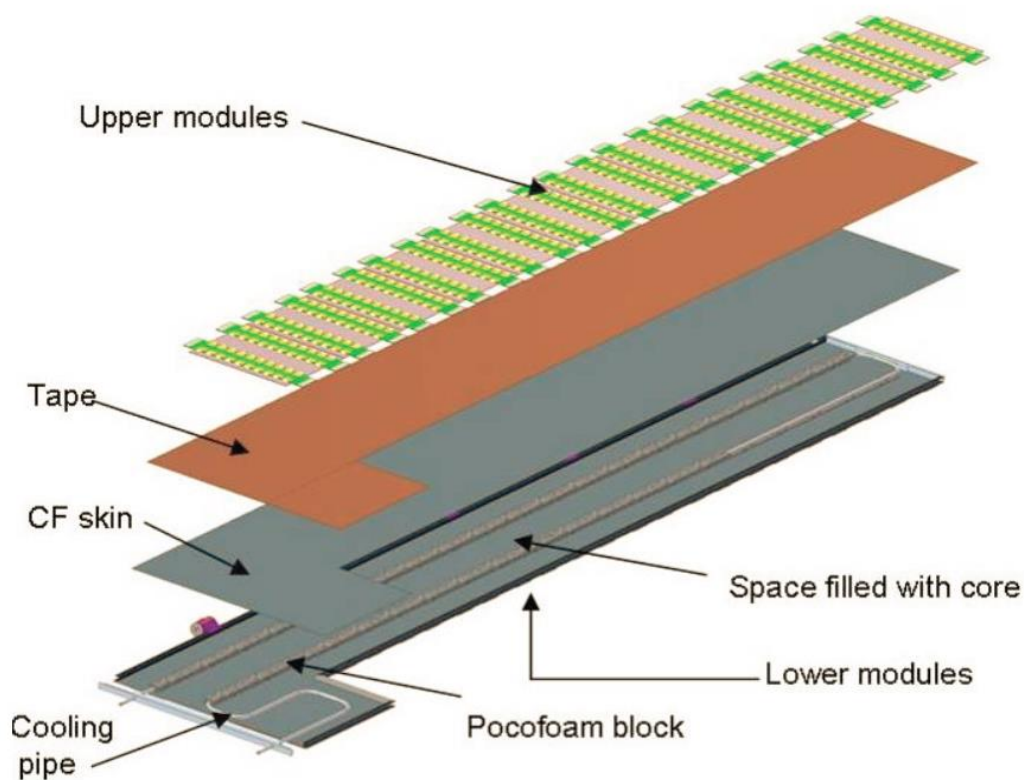
Figure 3-4   3D Rendering of the ATLAS Upgrade Stave Concept 2006 [59]

The ATLAS Upgrade Review of the Module Integration, held on 5th June, evaluating these new detector concepts summarised that the Stave solution with CO_2 cooling is expected to have less material per layer if direct gluing of the hybrid is viable, and is expected to meet the required thermal specifications. Prototype Stave designs 07, 08 and 09, based on the ABC readout chip power consumption of 0.25W per chip, were required to remove around 250W to 300W of heat from the $100mm^2$ silicon sensors.

The requirements of sensor modularity (lower cost) combined with considerations of services (powering, cooling and readout) and important constraints in space and production time drove the decision to adopt the stave solution as a baseline [Fig.3-4] [A.6].

The Stave concept, which is now the final production solution for the ATLAS ITk Strip detector, builds on methodologies demonstrated in the ATALS IBL detector. Thermal stresses in rigidly bonded Staves were of great concern and required investigation. Finite Element Analysis (FEA) studies of the thermo-mechanical performance of Staves with rigidly bonded cooling tubes were analysed [60].

FEA simulations indicated that a stave object cooled from ambient temperature, using C02 cooling to -30C contracted by 0.2mm. For a positional sensitive tracking detector, this thermal contraction would render tracking at high occupancy impossible. Before silicon
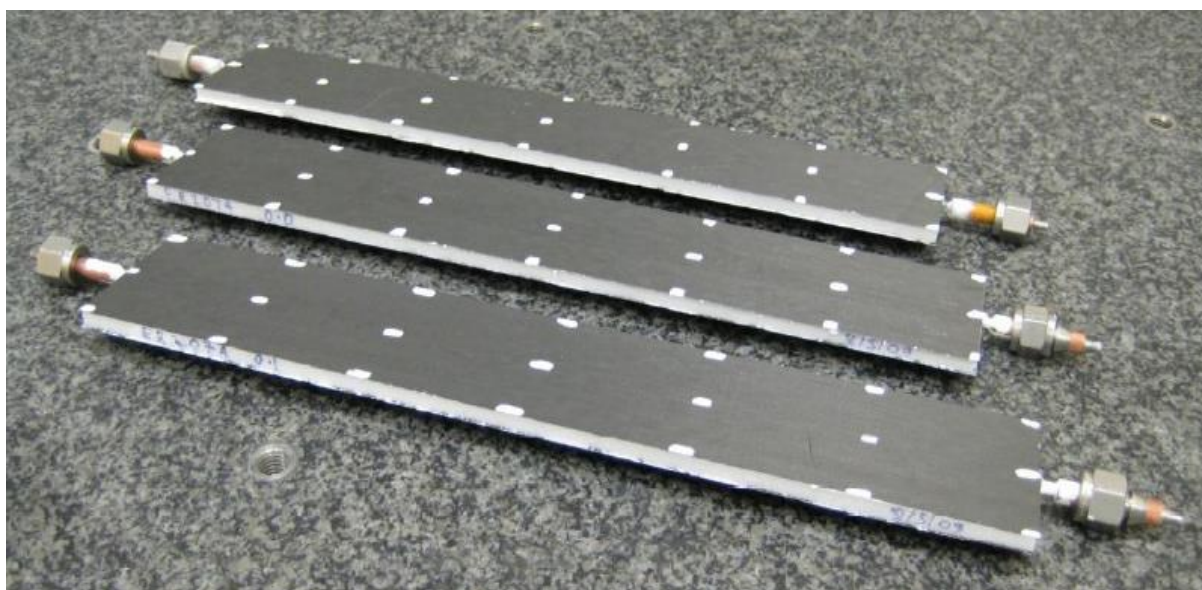
Figure 3-5   Image of 3x prototype strip Staves under adhesive evaluation [61]

sensors could be mounted to the Stave support structure the thermal expansion needed to be investigated and understood.

Expected influences to the thermo-mechanical behaviour [Fig.3-6] of a Stave are largely attributed to the coefficients of thermal expansion and the thermal conductivities of the components. Comparison of the stresses (tensile and three point bend) in the component materials gives valuable information to design safety in relation to ATLAS ITk design parameters.

The author was involved in the production of the cooling tubes required for three test prototypes manufactured and tested in Liverpool in 2009 [Fig.3-5] [A.7, A.10], used to evaluate the properties of the hard epoxy or compliant adhesive layers coupling the cooling tube to the carbon foam core of the Stave [57].

All prototypes use the baseline [57] cooling tube system of a 1/8" (3.18mm) OD (outside diameter) stainless steel tube bonded into a pair of 300x5mm^2 carbon foam (Pocofoam™) blocks in a machined groove +0.1mm larger in diameter than the tube itself. The tube and carbon foam sub-assembly is bonded between a two 300 x 55 x 0.26mm Mitsubishi K13D2U/RS-3 (0-90-0) laminate face sheets using Rohacell™ foam as a lateral in-fill.

Initial test results from the three rigidly bonded prototype Staves and comparison with existing and later FEA tests indicated that the structural integrity of a rigidly bonded thermo-mechanical stave was suitable for further investigation. Avoidance of inducing high internal stresses within the structure are made by substitution of the cooling tube material to one with a similar CTE to the stave structure. For this reason, the cooling tube material was changed

Material	Thermal expansion ppm	Thickness (mm)	Modulus N/mm^2
Composite Facing CFRP	0	0.25	60,000
Honeycomb Core	0	5	Shear L99 W50
Tube/PocoFoam Glue	8	0.06	10,000
PocoFoam	1.3	5	2,000
Skin Glue	8	0.1	10,000
Stainless Steel Tube	18	OD 3.18mm X 0.22mm wall	200,000

Figure 3-6   Expected material properties for thermo-mechanical stave [62]

from stainless steel to titanium. The author began the development of an all-new titanium cooling tube with a significant materials investigation. This work is now adopted as the ATLAS ITk baseline material for future production [57] [63]

3.5   ITk Module Research and Development

The ITk Stave modules required further R&D to achieve robustness. The author was initially involved in the R&D of direct gluing of the hybrid to silicon [64]. Trials used twelve HPK ATLAS-07 "mini" (10mm^2) silicon sensors [Fig.3-7]. Sensor characterisation tests were conducted independently at the Universities of Sheffield, Liverpool and Glasgow to determine glue effects on silicon sensor performance [A.5, A.7, A.8, A.9].

Figure 3-7   HPK Mini Silicon Sensor used in glue trials [65]

Using semi-conductor grade clean rooms for their controlled environment, comparison of a structural epoxy adhesive (Araldite 2011) was compared with an electronics grade epoxy adhesive (Fuller Epolite 5313). Araldite 2011 was used extensively in the construction of both the ATLAS and CMS detectors and was known to be radiation hard. Fermilab had previously tested the Epolite epoxy in trials for the BTeV Pixel with good results [66].

The measurements were performed with AC coupled p-in-n "mini" 10mm^2 micro-strip detectors produced by Hamamatsu Photonics (HPK) for the ATLAS Upgrade. The sensors have a strip pitch of ~250μm and strip width of ~20μm. The full depletion voltage is typically below 75V. All measurements reported here were made at a bias voltage of 1000V, chosen as an operating voltage for ATLAS Upgrade Strip Tracker.

The inter-strip capacitance was measured at a frequency of 1 MHz between a selected aluminium AC readout strip and the two adjacent strips connected together. These three strips were DC grounded while all the other Al strips remained floating. All p+ implant strips were kept at the ground potential. The "mini" sensor was mounted on a Wentworth AWP1050 semi-automatic probe station equipped with a vacuum chuck.

The electrical isolation between neighbouring strips is demonstrated by the inter-strip resistance values (R_{int}). The inter-strip resistance measurements were performed by the induced current method where three adjacent DC pads are contacted by three probes. The standard approach is to connect between a strip and the bias rail a source-meter unit (SMU) providing potential V_0 varying by a few volts around zero. This potential will sometimes be called V_{master}. Measuring the current flowing out of the SMU provides R_0. Simultaneously, a voltmeter connected between a nearest (or next) neighbour strip and the bias rail measures the potential U (U_{slave}) as a function of V_0.
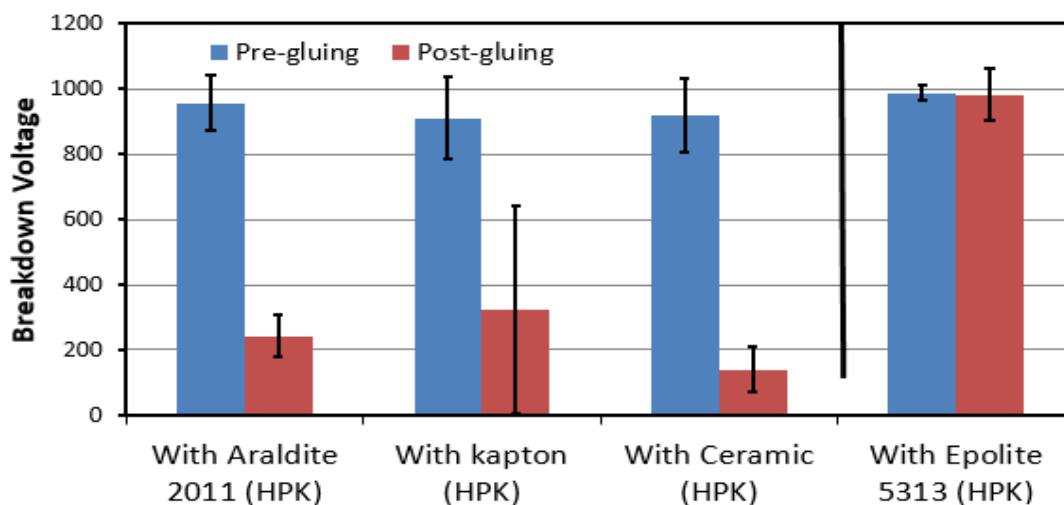
Figure 3-8   Breakdown Voltage Result Summary [67]

When potential V_0 is applied between a strip and the bias rail it induces a current flowing via R_{is} to the neighbouring strips. This current can be measured either directly or indirectly by connecting an ammeter or voltmeter parallel to the bias resistor, R_b, of the investigated strip. All 12 sensors [Fig.3-8] glued with the Araldite 2011 demonstrated decreased breakdown voltage (V_{bd}) when compared with the sensor with no glue used as a reference.
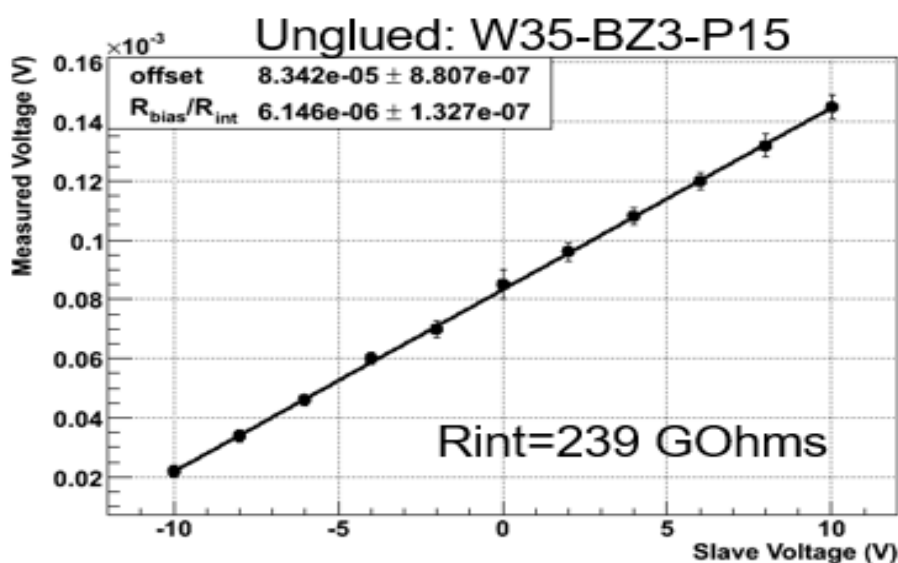
Figure 3-9   No glue, Rinterstrip Measurement at Vbias = 200V [68]

To characterise inter-strip isolation the slope $S=\mathrm{d}U/\mathrm{d}V_0$ is used because the induced potential U is not proportional to V_0 ratio. A voltage (V_{app}) was applied by a Keithley 2410 high voltage source meter instrument (SMU), to the outer strips, the current (I_{int}) was measured on the central strip. The IV characteristics were recorded as a function of time on both test series of sensors [Fig.3.9, 3.10, 3.11] [A.5].

The reverse currents (R_{int}) were measured in the sensors [Fig. 3-9, 3-10, 3-11]. The sensor bonded with Epolite [Fig. 3.11] showed little V_{bd} when tested at 1000V when compared with the control, unglued, sensors [Fig.3-9]. When compared with the R_{int} measured in the sensors bonded with Araldite 2011 [Fig 3-10], high V_{bd} was observed when tested at 1000V when compared with the control, unglued, sensors.
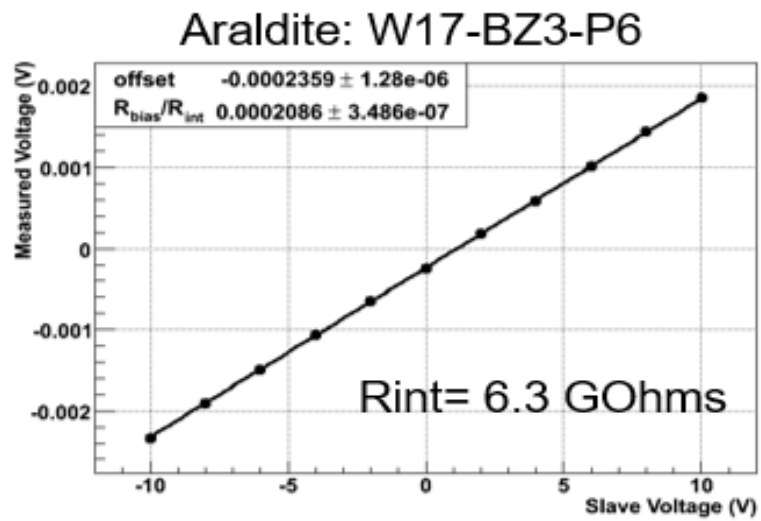
Figure 3-10   Araldite, Rinterstrip Measurment at Vbias =200V [69]
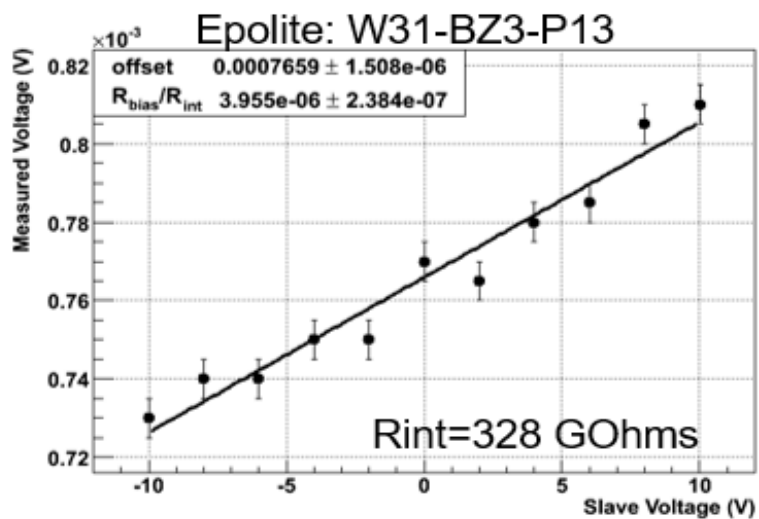
Figure 3-11   Epolite, Rinterstrip Measurement at Vbias =200V [70]

Additional reverse inter-strip (R_{is}) measurements, made by the author in the Sheffield clean rooms, confirmed the behaviour seen in the sensor breakdown voltage [Figs. 3-10, 3-11] when compared with the control sample [Fig.3-9].

Interstrip capacitance is the biggest contributor to noise in silicon detector systems, which affects tracking performance. The R_{int} decreased with bias, normal sensor function dictates that R_{int} grows or at least remains constant. At a fixed bias the R_{int} also decreased with time, electrical properties determine this is due to a current generated near the surface and reducing R_{int}. This model is also consistent with the reverse breakdown voltage behaviour shown in [Fig.3-8].

Confirmation of good sensor performance with the Epolite epoxy adhesive used to bond a silicon sensor to the control hybrid was made which allowed the author to develop a Thermo-Mechanical module within the same collaboration in 2009 [Fig.3-13]. A prototype ITk Stave design was emerging [Fig.3-12, 3-13, 3-37], following a similar design ethos as the IBL detector Stave [Fig.2-46].

This R&D would provide the final deliverables of the existing UK ATLAS Upgrade programme; a fully tested realistic thermo-mechanical prototype assembled in the UK and the first fully instrumented electrical prototype assembled as part of an international programme (STAVE09). The sensor technology work is documented in A.7, A.8,A.10, A.11]. Developments presented by the author were at the annual ATLAS-UK meeting 7-9/1/2009 [73].

The thermo-mechanical module [Fig. 3-12] utilised a special thermal hybrid [Fig.3-13] designed in Liverpool. The hybrid used a network of surface mount device (SMD) resistors to deliver the equivalent heat load to the silicon sensor allowing for thermal performance studies.
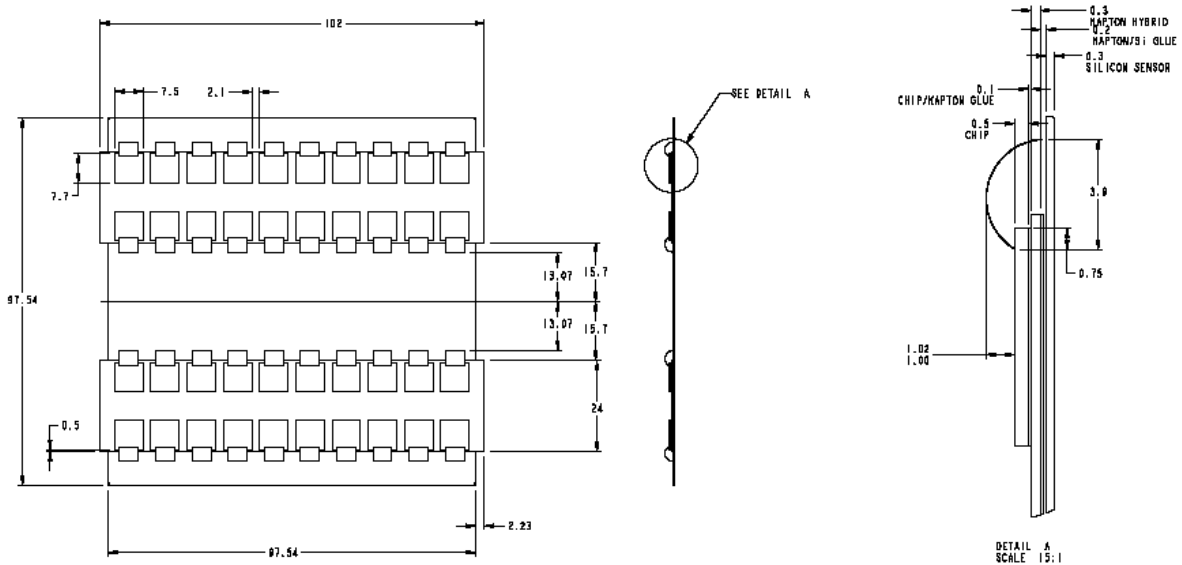
Figure 3-12   Drawing of Stave thermo-mechanical module [71]
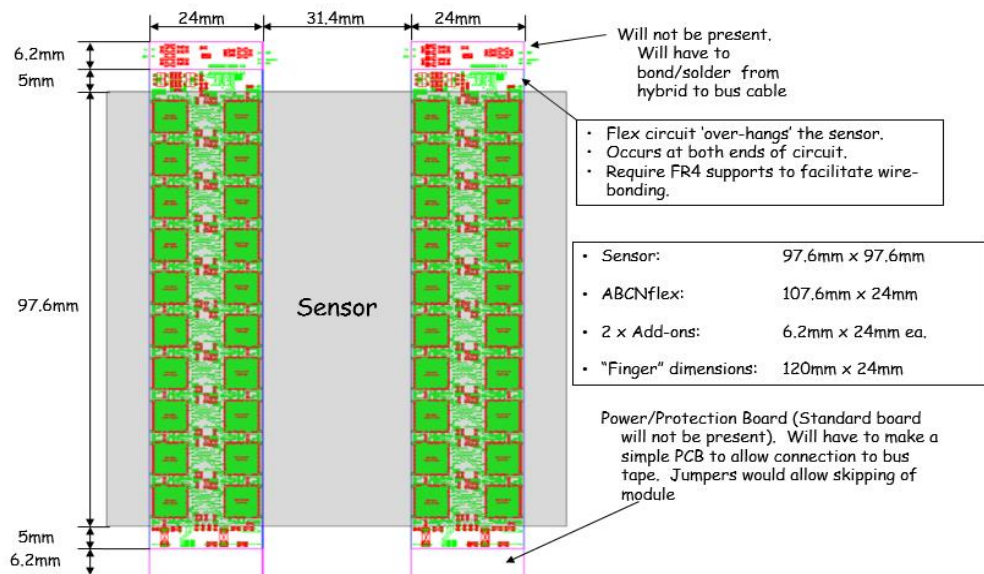
Figure 3-13   STAVE09 Thermo-mechanical Hybrid layout [74]

Working in collaboration with Glasgow, the author developed a successful glue pattern for the silicon module to bond to the hybrid. The principle was to deliver a low cost prototype for module and Stave [Fig 3.14] thermal analysis [A.6].
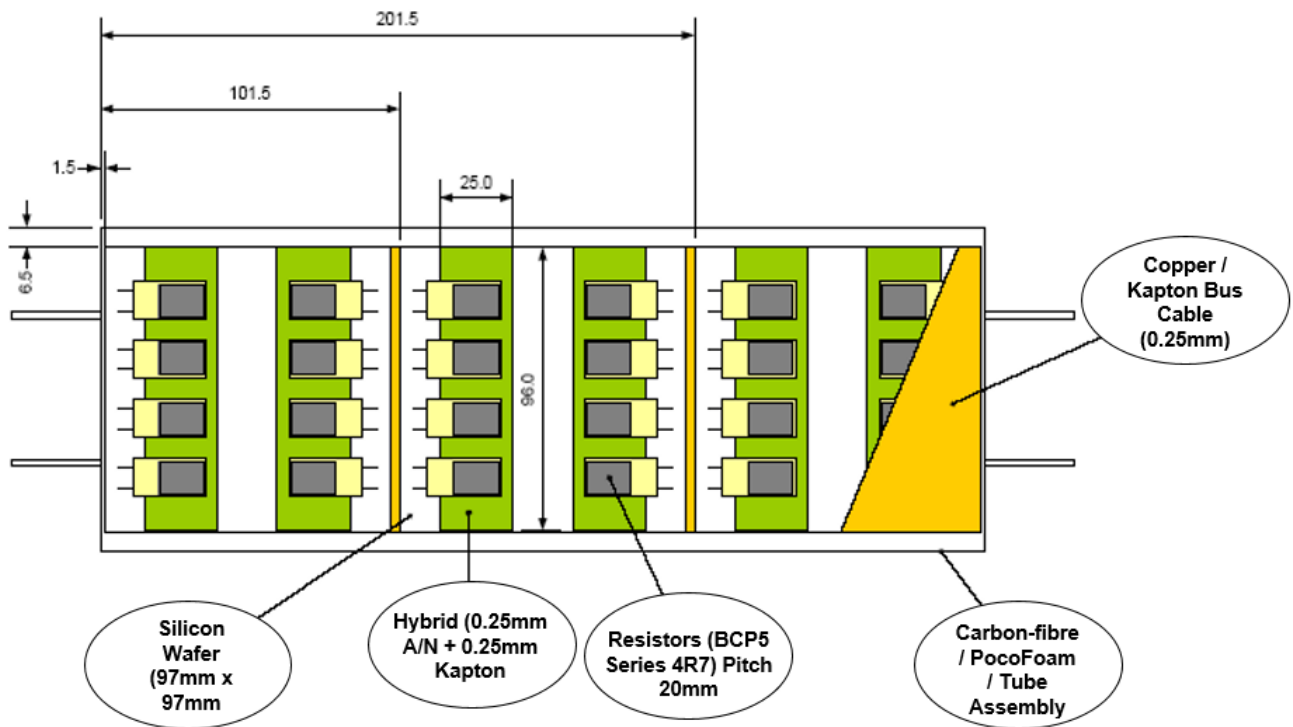
Figure 3-14   Prototype Stave module layout [72]

The final deliverable of the thermal mechanical module programme was to provide a minimum of 50 working thermal replica modules to the ATLAS-UK Work-Package 7 (WP7) group for mounting to the thermally functional prototype Stave. For the initial prototype the silicon MCC equipped hybrids [Fig.3-14] were replicated in terms of dimension, assembly method [Fig.3-17] and heat (power dissipated in Watts). An overall accuracy of construction was to be +/-0.2mm and assembled by hand for speed [A.8].
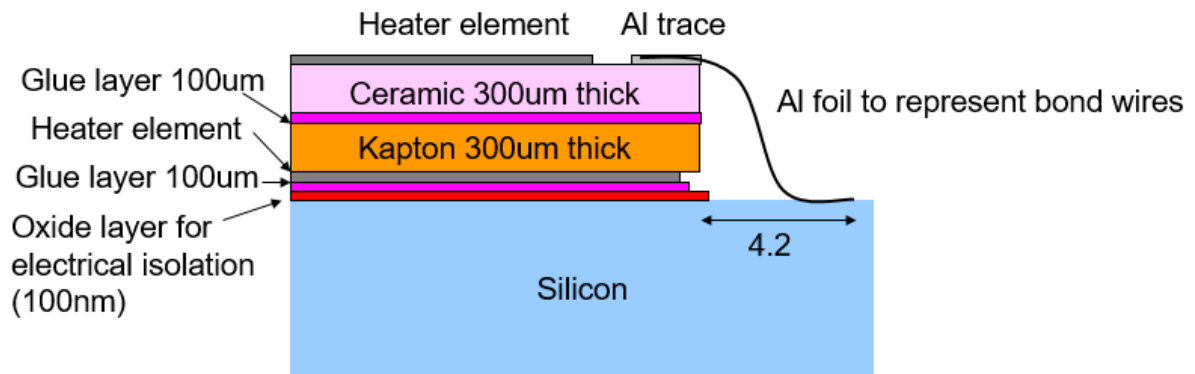
Figure 3-15   Layout of thermo-mechanical module [75]

The hybrid SMD resistors provided a sufficient heat load conducted through a representative structure [Fig.3-15, 3-16] [A.6].
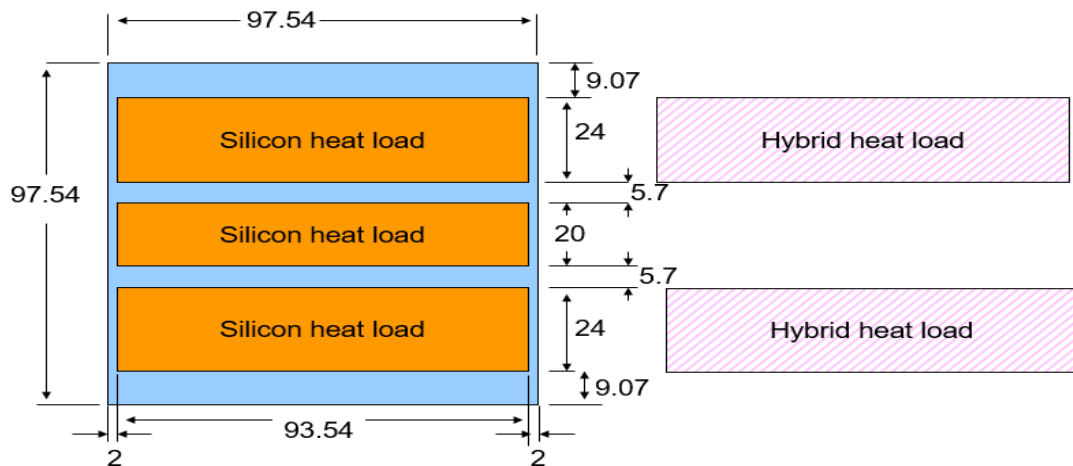
Figure 3-16   Thermal module layout 04/09 [76]

Power requirements would match that of the proposed electrical modules under development. The silicon power dissipation is in the region of 2W max / 20uA per cm^2 at 500V (-10C). Extrapolating this number to a 100mm^2 sensor, we calculated that powered at 2mA would generate 1W. Experimental testing of the thermal-mechanical module powering was from a standard laboratory power supply of 35V / 5A max [A.7].

The thermo-mechanical modules needed to be produced with the same flatness and uniformity as expected for the real silicon modules. Tooling to place the hybrid panels in a precise location with the correct height, to enable uniform glue thickness, was adapted by the author from the initial CAD designs for the Stave module tooling [Fig.3-17].
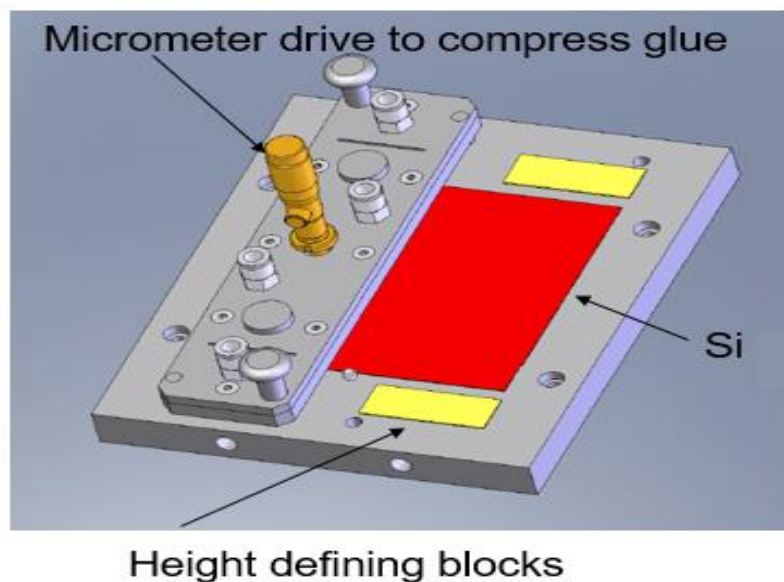
Figure 3-17   STAVE09 Module Construction Tooling [77]

The author located secondary silicon suppliers and began fabrication of the bare non-electrically operative sensor with dimensions of 100mm2 x 300µm [Fig.3-18]. This type 100 silicon sourced from the Ukraine was cleaved into wafers from standard 6" diameter silicon. To achieve a replica of the electrical module heat load a resistive thin film coating of 30 Ohms (<25µm Ti Nitride) was provided by manufacturer and the wafer was polished to achieve an identical sub-micron surface finish found on the ITk sensors.
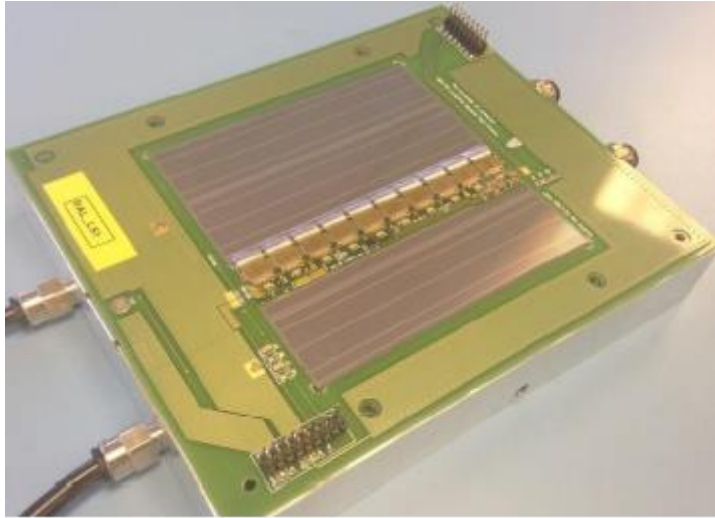
Figure 3-18   Image of thermo-mechanical module [78]

The thermo-mechanical module programme allowed for the successful characterisation of module temperatures for a range of module powers, and a range of active modules. Performance of the first and last modules on the stave could now be tested, providing information to both the sensor and hybrid designers but also to the cooling system designers.

The programme of research and development allowed measurement of mechanical distortions due to thermal loads by the; Measure edge shapes under a range of thermal loads; Measure length changes under a range of thermal loads; Observation of the effects on the stave mounting mechanism. Verification of previous FEA (free state) static load data would be confirmed by measurement of mechanical distortions of free edges.

3.6   Silicon Sensor Radiation Performance

ATLAS ITk tracking performance will be in a high occupancy environment, this corresponds to a particle fluence or radiation dose of $10^{15} n_{eq}/cm^2$ at approximately R=300mm from the LHC beam. The prototype silicon sensors require a full evaluation to the equivalent HL-LHC fluence as radiation damage by hadronic particles (pions, protons, neutrons, etc.) creates acceptor-like energy levels in the silicon bulk region. N-type silicon transforms into p-type, and increasing the full depletion voltage (FDV) as fluence is accumulated. [79] Operation in the partially depleted state is advantageous to ATLAS because the p–n junction is always on the signal collecting side, making the sensor highly radiation tolerant.

Development of highly radiation tolerant micro strip sensors for use in ATLAS [A.8] attracts a number of challenges that are effectively design requirements. Basic semi-conductor theory applies [79], the silicon materials must use the smallest FDV possible, and ideally a FDV that is capable of increasing as a function of fluence received. The required signal strength is obtained from the operational bias voltage, and electrical field minimisation is found through optimisation of the surface structures. P-type ion concentration in the surface must be determined so the micro-discharge onset voltage exceeds the operation bias voltage leaving the n-implant strips isolated.

Radiation damage is classified as either macroscopic damage, caused by electrically active microscopic defects known as bulk damage, or surface damage, which is microscopic damage due to ionising energy loss or surface effects. Within the bulk of the semi-conductor detector, when exposed to increasing radiation, the properties of the semi-conductor can deteriorate causing increases in sensor leakage current, depletion voltage and a reduction in signal strength.

Semiconductor processing techniques and design allow the manufacture of the bulks radiation hard material, ensuring operation after irradiation and at high voltages. N-in-P type detectors are advantageous to use because no radiation induced type inversions occur, unlike p-in-n detectors which read out holes [A.6]. The n-type bulk carrier concentration decreases

with irradiation, effectively becoming p-type, experiencing type inversion and the sensors undergo rapid deterioration [A.7].

Environmental conditions within ATLAS are harsh. It is essential that the assembled module (silicon + hybrid) can withstand a service life of ten years in HL-LHC. The following description of work charts the author's involvement in the confirmation of radiation tolerance for the ATLAS-07 silicon sensors [Fig 3-17] and their development [A.6, A.7, A8, A.9]. To reduce costs, smaller 10mm^2 silicon miniature detectors are irradiated.
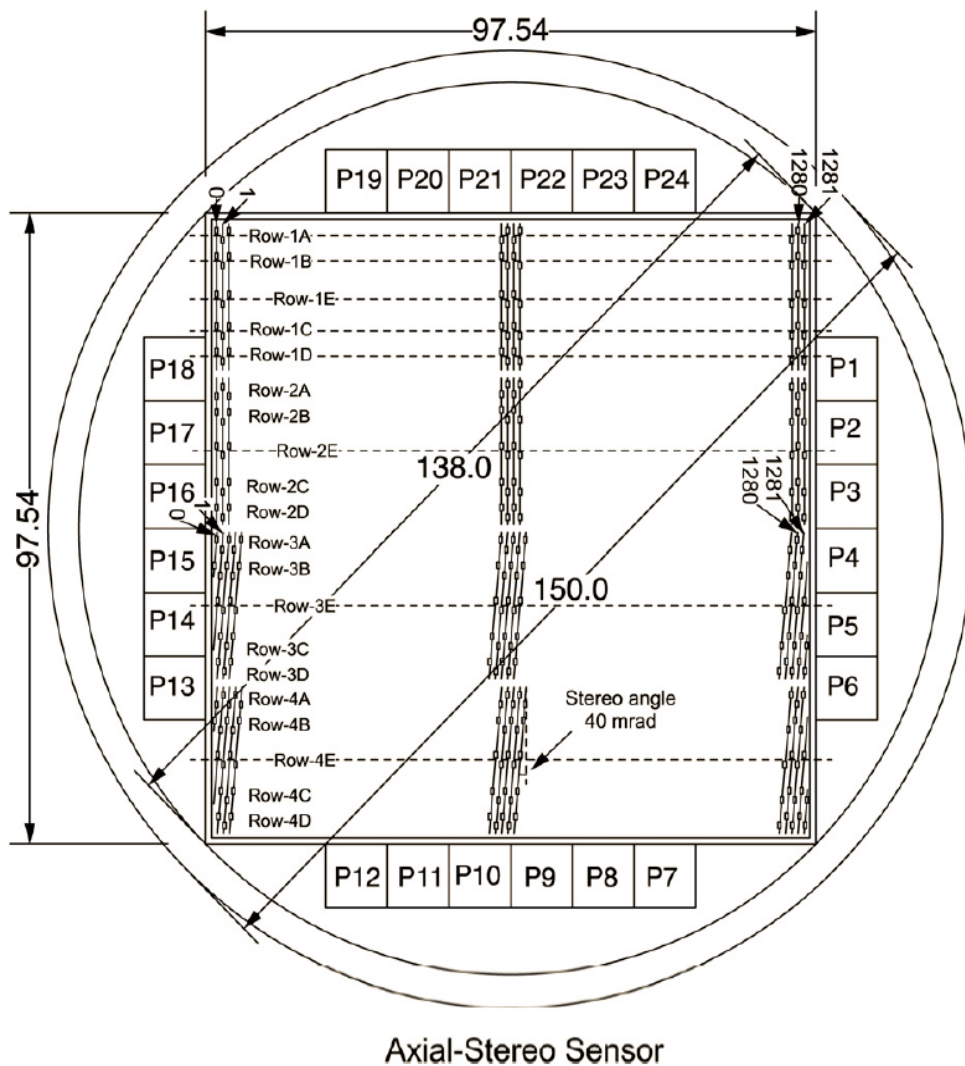
Figure 3-19   Image of the ATLAS07 silicon sensor layout [80]

Due to the high density of the active region within large scale tracking detectors, silicon material represents a low cost option when compared with other materials. [Fig.3-19] shows a 6" silicon wafer divided into active region, the central piece are a 97.5mm^2 main sensor and regions P1–P24 are the "minis" 10mm^2. Single crystal silicon wafers can have their growth technique manipulated to determine the sensor performance. Commonly used high purity crystal growth techniques are Czochralski (Cz) and Float zone (FZ). The FZ technique has been used to manufacture silicon p-type wafers for ATLAS12 devices [A.11]. Fabrication of thin wafers and silicon semiconductor devices are processed with pn-junctions creating a large depletion region. This allows the silicon to perform as a solid-state ionisation chamber thus capable of particle detection [A.7].

Sensor annealing must be avoided as temperature increase mobilises defects within an atom as loosely bound to lattice positions. Complex defects can disappear in a sink or can return to their original lattice position potentially recovering the damage from annealing. To reduce post irradiation radiation damage effects, annealing is performed for approximately 80 minutes at around 60℃. Parameterisation of the reverse annealing is best described by the Hamburg model [81].
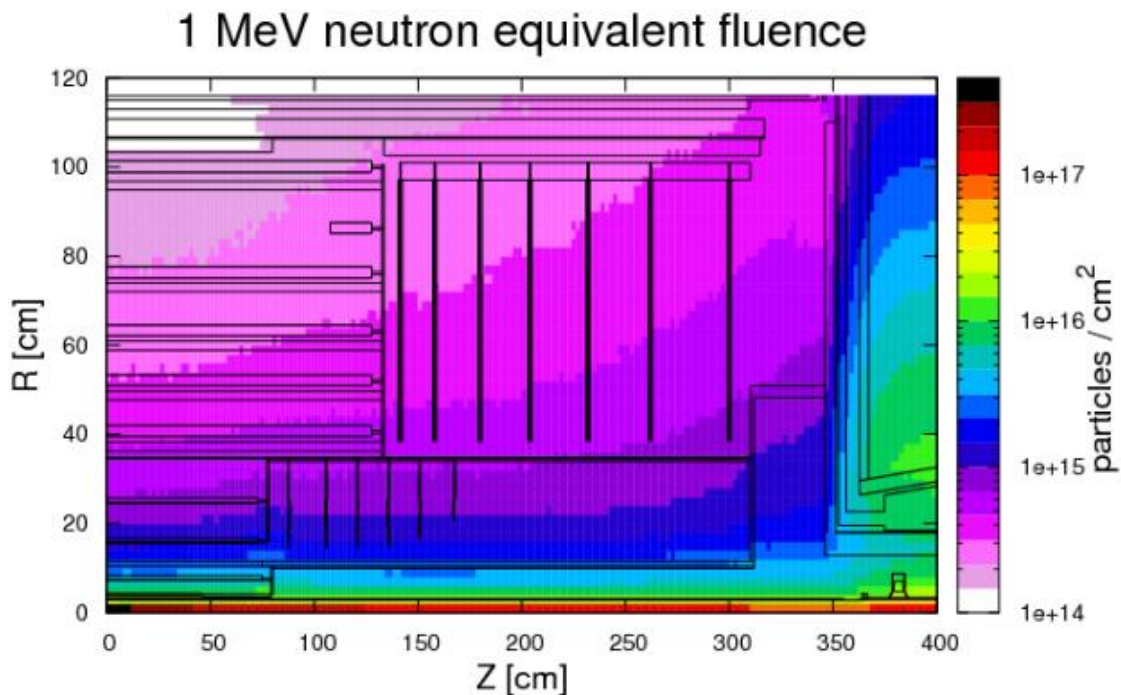
Figure 3-20   FLUKA Image of ITk LoI Layout [82]

Utilisation of Monte Carlo based radiation simulations are a time and cost saving method of predicting expected fluences. Using the baseline ITk layout as described in the ATLAS ITk LoI [Fig.3-3] a FLUKA simulation of the expected fluence can be made [Fig.3-20]. Using approximate data from the radiation simulations, reliable estimations of detector performance can be given. However true qualification of a sensor for use in a high radiation environment requires an active irradiation test programme, sometimes referred to as a "test beam" [A.10].

3.7   Sensor   Irradiation   and   Facilities Development

Using the CERN PS IRRAD facilities [Chapter 1.6], the standard proton irradiation beam with a momentum of 24 GeV/c is extracted from the PS ring into the T8 beam line in "spills" of about 5×10^{11} particles. Beam intensity is dependent on the number of spills per PS super cycle (CPS). CPS spills delivered to the irradiation facilities during high intensity periods decreases the spill from three or more to one or two when other IRRAD or CHARM experiments require the beam or when the PS serves as injector for the other accelerators of the CERN complex. [A.6, A.11]

Full sized ATLAS12 silicon detectors - Hamamatsu Photonics HPK 97.4mm² with 5120 strips, required irradiation at the CERN-PS allowing evaluation of its ten year service life performance to $10^{15}/cm^2 n_{eq}$. These ATLAS ITk large area sensors of the Strip Tracker posed an unusual dimensional problem for the conventional IRRAD T7 facility at CERN. The author's involvement in solving this challenge follows below.

The ITk 100mm^2 sensor was simply was too big for the existing IRRAD T7 environmental chambers beam aperture. Irradiated detectors required a bias of up to 500Vmax and needed significant cooling to allow operation at -25°C to control the reverse current, avoid thermal runaway and reduce the shot noise produced by the bias current (independent of incident radiation) and the discrete flow of carrier in the semiconductor. Solving the issue was to simply tilt the silicon sensors at an angle [Fig.3-21], effectively reducing the proton path from Z=300mm to Z=>10mm allowing the full sensor to have uniform irradiation.
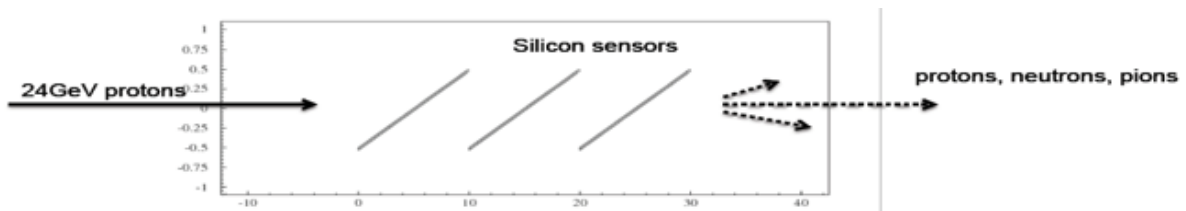
Figure 3-21   Proton path with tilted silicon sensors in CERN IRRAD T7 cold box [83]
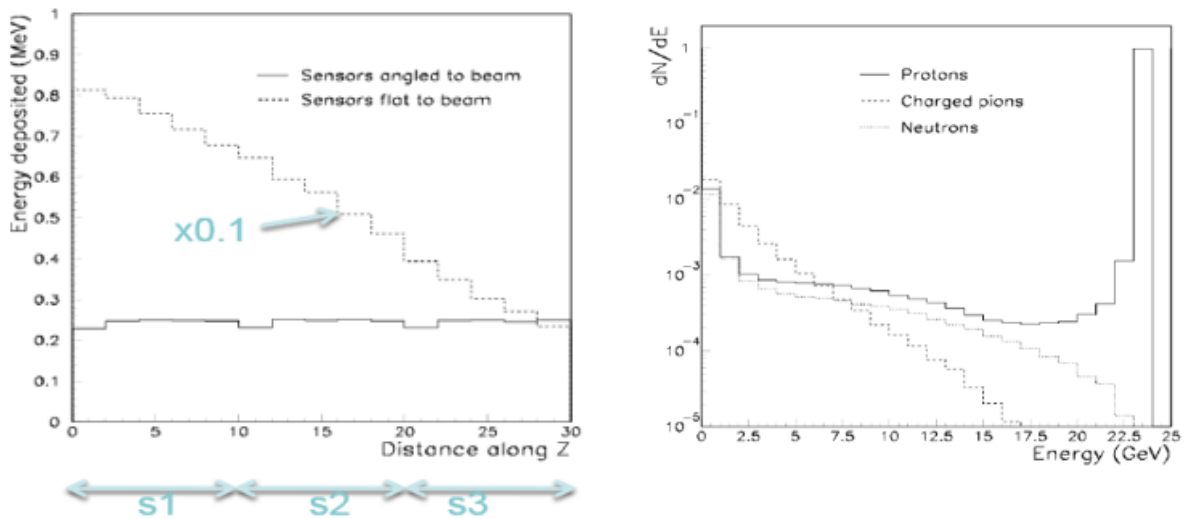
Figure 3-22   FLUKA silicon sensor mounting simulation [84]
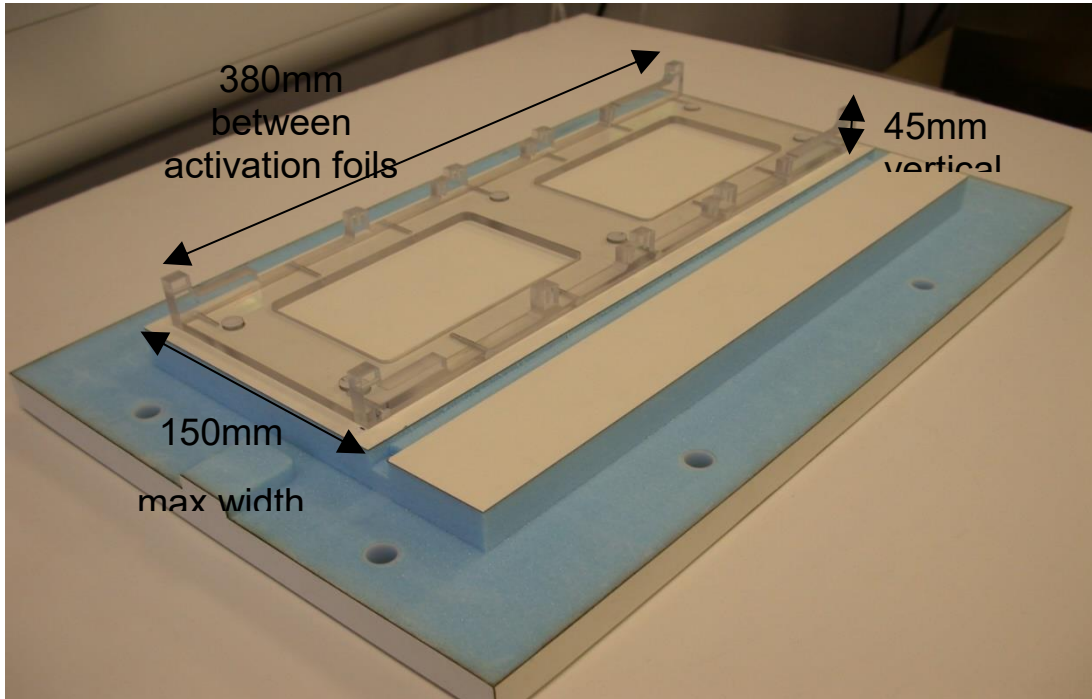
Figure 3-23   CERN IRRAD Silicon sensor mounting frame [85]

With the silicon sensors tilted secondary radiation effects could be minimised, however verification by analysis was needed. For this, a FLUKA simulation was produced [Fig.3-22]. Simulation results confirmed initial estimations (extracted from a previous proton beam profile of the 10mm^2 mini sensors flux of 1-3E13 protons/hour/cm^2) indicated that the run duration would be in the region of two weeks [A.7].

Preparations to irradiate the sensors required new mounting rails [Fig.3-23] for the silicon detector, temperature and relative humidity sensors along with all the necessary module powering and signal cables required for an "active" irradiation as opposed to just passive, non-powered sensors.
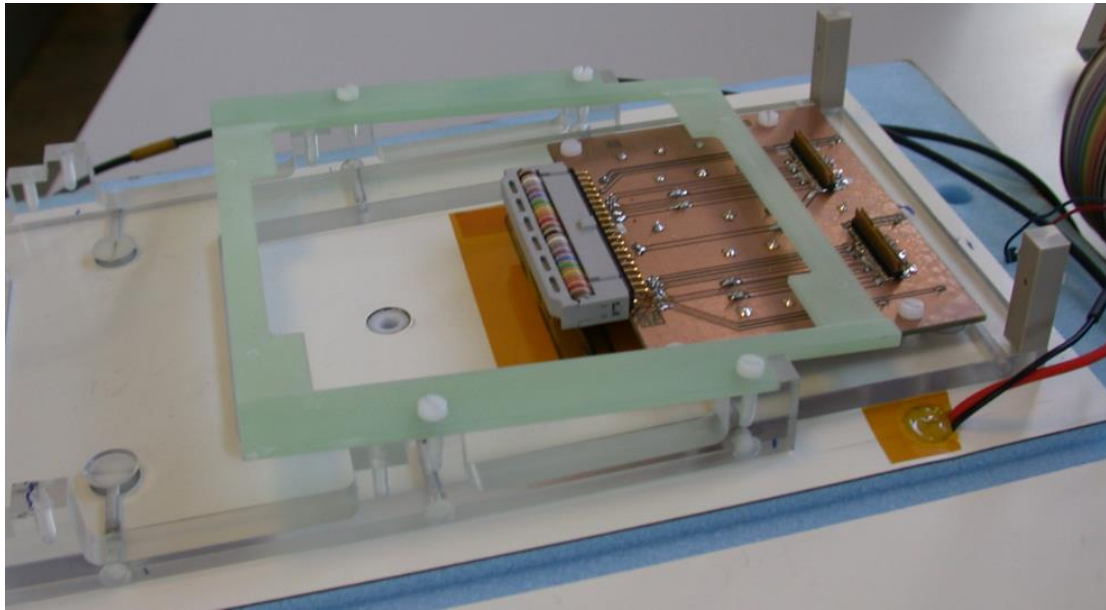
Figure 3-24   Sensor frame and module PCB mounting [86]

Downstream dosimetry was made possible by mounting a Ni activation foil in a spare sensor mount [Fig.3-24]. The hybrid equipped sensor was mounted in the upstream location allowing full measurement of dose received [Fig.3-25].
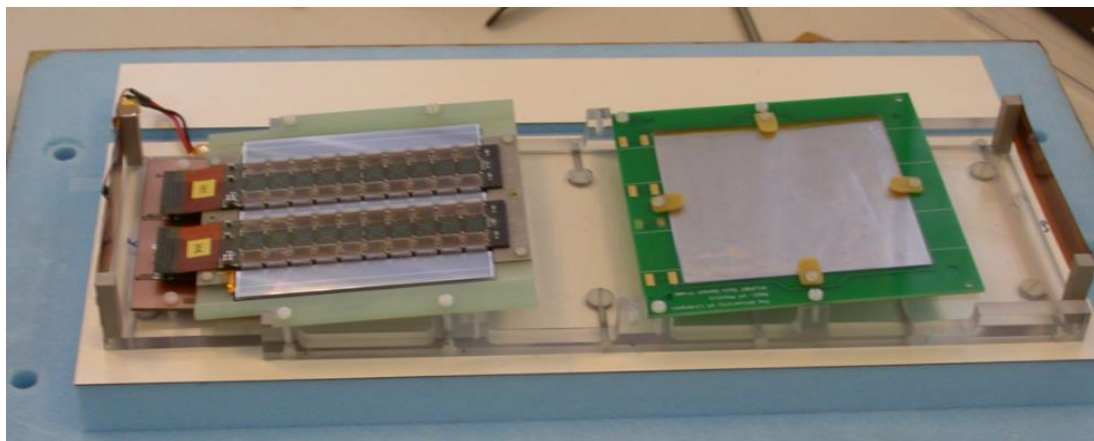
Figure 3-25   ITk Si Module mounted for irradiation [86]
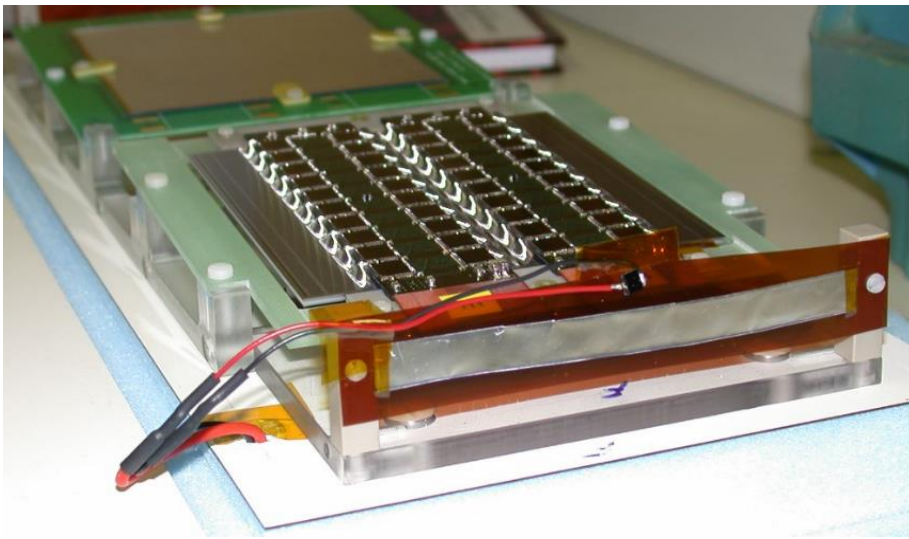
Figure 3-26   BPM mounting in front of module [87]

Further dosimetry was provided by use of a Beam Position Monitor (BPM) which would allow for beam entry and exit measurements plus position. The BPM would be mounted vertically at each end of the sensor mount rails [Fig.3-26 and 3-27].

The full sensor irradiation took place in 2010 and proved that the first ITk silicon module could withstand a total fluence of $10^{15} n_{eq}/cm^2$.
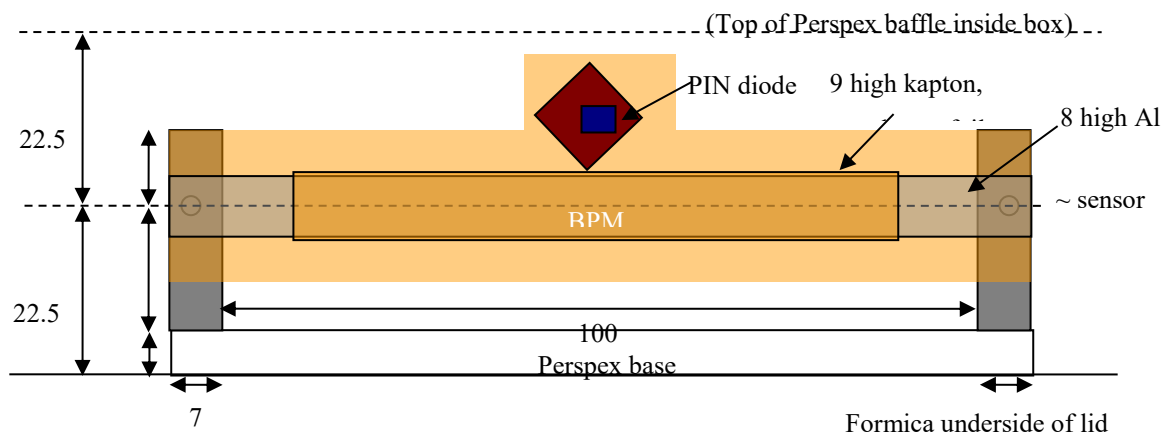
Figure 3-27   Location of dose monitor assembly at front and back of PS_ Lid_1 at 29/4/2010 [88]

3.8   UK ATLAS Irradiation Facility

Sited at Birmingham University (UK), replacement of the antiquated Radial Ridge Cyclotron with a Scanditronix MC40 variable energy cyclotron provided the ATLAS UK groups of Sheffield, Liverpool and Birmingham with a joint concept for the development of the beam line to establish a UK-ATLAS irradiation facility. Use of this modern cyclotron enabled the fast study of radiation effects on semiconductors and passive materials for UK particle physics. The goal once instrumented and tested; would allow the facility to become available to the wider Particle Physics community as a source of medium energy ion beams.

On the 21st May 2009 a meeting was held to discuss the possibility of using the Birmingham Medical Physics Scanditronix MC40 Cyclotron to irradiate passive materials and semi-conductor devices for the ATLAS experiment. The meeting between, D. Parker, J. Wilson (Birmingham), G. Casse, A. Affolder (Liverpool) & the author (Sheffield) was to establish viability of the Cyclotron. Proof of concept was to calibrate the radiation hardness factor. The following section describes the authors contribution to this new facility development [A.10, A12, A.13].

Calibration of the radiation hardness factor was by temperature measurement of the silicon sensor under a beam spot of $10mm^2$. Mounted on the silicon would be a PT100 temperature sensor to allow estimation of the upper limit of beam intensity relative to the specific constraint: Si T $<= 5°C$, the activation profiles of Ti dosimetry foils using a Bragg peak measurement [A.10, A.11].

Calibration and proof of concept was achieved on 11/09/2009 with the beam measured at 1 micro–Amp of 29MeV protons. This gave significant dose rates of radiation in the surrounding rooms, later corrected, to acceptable levels with the addition of new radiation shielding. Run-time calculations of approximate efficiency of the Cyclotron to irradiate a $100mm^2$ sensor area were made. 8 hours of running would give a fluence of $1.8x10^{15}cm$-2.

Results showed a clear requirement for increased beam current to shorten the running time however, the facility was ideal for ATLAS Upgrade irradiation purposes. [A.10, A.11]

Initial requirements to demonstrate the potential of this source of protons required the author to design and construct a Cartesian robotic scanning system to move test samples uniformly through the beam. The original 3D linier positioning stages, X & Z were controlled by two P.I Micro-positioning translation stages utilising a pizo-electric encoder system for positioning. These used a PCI interface with NI LabVIEW drivers. Movement in Y (vertical) was by means of a SKF "Telemag" telescopic pillar, driven by a stepper motor with no positional accuracy but a high payload handling capability. Directional control was via a relay switching system, a liner encoder provided position. X,Y and Z were interfaced with LabVIEW and a control PC in the adjacent control room providing the necessary computing power.

Cooling of the samples (essential to prevent annealing or heating effects from the energy of the proton beam) was from two Hakke Kryothermat 800W recirculating fluid chillers, controlled remotely with a serial *RS-232* port, again interfaced in LabVIEW.
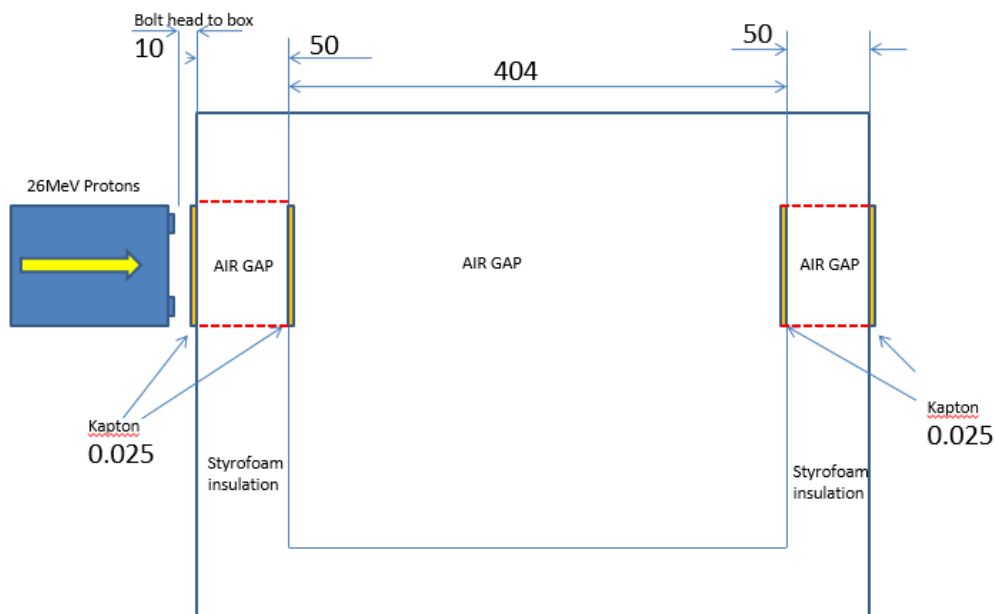
Figure 3-28   Cold Box window and air gap dimensions [89]

The local environmental control was provided by a custom thermal chamber or cold box [Fig.3-28] mounted on top of the robotic system. Heat is removed from the device under

test by means of circulating cooled Glycol through a heat exchanger. Forced convention generated by means of a fan system ducts cold air through the chamber and to the device.

Temperature and relative humidity sensors provide fine environmental control and monitoring inside the thermal chamber. Beam energy loss and scattering calculations were made to understand the beam interaction with the cold box window materials of Polyamide and acrylic [Fig.3-29, 3-30].
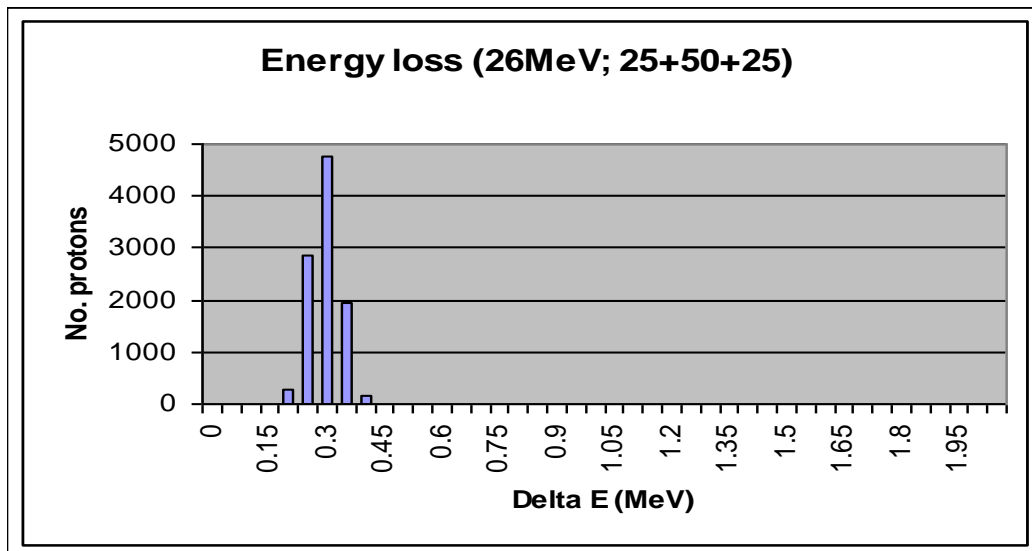
Figure 3-29   26MeV energy loss calculations for Polyamide & Acrylic in beam of cyclotron.[90]

Following signification construction work documented in [A.9] the facility was near to qualification. On the 24th November 2011 the first ATLAS ITk Optical Fibre materials irradiation began with testing of the scanning system and full exercising of the beam line at Birmingham [A.13].
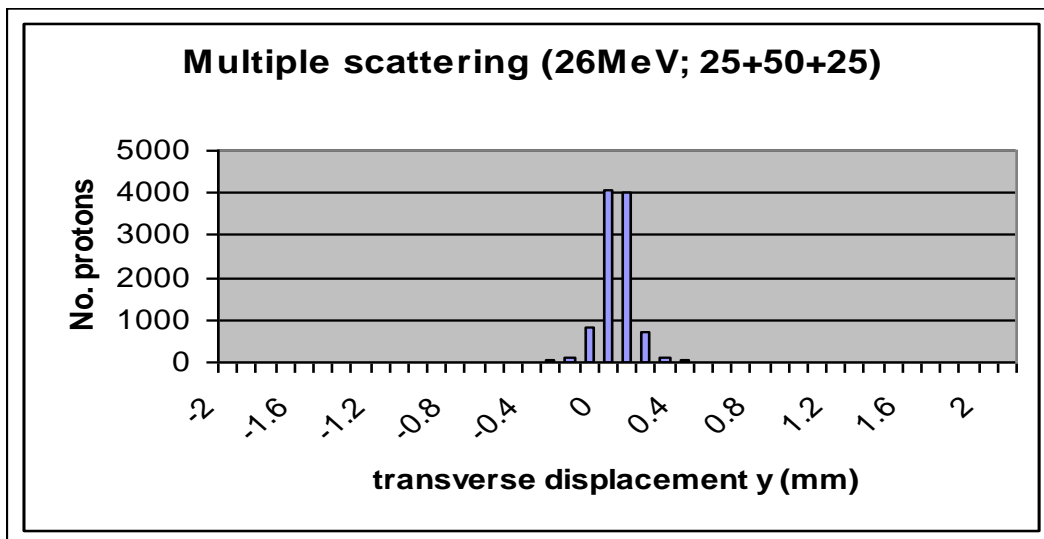
Figure 3-30   Energy scattering calculations for Polyamide and acrylic in beam of cyclotron [91]
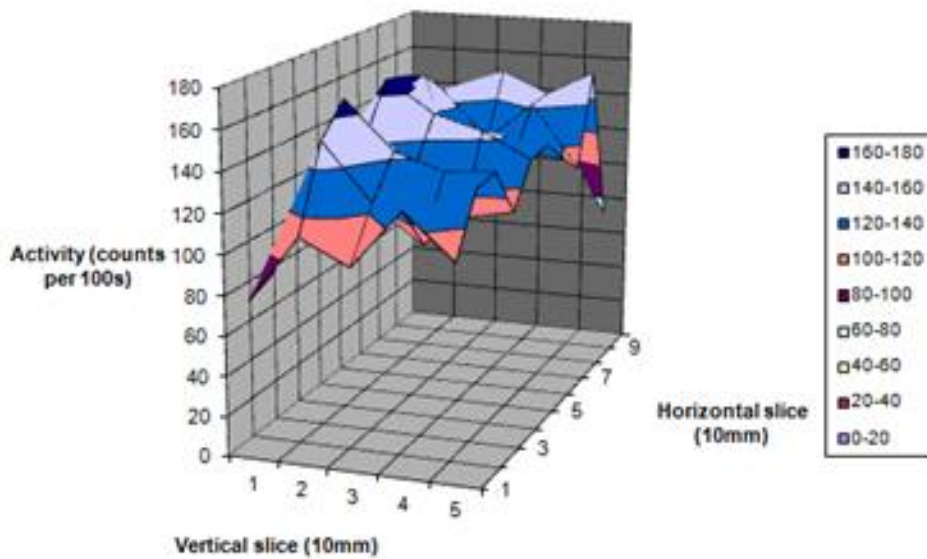
Figure 3-31   Ti activation foil uniformity measurements from Run1 [92]

Checks of the beam profile, dose rate measured with Ni activation foil and Gafchromic film tests [Fig. 3-31]. Gafchromic film is a self-developing radio-chromic film containing a colour changing dye, when exposed to ionising radiation the colour change indicates immediately the level of exposure and beam profile to be characterised. The Ni activation foil decay spectrum measurement using a hyper-pure Ge detector clearly showed [44]Sc with two

distinctly separated ɣ peaks from annihilation (511keV) and the 1.157MeV scandium decay [Fig.3-32].
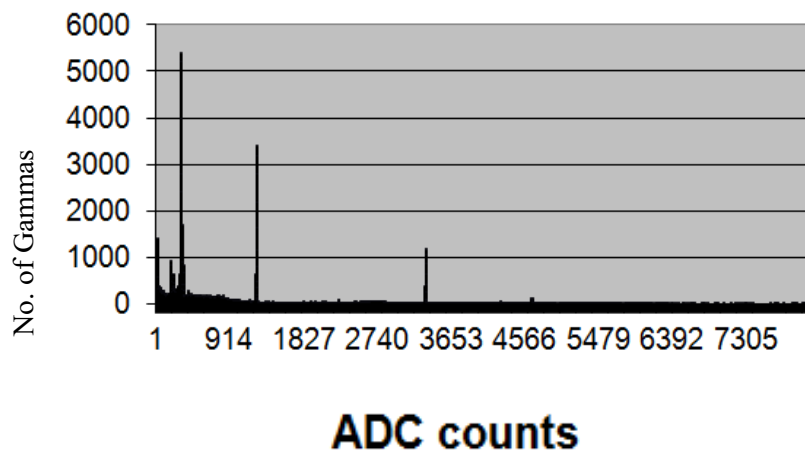
Figure 3-32   Gamma spectrum of activated foil (Ge Spectrometer) [93]

This simple calibration (roughly by doubling the exposure time in the beam) resulted in approximately twice the rate of ɣs detected. Verification of the results was by using auto-irradiation (placement of the irradiated Ti sample on a piece of Gafchromic film) which produced a clear image of the irradiated section. Results gave confidence that the dosimetry foil [Fig.3-33] information was providing a reliable crosscheck of fluence.

Optical Fibre irradiation commenced on 26/11/2011 with a beam current of 0.4uA (3-hour run to irradiate an area of 100x50mm). The Irradiation run ended at 15:45 on 28/11/2011 providing the samples with a fluence of 5x10^14 26 MeV protons which corresponds to 10^{15} (1MeV neutrons). [94]

In an exercise to reduce labour costs, commercial off the shelf technology was selected using knowledge gained from CERN as to the durability of electronics in a high radiation environment. Later operations were combined with the EU Framework 7 programme AIDA, a European Infrastructure project which allows the majority of the UK and EU P.P groups beam access or the provision of detector and passive object irradiation on a demand basis once tested and proven [95] [A.12, A.13].
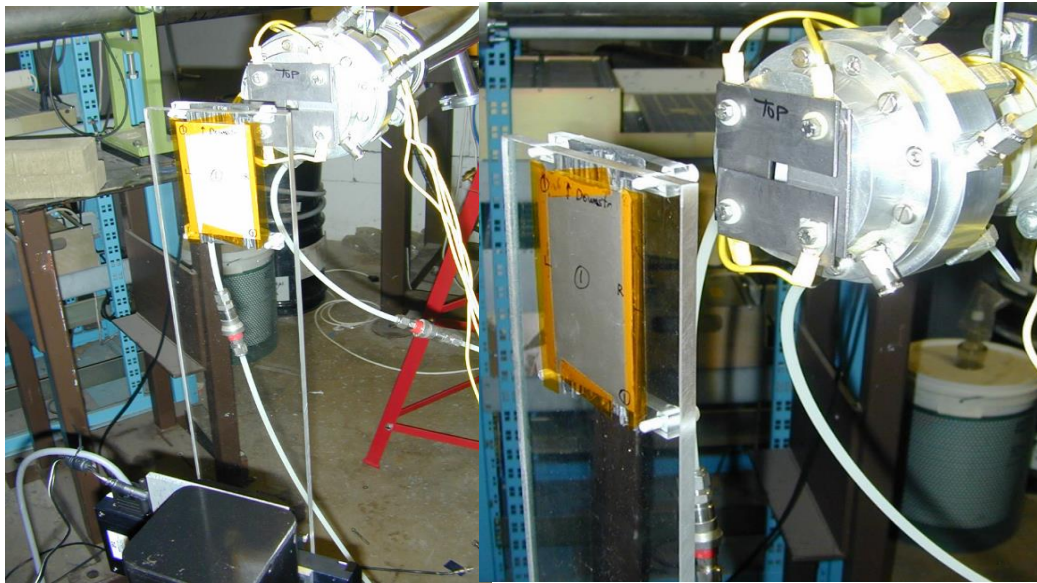
Figure 3-33   Ti Activation Foil tests of beam 24/11/2011 [96]
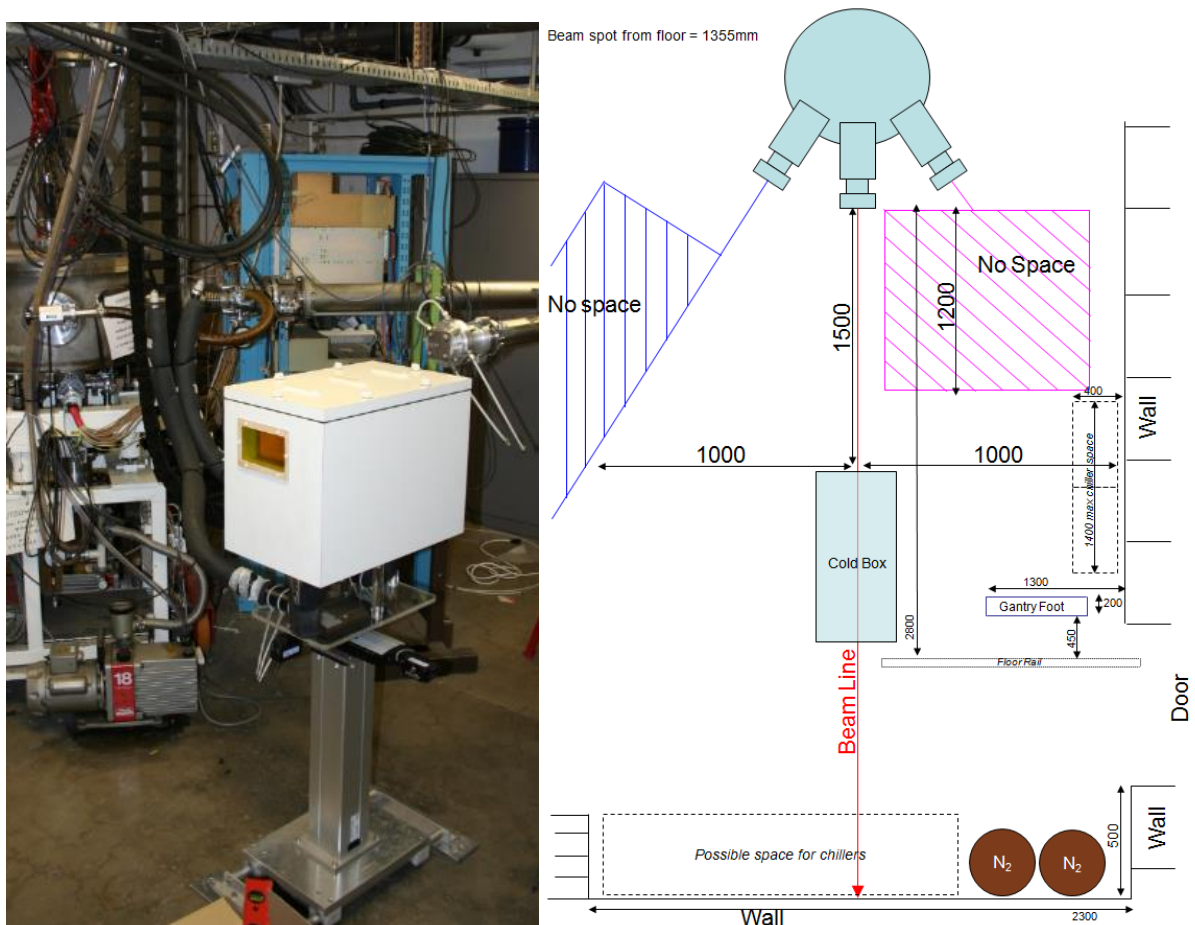
Figure 3-34   Image of Scanning Robot (L) and 2009 Low Energy Irradiation Area Layout [97]

Limitations to the maximum duration of irradiation periods at the Cyclotron required increased beam energies effectively providing a dose of very high intensity radiation to the samples. The 2009 layout [Fig.3-34] required additional shielding, a new area design [Fig.3-35] with installation of a new scanning system ready for construction in 2012 [A.12, A.13].
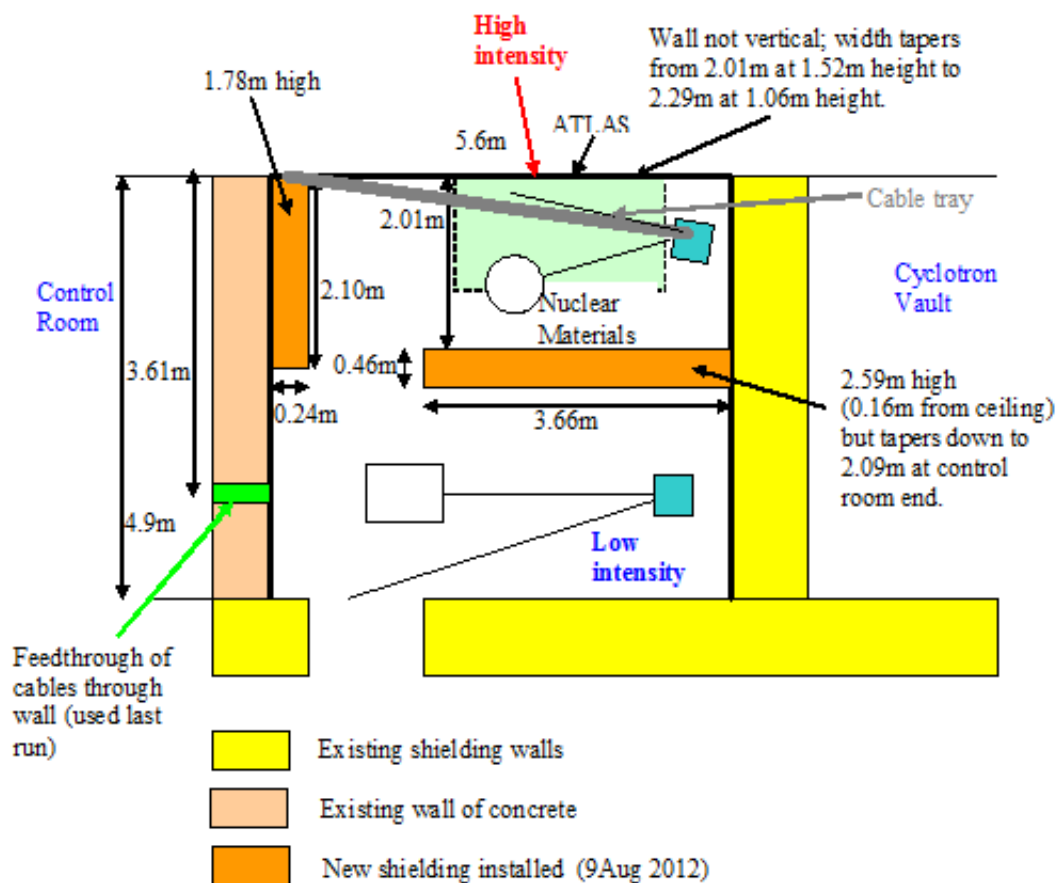
Figure 3-35   Upgraded high energy irradiation layout proposal 2012 [98]

From initial test beam results in 2010, the 26MeV proton beam at 0.4 micro amp irradiation on the optical fibres provided the opportunity for the development of the UK-ATLAS facility to operate up to 0.8 micro amps by 2012. The author made a significant contribution to the development of this new, high-energy irradiation area. Design and construction of an entirely new Cartesian Robotic Scanning System, with new high-density concrete shielding [Fig.3-35] took place. Now, thousands of sensor irradiations have taken place and in 2017 the new robotic system installed in the high energy area [Fig.3-36] is capable of remote operation from Sheffield [A.13].

Figure 3-36   Upgraded cold box and robotic scanning systems [99]

3.9   ATLAS ITk Cooling Research & Development

Building on the author's expertise obtained from the ATLAS Inner Detector cooling system and the statement "The mechanical support design is based on carbon-fibre composites and CO_2 evaporative cooling in titanium pipes [A.6]. Significant improvements in materials and assembly techniques, coupled with the reduced size cooling pipes needed by CO_2, result in a large reduction of detector mass relative to the Run 1 pixel detector." [47]

The ATLAS ITk Strip Stave design is understood, based on the LoI layout, a series of design specifications are now fixed. Stave design is described in [Section 3.3] and the silicon detectors or modules are discussed in [Section 3.4]. Heat load removal from the Stave is calculated to be 140W [66]. Maximum evaporation temperature of the future ATLAS ID cooling system is -35°C to maintain stability within the PIXEL detector [16].
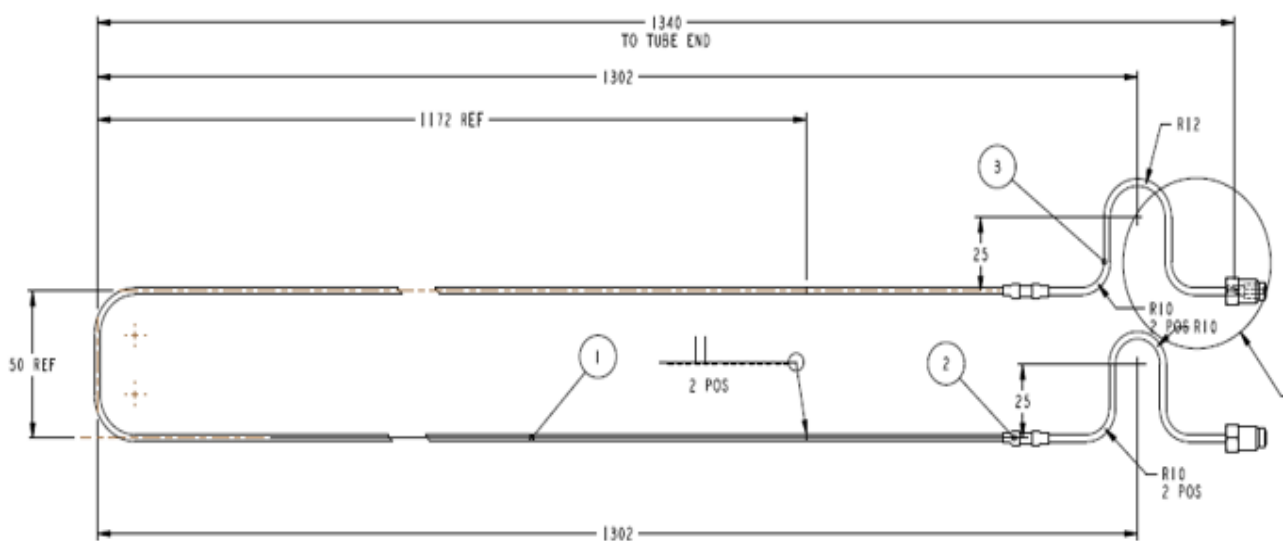
Figure 3-37   ITk Strip Stave Core Design [100]

Production efficiency and cost reduction uses one single design for the stave core, regardless of overall length or module occupancy. This dictates that the cooling tube using evaporative CO_2 cooling [Fig.3-37], must remove heat from the highest powered scenario. The author has made a considerable contribution to the materials section and joining methods now adopted as a baseline ITk technique.

Two materials of choice were studied in depth. Initially development of 316L stainless steel cooling tubes with an outer diameter (OD) of 3.175mm and a wall thickness (WT) of 0.22mm were adopted for the STAVE250 solution with high-powered modules. The advent of the ABCn (130nm chip) and the ATALS08/12 Silicon sensor based module [A.11], reduced cooling requirements considerably. Smaller diameter tubes could be used to achieve the same cooling performance of -35°C within the STAVE09 [A.8] design concept [Fig.3-38].
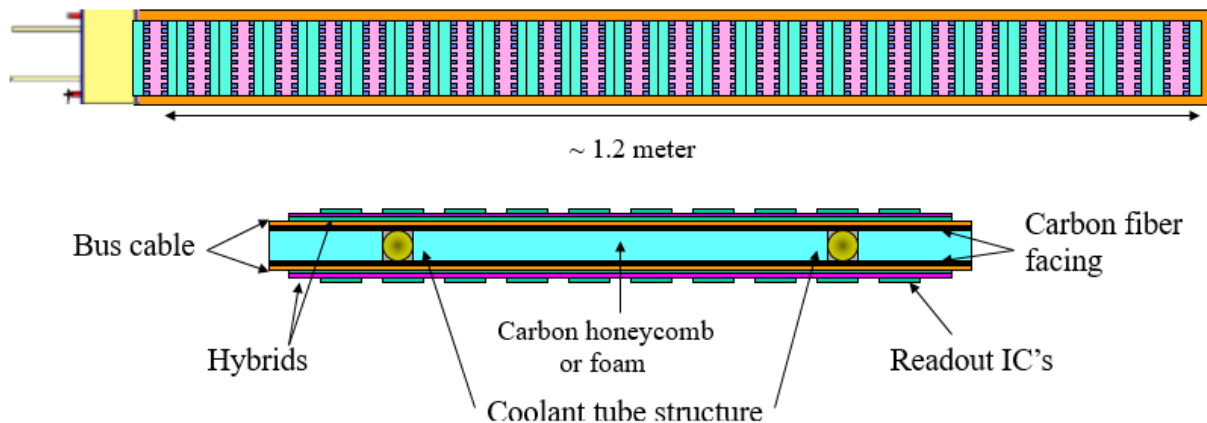
Figure 3-38   ATLAS ITk Stave09 Design [101]

Induced internal stresses from the cooling tube in a rigidly bonded Stave [Chapter 3.3] brought about the need to investigate titanium material. Dramatic advantages could be achieved with the switch to titanium. The CTE of titanium is closely matched to the Stave carbon

composite materials and has improved thermal conductivity. Tracking is improved due to the lower materials mass of titanium improving radiation length (XO) [Fig.3-39].

Using a representative calculation of 2.2mm OD x 0.14mm WT tubes, exchanging the 316L stainless steel tube with titanium improves the XO from 0.283% (316L) to 0.095% (Titanium). This dramatic difference reduces active material exiting the Strip Tracker in front of the ITk ECs, which improves tracking within the forward region.
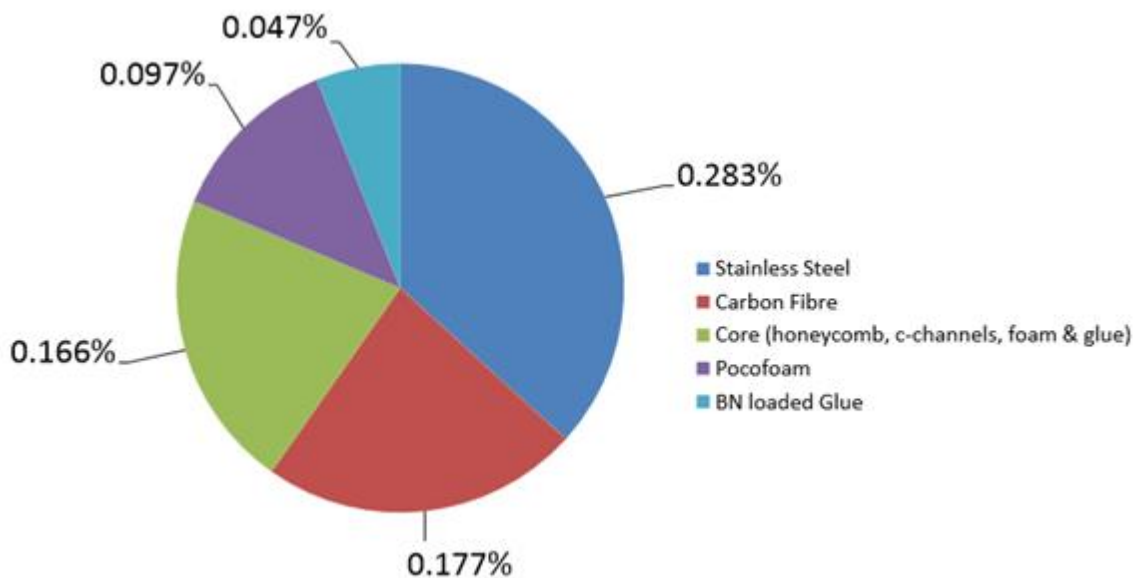
Figure 3-39   Stave core materials radiation length [102]

To cope with high pressure CO_2, and allow operation of a enclosed pressure vessel, investigation of a number of design standards were carried out [66]. These pressure handling calculations proved that with application of a safety factor (SY) of SYx1.5 using Von Mises theorem [125] (collapsing thin-wall pressure vessels) and manufacturing constraints (raw stock tube dimensions) the design of titanium tubes allowed for a much stronger tube with less material.

Joining of the cooling tubes plagued the existing ATLAS SCT ID with faults previously described in Chapter 2.8. The compression type fittings used also represented considerable mass or increase in XO. The author pioneered the development of fusion welding for the tubes, to avoid issues seen with fluxes contaminated brazed joints and incorrect joint limit and fit tolerances. Advanced gas tungsten arc welding (GTAW) or tungsten inert gas (TIG) with an orbital weld head attachment was developed for the ITk to produce a welded tube-to-tube joint in 220µm WT stainless steel tube [Fig.3-40].
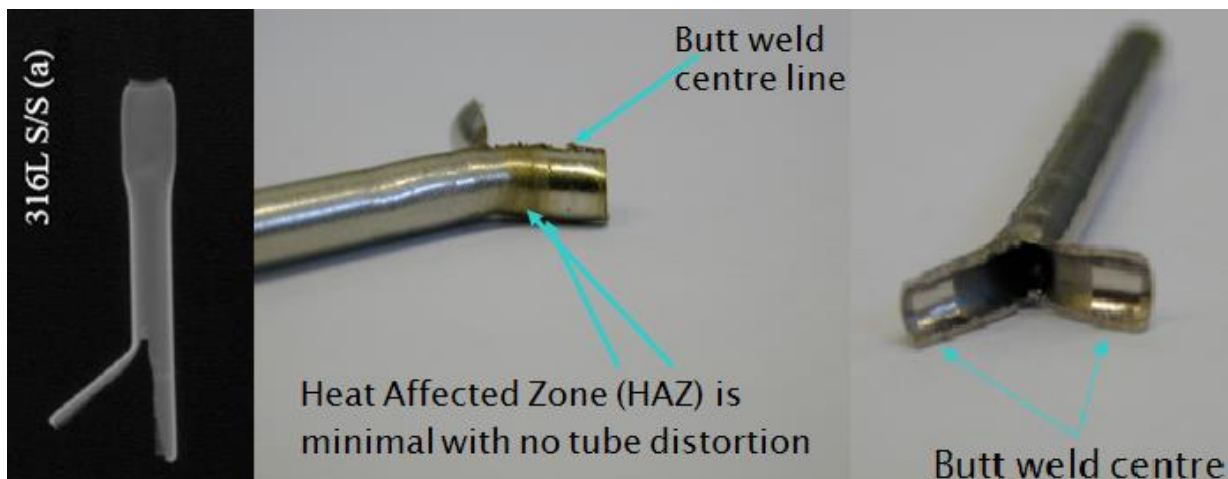
Figure 3-40   316L tube welding, X-Ray (a) and images of joint [103]

Tube-to-tube fusion welding using the TIG orbital welding process on stainless steel tubes used in the ATLAS ITk produced a highly reliable production yield with few failures. The author conducted a series of welding trials on the 3.175mm OD 316L tubes that allowed a statistically significant evaluation of the quality and robustness of the welds, including novel QA inspection and non-destructive testing methods [Fig.3-40]. Analysis by use of micro-focus CT x-ray was carried out by the author to verify if the testing methods were appropriate for use on a potential 6000 welded joints found in the ITk cooling system [Fig.3-41].
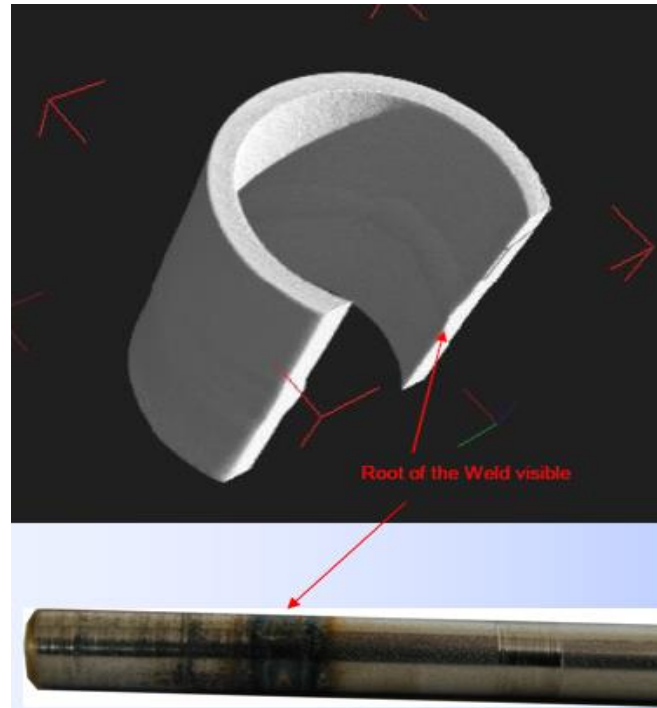
Figure 3-41   Micro-focus CT x-ray image of 316L tube-tube [104] joint.

Verification of the 316L welded joint was supported by conventional destructive testing (DT). Six tube-to-tube weld samples were longitudinally cross-sectioned, polished and etched (etchant 13a of ASTM E407). Metallographic examination was carried out using a LEICA MZ16 stereomicroscope at CERN Fig.3-41. Micro-hardness profiles across the weld bead were
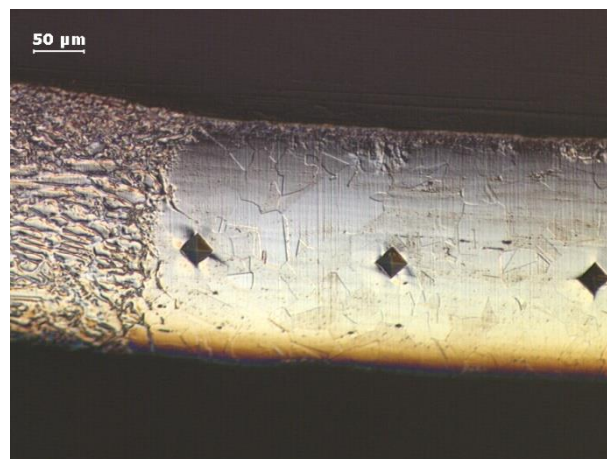
Figure 3-42   200x magnification cross sectional view of 316L weld sample [105]

checked using a WOLPERT 402 MVD micro-hardness tester [Fig.3-43]. Tensile tests were performed on a UTS tensile test machine equipped with auto-tightening grips and a 200 kN load cell [Fig.3-44].

Sample 137	Base material			HAZ			Weld			HAZ			Base material		
	175	170	191	181	204	179	198	201	185	163	172	176	166	167	169
Sample 428	Base material			HAZ			Weld			HAZ			Base material		
	195	192	212	191	191	205	207	215	231	219	212	210	234	217	217
Sample 968	Base material			HAZ			Weld			HAZ			Base material		
	207	192	189	209	204	190	217	210	193	216	197	195	210	196	203

Figure 3-43   Micro-hardness profiles of 316L tube weld sample [106]

Results of the destructive testing demonstrated through micro-optical observations neither structural nor geometrical imperfections could be detected [Fig.3-41]. The micro-hardness tests (according to NF EN 1043-2) produced a maximum value in the weld bead of 231 $HV_{0.1}$ [Fig.3-43]. Micro-hardness profiles are obtained by observation of the sample material's ability to resist plastic deformation from the base, or parent material.
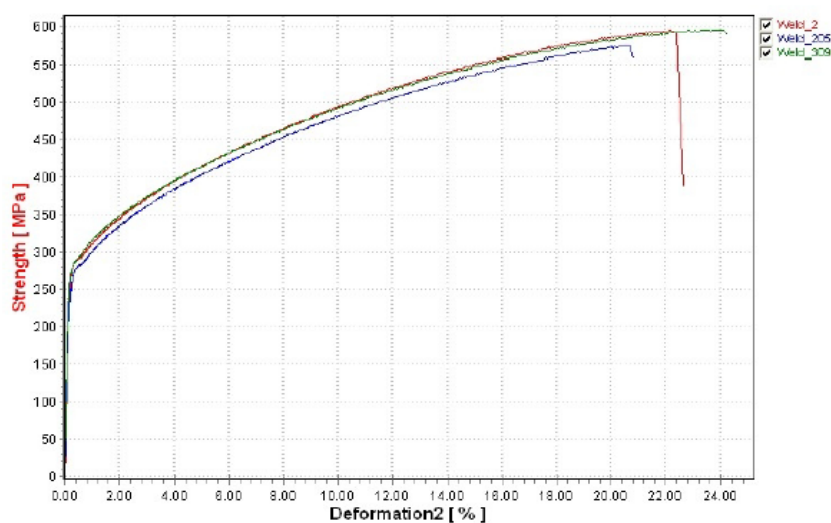
Figure 3-44   Tensile Test results of 316L tube sample elongation [107]

For the tensile tests [Fig.3-44], all samples broke in the weld. The average Ultimate Tensile Strength (UTS) is 588 ± 11 MPa. According to NF EN 288-3, the UTS should not be less than the minimum specified value of the parent metal. The minimum UTS value for AISI 316L pipes as stated in ASTM A312 is 485 MPa [A.8].

Comparison with the ATLAS tube results with previous welding to a tube with OD 4 mm x 0.5 mm WT used by the AMS experiment were consistent [108] with similar results at around 550-600 MPa for UTS. Due to the thin wall of the tube, it was not possible to use an extensometer to determine RP0.2 so an estimation was made according to elastic-plastic transition on the curve around 300 MPa. Elongation determined with measurement of the whole sample before and after test was about 20 %. Failure occurred either in the weld or in the HAZ (Heat Affected Zone). Results obtained for our pipes are very similar to these ones.

The conclusion made by the author was that the parent and weld material hardness and strength is not too hard or brittle. The weld bead grain is correct when compared to other 316L welds (grain size). The adjacent grains in the tube look marginally bigger, (assumed not through the heat generated by welding). Enough grains of material were present through the cross section not to have potential leak path issues via grain boundaries. Both destructive and non-destructive test data supported the process of TIG tube to tube welding of 316L pipes.

The exchange of the cooling tube material to titanium required a new approach as the conventional TIG orbital welding equipment could not join 125μm WT commercially pure Grade 2 titanium (CP2Ti) without distortion or significant damage [Fig.3-45]. This work, funded by the STFC Industrial Partnerships Scheme, was carried out in conjunction with industry and has now led to several aerospace applications, [111,112,113] discussed in Chapter 4.3.

Figure 3-45   ITk Stave CP2Ti welded tube joint 3.175mm OD x 220µm WT [109]

In depth investigations were required to be made by the author to determine how to minimise the titanium material in the ITk Stave. The 220µm wall thickness of the tube was, at the time, too thick even though significant materials reduction found from the use of CP2Ti. Problems with initial tube welding were mainly due to the thick layer of oxide found on the tube, which occurred during the manufacturing process [Fig. 3-46].
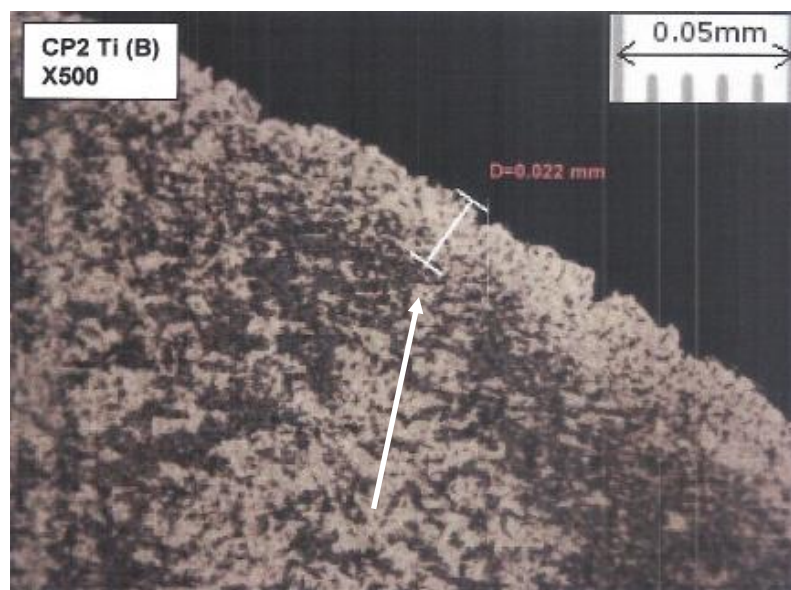
Figure 3-46   500x magnification image of CP2 Ti Oxide layer [110]

A series of chemical etching trials [Fig.3-47] were made to attempt to remove this oxide to ensure a robust welding process. The titanium oxide creates flaws in the welded joint through sulphur, carbon and other impurities.

Figure 3-47   HF etching trial Ti tube sample results [114]

Following the success with a diluted HN03: HF solution, a commercially available equivalent etchant was obtained to "pickle" the tubes. This pickling was adopted by the tube manufacturer and used on ITk production tubes with a thorough cleaning process [Fig.3-48]. Oxide free welding would now be possible for the ITk. This 2.275mm OD x 215μm CP2Ti tube, developed by the author, was used for the ATALS IBL Stave cooling system detailed in Chapter 2.10.
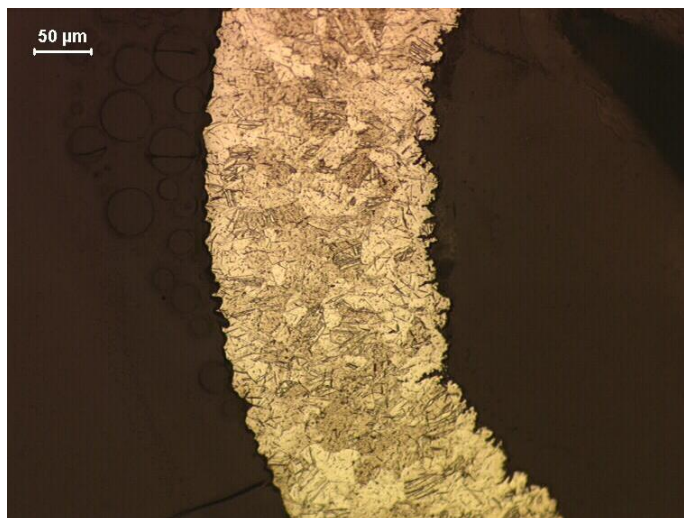
Figure 3-48   50um image of CP2 Ti tube end view [115]

Grounding and shielding is a major consideration for ITk cooling system design. The sensitivity of the detector electronics is such that pick up and sources of external noise should be minimised as discussed in Chapter 2.5 [8]. The ITk faraday cage requires a screen to absorb the cable ground loops with minimal EMI attenuation. The ITk Strip Staves receive a single point referencing through the services cable shield and the ITk inner power cables have an existing shield [Fig.3-49].
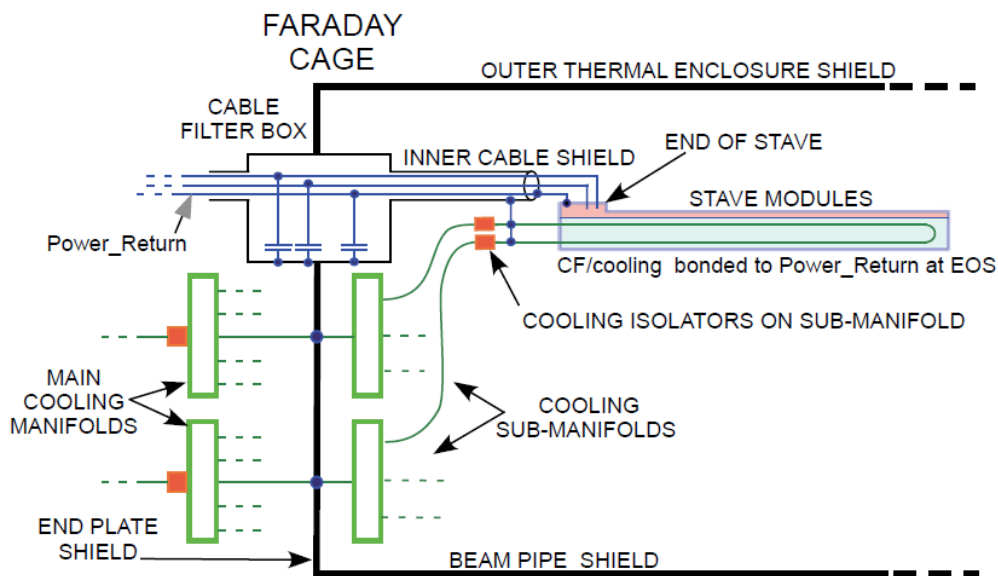
Figure 3-49   One quarter section diagram of ITk Faraday Cage [116]

The Stave core carbon composite structure with embedded cooling tubes requires referencing to the inner cable shield. Isolators will be required to allow the Faraday cage to have isolation except for the single ground cable to earth. Secondary isolators are required to allow the Stave cooling circuit to reference to ground by the Stave cable shield. [8]

The author was required to develop a robust electrical isolator for the ITk Stave cooling tubes. Using the electrical isolator from the IBL as a base example [Fig.3-50], he developed an all titanium version to reduce detector XO. The principle was to make a simplified item using brazed ceramic.
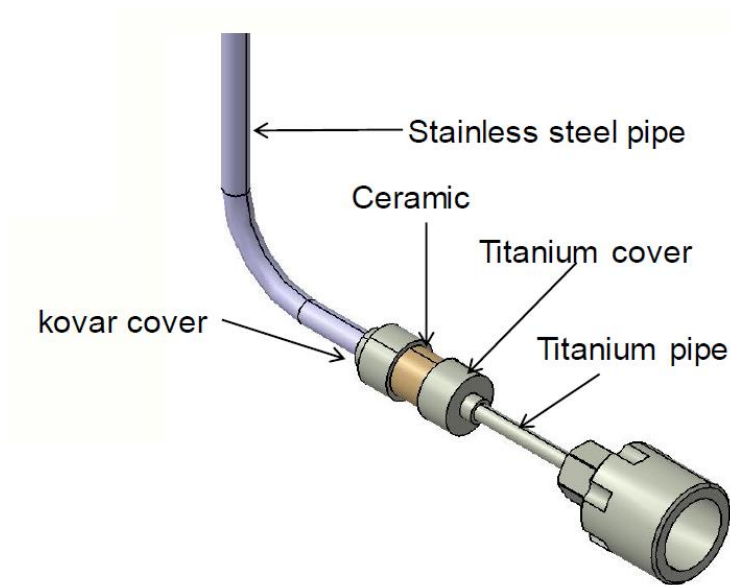
Figure 3-50   Diagram of IBL cooling tube electrical isolator [117]

R&D into ceramic materials brazed to ceramic by the author resulted in braze alloy selection criteria of; suitable ductility for avoidance of stress failure during the cooling cycle combined with a low as possible solidus temperature which will minimise ΔT where shrinkage is likely occur [118]. In this case titanium material has a coefficient of thermal expansion which is close to that of alumina therefore the brazing process is likely to be successful.

Known ceramics were tested with the vacuum brazing process with three typical braze alloys or fillers; silver-copper-palladium and silver-copper eutectic, the latter was selected due to ease of repetition and the lower cost of Cu/Ag eutectic alloy. This was demonstrated to work with the ITk CP2 Ti tube mated with a Macor machinable glass ceramic. A prototype Macor ceramic-to-titanium seal was produced [Fig.3-51 & 3-52] and tested to achieve a joint shear strength of 8,000-psi then vacuum leak checked to 10^{12} mBar/LS.
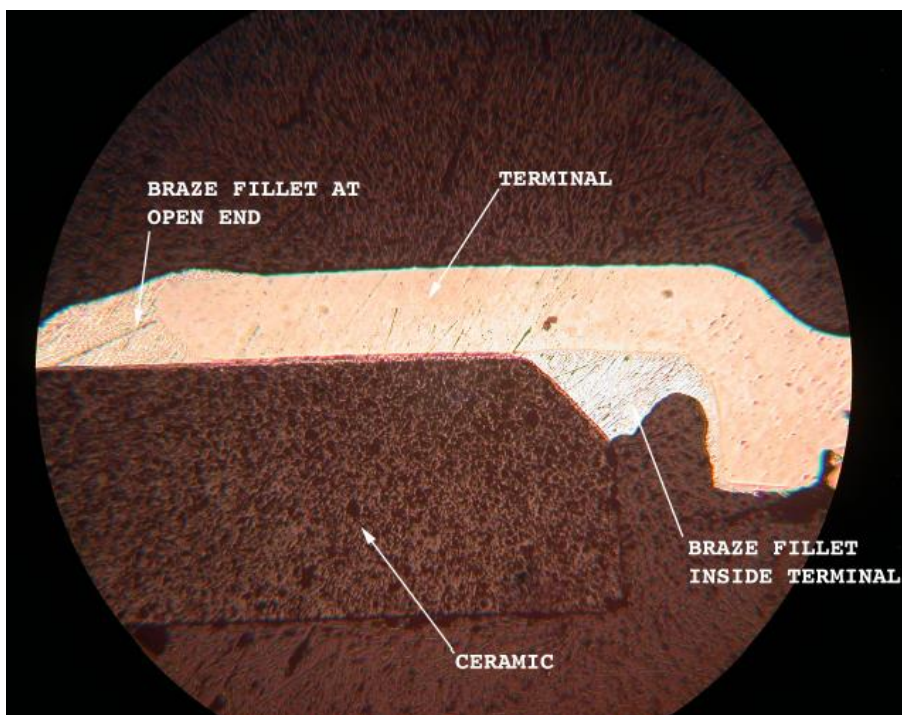
Figure 3-51   500x magnification Cp2 Ti brazed with VBC CuSil alloy to Macor [119]

The ITk Stave cooling system development nears completion; the first production Stave tooling has been produced with electrical isolators [Fig.3-53], to enable the manufacture of a high volume of cooling circuits for both the ITk Strip and Forward PIXEL detector [Fig. 3-54]. A great deal of metallurgical understanding was required to allow titanium use in the ITk tracker cooling system [Fig.3-55].

Figure 3-52   Image of prototype ITk Strip electrical isolator [97]
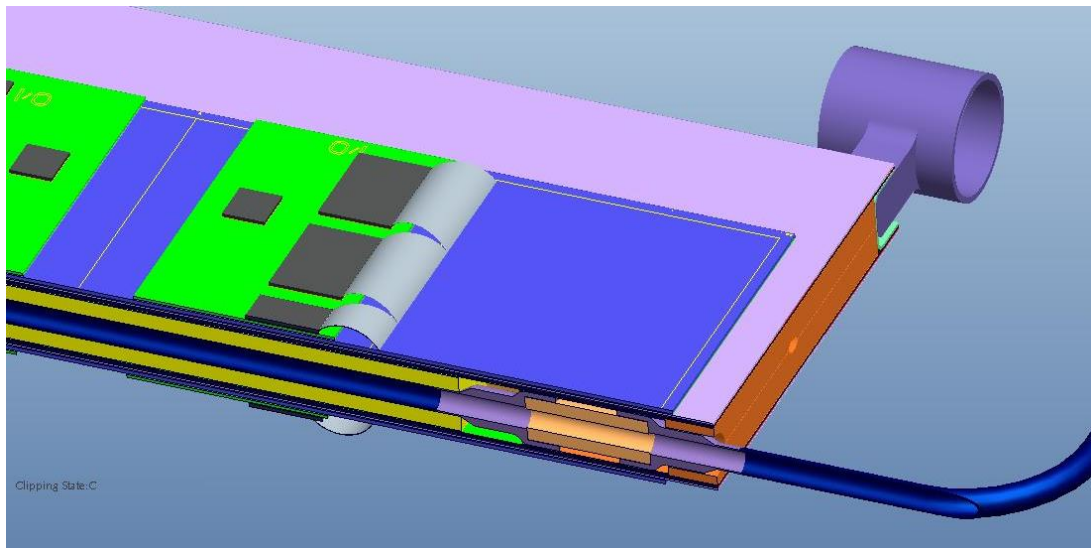
Figure 3-53   CAD Rendering showing encapsulated electrical isolator in Stave [98]
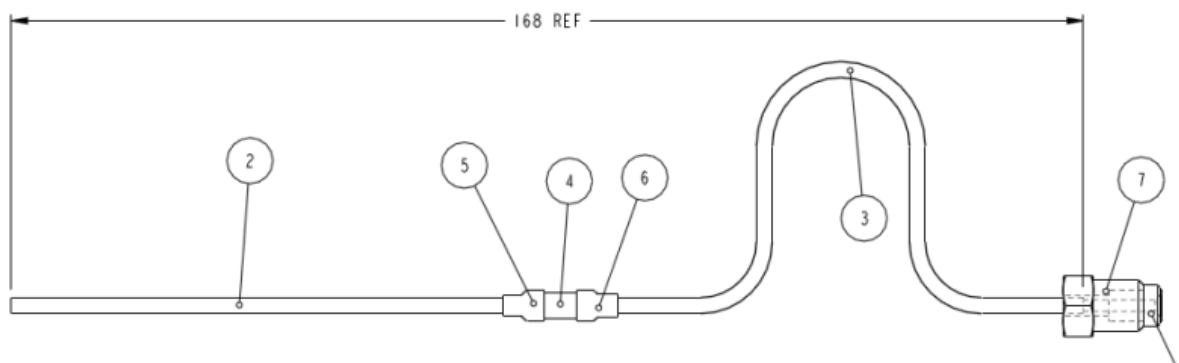
Figure 3-54   Drawing of production version of Strip electrical isolator assembly [99]

Chapter 4   Lessons Learned

4.1   Introduction

The design and construction of large-scale particle physics detectors such as ATLAS, due to the sheer complexity of the sub-systems and sub-detectors, draws on skills and technologies from numerous disciplines. This chapter highlights the author's experiences and the lessons learned from the construction and on the fly modification for the ATLAS SCT. His later involvement with the development of CO_2 cooling systems and the testing of materials, electronics and passive component radiation tolerance has progressed detector technology and its implementation is discussed.

The engineering design and materials used within modern particle physics detectors uses modern low mass, high strength materials to improve physics tracking performance. These material and design characteristics translate directly into wider engineering applications such as aerospace and the nuclear industry. Examples of the author's application of technology developed for industry is presented in a case study format.

4.2   Implementation of solutions

During the construction and installation of the ATLAS SCT, a number of critical failures in the cooling system occurred requiring on the fly modifications. The main issue, faced by all large-scale particle physics detector construction projects, is the fact that the cooling system and services are often overlooked in favour of the development of on-detector or front end electronics. This is a logical conclusion as the module power consumption and heat load data is required to design an efficient, low mass cooling system, is only obtained during final semi-conductor sensor or module testing.

Real module performance data is dependent on estimating operating environment of the detector such as, the levels of radiation at expected peak performance, the design physics

performance requirements of the detector and the total radiation length of the detector. Testing and verification of these design parameters never reaches a conclusion because the technology is constantly evolving. Final detector operation during physics data taking sees numerous hardware improvements rolled out through the detector lifetime.

There is a subtle detail, which is seldom published but widely understood; the cooling system design and prototyping is based largely on estimated data from the detector front end electronics. Financially the research and development phase of detector construction requires that both the on-detector electronics and services (cooling) be developed in parallel. This means that by the time the detector enters into the production and construction phases, little or no time remains for any adjustment to compensate for system design or specification change. As a result, on the fly and in-situ modifications are required to ensure system reliability and performance during the expected service operation of the detector.

One element of previous detector technology that is a useful guide for future detector design and construction is the retention and evolution of the components and materials that performed well. The shift from CFC refrigerant gas to high pressure CO_2 cooling is not exceptionally new. At the turn of the nineteenth century CO_2 was one of the most widely used refrigerants alongside ammonia in the early 20th century, but was displaced by the early CFC refrigerants, and practically disappeared from use as refrigerant by the 1950's.

The AMS on the International Space Station and the LHCb detector have been equipped with CO_2 cooling; this has now transferred to the ATLAS IBL detector equipped with a CO_2 high pressure two phase accumulator loop controlled cooling system [Fig.2-45]. However, at the time of ATLAS SCT research and development, direct gluing of the sensor to the detector structure was not possible. The failures within the SCT cooling were driven by the way that the designers had chosen to specify the material and its dimensional tolerance in assembly.

The use of new materials such as carbon foam encapsulated between two CFRP skins to better conduct module heat while retaining high strength coupled with the techniques for reliable direct sensor gluing to the detector support structure, has allowed adoption of a higher pressure, greater cooling capacity system.
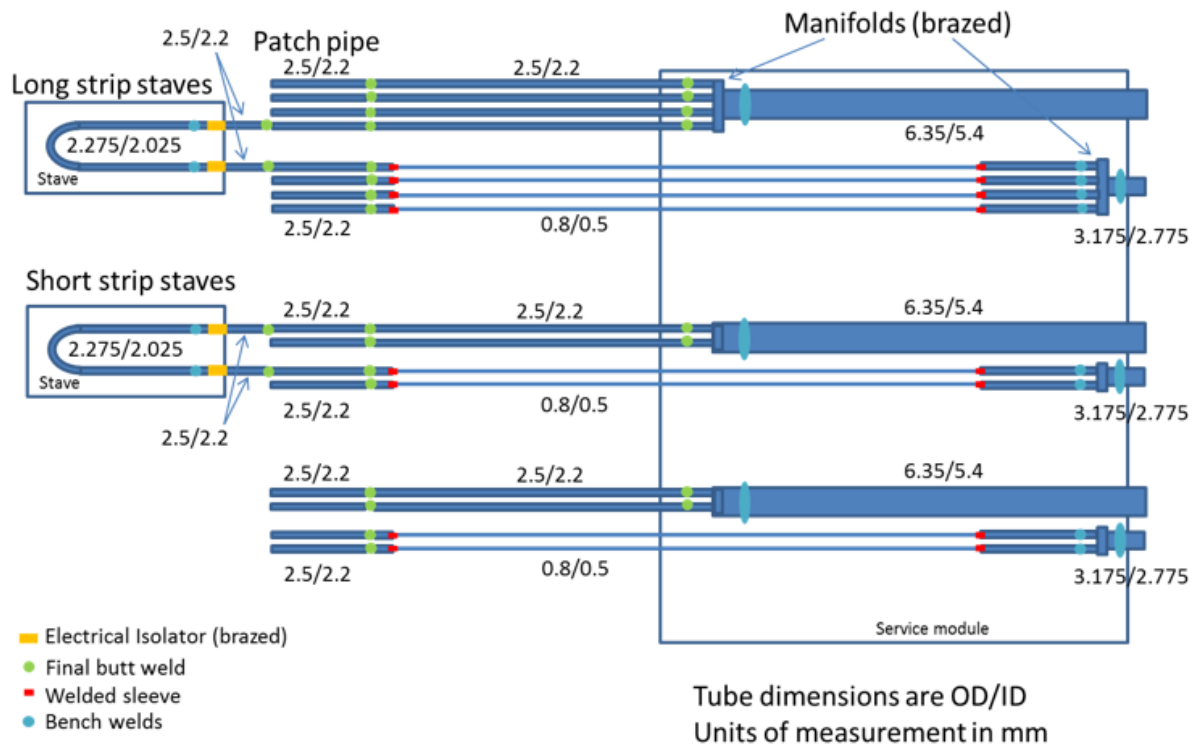
Figure 4-1   ITk Strip (Barrel) Detector Cooling System Layout [100]

As used by the IBL stave construction, its embedded cooling tube [56] was based on a proposal for CDF in the Tevatron Run IIb [55]. Now with the correct materials performance, the correct understaning of the application and evaluation of constructino techniques, the author has been able to adopt the best elements of these concepts into the new ITk Stave design. The fusion welding technology developed and titanium tubing is now the baseline specification for the ATLAS ITk cooling system [Fig. 4-1] to continue opperations at the HL-LHC.

4.3 Application of Particle Physics technology in wider engineering

Novel materials development for the ATLAS ITk cooling system by the author required development of novel technology to optimise performance of particle tracking and reliability. The author's development of ultra-thin advanced aerospace alloy joining was by use of an automated constricted TIG (Tungsten Inert Gas) or GTAW (gas tungsten arc welding) fusion welding technique [111]. This system was developed in partnership with industry for parallel applications, aerospace [112] and ATLAS.

The aerospace market is worth over £550B per year, with forms of welding to manufacture parts contributing to a high portion [113]. ATLAS Upgrade required the fusion welding of titanium alloy thin wall engineering tubing because of its properties; high strength and low mass. However, welding titanium has plagued many projects with failure, e.g. the NASA Galileo space project suffered £2.5M failures from manual welding of fuel lines.

The lack of commercially available welding equipment dictates small diameter tube joints are made manually with compression connectors, requiring thicker, heavier walled tubes compromising weight. In the case of particle physics, this weight or mass is detrimental to particle tracking, for aerospace this weight and size increase reduces fuel efficiency and reliability.

Figure 4-2   VBCie InterPulse power source, orbital welding head and 316L tube to tube joint

Fusion (TIG) welding is a very precise arc welding process, which can be automated and produces seamless welds, with no requirement for connecting tubes. However, due to high capital expenditure and lengthy R&D processes such equipment is not commercially available. VBCie (VBC Instrument Engineering Ltd) is a British manufacturing company that has been supplying welding equipment to the aerospace, medical, food, sensor, oil and gas markets for over 30 years. Their 'InterPulse' weld system [Fig. 4-2] is based on TIG principles and is so advanced it can effectively join razor blade edges together without heat distortion.

Through the support of UK research agency funding and investment from VBCie, a collaborative research and development project was set up with the objective of transferring the author's advanced technique and material development for ultra-thin wall aerospace metal based alloy tube joining, developed for ATLAS, to VBCie. Using VBCie's 'InterPulse' welding system, a modified prototype, was produced. The prototype demonstrated a significant performance advantage over commercially available welding equipment and the aerospace industry has adopted 'InterPulse' for salvage welding of difficult to weld metallic components.
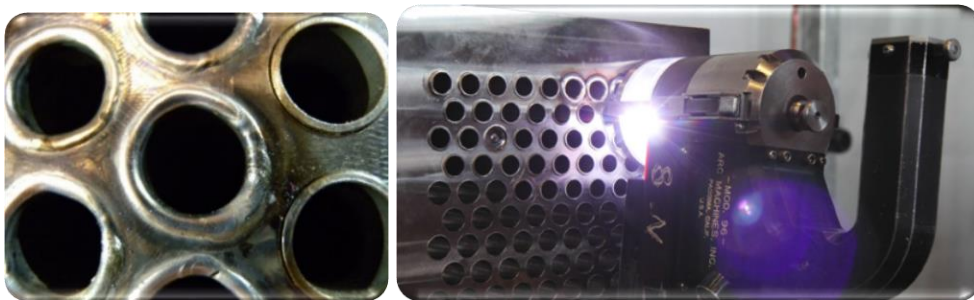
Figure 4-3   Example heat exchanger tube to plate weld for nuclear industry

The project produced a successful working prototype which automatically welds tubular material with enhanced precision, negating the need for connectors in component or system design. This allows reduced wall thickness, which in turn drives down mass and raw material use in line with aerospace, nuclear fabrication [Fig. 4-3] and automotive manufacturer's future requirements.
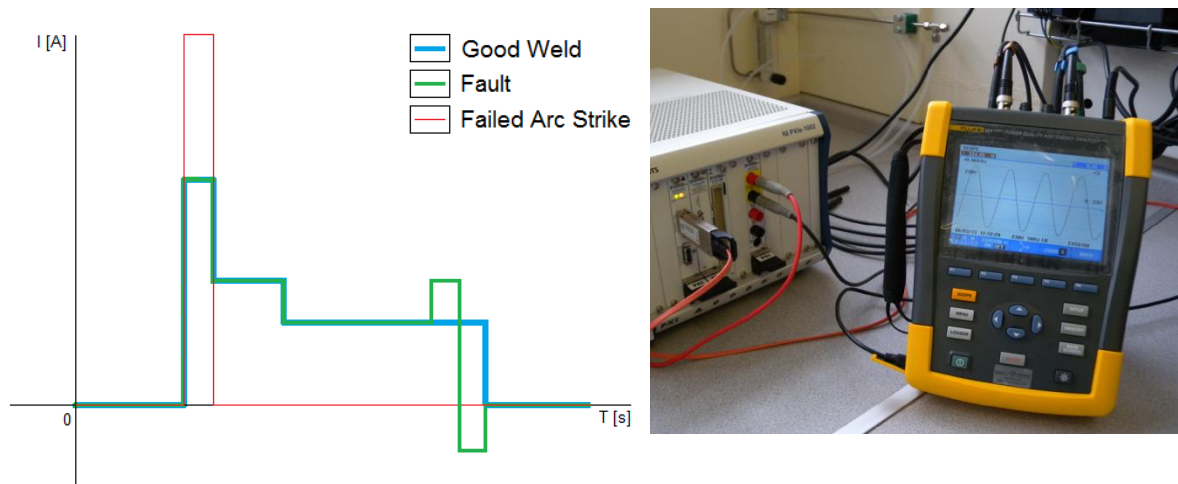
Figure 4-4   Representative welding arc voltage plot with real time monitoring DAQ

This initial instrument development project has now allowed development of new, advanced fusion welding and systems for the aerospace [113], nuclear and automotive industries that combine real time process monitoring, multi-agent robotic systems with novel vision, inspection and real time monitoring systems [Fig. 4-4].

4.4   Conclusion

This thesis contains a number of studies conducted by the author to establish the performance evaluation results of components and materials for the initial ATLAS experiment and its later upgrades in service. This work is essential to ensure a lengthy detector service life in a harsh environment, potentially without service access or intervention. Chapter 1 depicts the involvement of the author with the development of the CERN accelerator complex, allowing for early prototype testing for the HL LHC Experiment Upgrades.

The focus of chapter 2 is on the construction and installation of the ATLAS SCT detailing the authors contribution to the SCT EC-C through to its installation in the heart of ATLAS. Significant work was directed into investigations of a number of critical failures in the ATLAS ID cooling system occurred requiring on the fly modifications are highlighted. Once operational the SCT recorded the first events in ATLAS, this work and the testing methodology and results to enable physics data taking is noted. Further developments of the ATLAS ID cooling system are noted, with the shift to more reliable cooling technologies for the later detector upgrades, the IBL [2.10] and ITk [3.4] .

A significant amount of work in this thesis is focused on the ATLAS Upgrade module and Stave developments [3.5, 3.6] with testing under high levels of radiation at both the Birmingham irradiation facility and CERN PS. In preparation for the HL-LHC, materials are irradiated to high fluences in order to determine their performance and durability in this environment.

The Birmingham facility has been developed to use a cyclotron to irradiate to HL-LHC fluences within a short time-scale using a robotic scanning system to move samples within a thermal chamber, through the fixed beam spot. Chapter 3 describes the planned upgrades to the LHC and detector characterisation techniques. The Birmingham Irradiation Facility and CERN PS development through the EU AIDA framework, presents results from irradiations, upgrades to the system and tests performed to understand the proton beam.

Having established reliable thermal performance data of the ATLAS Upgrade modules, the final section of chapter 3 details the research and development work carried out on the ITk cooling system [3.9]. This follows the modern particle physics detector cooling system design methodology, the shifting away from CFC refrigerant gasses to CO_2 cooling, to construct a robust, lightweight tracking detector with embedded systems in the detector support structure.

By mirroring the application of technology used for and developed by the ATLAS Upgrade, chapter 4 demonstrated the industrial applications made possible by the drive to achieve high performance. Lightweight, high strength material performance with robust operation is desired, not only in particle physics, but also by the high value manufacturing industries such as aerospace and nuclear.

At the time of publication, the LHC in Run-II operation nears an end in preparation for the HL-LHC upgrades. The layout is nearing finalisation, the research and developments for the components, materials and specifications to be used for the ATLAS detector during Phase-II operation are being finalised. There is still a huge challenge in the successful modular construction of the ATLAS ITk allowing realisation of the full potential of the HL-LHC. When successful, this will establish more complete models of the fundamental forces and particles of nature.

Bibliography

[1]   The University of Sheffield, *"The University of Sheffield PhD by publication regulations"* WWW Document, (http://www.sheffield.ac.uk/polopoly_fs/1.379335!/file/PhDRegsbypublications.pdf)

[2]   CERN, "*Advanced European Infrastructures for Detectors at Accelerators*" WWW Document (http://aida2020.web.cern.ch/)

[3]   CERN, "*A detailed computer-generated image of the ATLAS detector and it' systems",* WWW Document, (http://atlasexperiment.org/photos/full-detector-cgi.html)

[4]   CERN, *"CERN's Accelerator Complex",* WWW Document, (http://cds.cern.ch/record/1621583?ln=en)

[5]   L. Rossi, *"Magnets for Upgrade of the Accelerator Complex at CERN",* 22nd Particle Accelerator Conference, Albuquerque, NM, USA, 25-29 Jun 2007, pp.3738

[6]   R French, *"Image of CERN LHC superconducting magnets"* 2006

[7]   CERN, "Image of the Proton Synchrotron", WWW Document, (https://home.cern/about/accelerators/proton-synchrotron)

[8]   CERN, *"The Accelerator Complex",* WWW Document, (https://home.cern/about/accelerators)

[9]   CERN, *"Drawing of the Proton Synchrotron Complex",* WWW Document, (https://ps.web.cern.ch/content/layout-integration-maps-0)

[10]   F. Ravotti, "Upgrade scenarios for irradiation lines", WWW Document, (https://cds.cern.ch/record/1951308/files/AIDA-D8_4.4.pdf)

[11]   CERN, *"Image of the ATLAS Inner Detector"*, WWW Document, (http://atlasexperiment.org/photos/inner-detector-combined.html)

[12]   R. Bates, "The ATLAS SCT grounding and shielding concept and implementation", JINST.**7**,305 (2012)

[13]   R.French, *"The barrel modules of the ATLAS semiconductor tracker"*, NIM.A. **568**, 642 (2006)

[14]   H. Pernegger, *"Image of Side-C IBL Installation"* 07-05-2014

[15]   CERN, "Rendered Image of the PIXEL Detector", WWW Document, (http://atlasexperiment.org/pixel-detector.html)

[16]   CERN, "ATLAS PIXEL Detector Description" WWW Document, (http://atlasexperiment.org/pixel-detector.html)

[17]   CERN, *"ATLAS PIXEL Module Image"*, WWW Document, (http://cds.cern.ch/record/854105)

[18]   R. French, *"Photograph of the 3rd ATLAS SCT Barrel"* 2005

[19]   R. French*, "The barrel modules of the ATLAS semiconductor tracker"*, 568 (2006)

[20]   ATLAS Collaboration, *"Studies of the performance of the ATLAS detector using cosmic-ray muons"* EPJ.3. **71**, 1593, (2011)

[21]   H. Pernegger, "Integration and test of the ATLAS Semiconductor Tracker", NIMA. **572**, 108 (2007)

[22]   ATLAS Collaboration*, "ATLAS Detector and physics performance Technical Design Report",* Volume 1, section 1.4.2, 25 May 1999, https://cds.cern.ch/record/391176

[23]   R. French, "*Photo of ATLAS ID Cooling Mock up (Macquette)*" 2006

[24]   A. Bitadze, *"Thermo-dynamical measurements for ATALS Inner Detector (evaporative cooling system)"* PhD Thesis, University of Glasgow (2016) (http://theses.gla.ac.uk/5186/7/2013BitadzePhd.pdf)

[25]   R. French, *"The ATLAS semiconductor tracker end-cap module"* NIMA. **575,** 353, (2007)

[26]   R. French, *"Photograph of the ATLAS SCT EC-C"* 2006

[27]   T. Jones, *"Image of the first completed SCT EC Disc"* 2003

[28]   R. French, "*Photo of LMT testing routing*" 2005

[29]   C. Doisters "*Drawing of EC temporary services frame TPPF1*" 2005

[30]   R. French, "*Photo of LMT testing (left) and failure (right)*" 2006

[31]   M. Gibson, *"Photo of Garlock Al Helicoflex seal (L)"* 2006

[32]   J. Tarrant, *"CAD drawing of EC connector assembly (R)"* 2006

[33]   R.French, *"Plot of performance of Garlock Al & Cu Helicoflex seal)"* 2006

[34]   J. Tarrant, *"EC PPF0 Cooling connector with Ti bolts (L) and 316L SS bolts (R)"* 2006

[35]   R. French, *"Image of Disc alignment target and EC-C discs in cylinder"* 2006

[36]   ATLAS Collaboration, *"Operation and performance of the ATLAS semiconductor tracker"* JINST9. P08009 (2014)

[37]   R. French, *"ATLAS SCT EC-C under construction at Liverpool UK"* 2006

[38]   R. French, *"Image of TRT prior to integration with SCT Barrel"* 2007

[39]   P. Cwetanski, *"Straw Performance Studies and quality assurance for the ATLAS transition radiation detector",* WWW Document, (https://cds.cern.ch/record/962570/files/thesis-2006-025.pdf)

[40]   R. French, *"Image of TRT being integrated into the SCT Barrel"* 2007

[41]   R. French, *"Image of the ATALS DCS FSM Control Display"* 2008

[42]   A. Barriuso, *"The detector control system of the ATLAS experiment"* www document, (https://cds.cern.ch/record/1268678/files/ATL-TILECAL-PROC-2010-004.pdf) (2008)

[43]   B. Hallgren, *"The Embedded Local Monitor Board (ELMB) in the LHC Front-end I/O Control System"* WWW Document (https://cds.cern.ch/record/530675/files/p325.pdf)

[44]   L. Rossi, *"SCT HEX fault notes"* 124th ATLAS EB meeting 2007, electronic communication to ATLAS SCT SG staff 2007

[45]   R. French, *"CAD Rendering of EC HEX Heater Modification"* 2007

[46]   K. Nagai, *"Image of a SCT cooling heater"* & "Thermocoax SCT heater drawing" 2007

[47]   S. McMahon, *"Endoscope (L) and SEM (R) image of SCT Heater corrosion"* 2007

[48]   R. French, *"Image of STFC D9C "186" connection (L) and fully installed (R)"* 2007

[49]   CERN, *"First event ever seen in ATLAS"* WWW Document (http://atlas.cern/updates/atlas-news/first-beam-and-first-events-atlas)

[50]   ATLAS Collaboration, *"The ATLAS Pixel Insertable B-Layer (IBL)",* NIMA.**650**, 45 (2010)

[51]   B. Verlaat, *"The IBL CO_2 Cooling System",* Proceedings of PIXEL Detectors for Particles and Imaging (PIXEL2016), 5-9 September 2016, Sestri Levante, Italy, available at https://cds.cern.ch/record/2212282

[52]   R. French, *"IBL Cooling Review Recommendations"*, WWW Document, (http://indico.cern.ch/event/190113)

[53]   S. Coelli, *"Development and test of the CO_2 evaporative cooling system for the LHCb UT Detector"*, CERN-Poster-2016-558

[54]   Albert, *"Prototype ATLAS IBL Modules using the FE-I4 Font-End Readout Chip",* JINST.7,**646** (2012)

[55]   R. Lu *"CDF Run IIB Silicon: Stave design and testing"* http://lss.fnal.gov/archive/2003/conf/fermilab-conf-03-368-e.pdf

[56]   ATLAS collaboration, *"ATLAS Insertable B-Layer Technical Design Report"*, WWW Document, (http://cds.cern.ch/record/1291633)

[57]   ATLAS Collaboration, *" ATLAS Phase-II Upgrade Scoping Document"* WWW Document, (https://cds.cern.ch/record/2055248/files/LHCC-G-166.pdf)

[58]   P. Allport, *"Letter of Intent for the Phase-I Upgrade of the ATLAS Experiment"* WWW Document (https://cds.cern.ch/record/1402470)

[59]   P. Sutcliffe, *"3D Rendering of the ATLAS Upgrade Stave Concept 2006"* 2006

[60]   I. Wilmut, *"Stave Stress Calculations, Materials and Thermal FEA 2008"* WWW Document (https://indico.cern.ch/event/32084/contributions/1700432/)

[61]   T. Jones, *"Image of 3x prototype strip Staves under adhesive evaluation"* 2009

[62]   T. Jones, *"Expected material properties for thermo-mechanical stave"* 2009

[63]   R. French, *"Pipes and connectors, ATLAS Tracker Upgrade Workshop 2008"* WWW Document (https://indico.cern.ch/event/32084/contributions/1700315/)

[64]   R. French, *"Interstrip Measurements After Gluing, NIKHEF 2008"* WWW Document (https://indico.cern.ch.event/32084/contributions/1700405)

[65]   R. French, *"HPK Mini Silicon Sensor used in glue trials"* 2008

[66]   L. Poley, *"Alternative glues for the production of the ATLAS Silicon strip modules for the phase-II upgrade of the ATLAS Inner Detector"* WWW Document, (https://arxiv.org/abs/1508.05912)

[67]   A. Affolder, "Breakdown Voltage Result Summary" 2008

[68]   R. French, *"No glue, Rinterstrip Measurement at Vbias = 200V"* 07-01-2009

[69]   R. French, *"Araldite, Rinterstrip Measurement at Vbias =200V"* 07-01-2009

[70]   R. French, *"Epolite, Rinterstrip Measurement at Vbias =200V"* 07-01-2009

[71]   P. Sutcliffe, *"Drawing of Stave thermo-mechanical module"* WWW Document (https://twiki.cern.ch/twiki/bin/view/Atlas/ITK)

[72]   R. French, *"Prototype Stave module layout"* 2009 WWW Document, (https://twiki.cern.ch/twiki/bin/view/Atlas/ITK)

[73]   R. French, "*First results of ATLAS ITk Irradiation Programme"* WWW Document, (http://www2.physics.ox.ac.uk/atlas2009/index.asp)

[74]   A. Greenall, *"STAVE09 Thermo-mechanical Hybrid layout"* 2009

[75]   R. Bates, *"Layout of thermo-mechanical module"* 2009

[76]   R. French, *"Thermal module layout 04/09"* 2009

[77]   R. Bates, *"STAVE09 Module Construction Tooling"* 2009

[78]   R. French, *"Image of thermo-mechanical module"* 2009

[79]   H. Sadrozinski, "*Bulk radiation damage in silicon detector and implications for LHC experiments*" NIMA,.**381**, 338, (1996)

[80]   *"Image of the ATLAS07 silicon sensor layout"* 2009

[81]   P. Riedler, "*Radiation Damage Effects and Performance of Silicon Strip Detectors using LHC Readout Electronics*" WWW Document, https://inspirehep.net/record/486390/files/cer-002171220.pdf

[82]   I. Dawson, *"Proton path with tilted silicon sensors in CERN IRRAD T7 cold box"* 2009

[83]   I. Dawson, *"FLUKA silicon sensor mounting simulation"* 2009

[84]   R. French, *"CERN IRRAD Silicon sensor mounting frame"* 2010

[85]   R. French, *"Sensor frame and module PCB mounting"* 2010

[86]   R. French, *"ITk Si Module mounted for irradiation"* 2010

[87]   G. Beck, *"Location of dose monitor assy at front and back of PS_ Lid_1 at 29/4/2010"* 2010

[88]   R. French, *"BPM mounting in front of module"* 2010

[89]   R. French, "Cold Box window and air gap dimensions" 2010

[90] J. Wilson, *"26MeV energy loss calculations for Polyamide & Acrylic in beam of cyclotron."* 2010

[91] J. Wilson, *"energy scattering calculations for Polyamide and acrylic in beam of cyclotron"* 2011

[92] J. Wilson, *"Ti activation foil uniformity measurements from Run1"* 2011

[93] J. Wilson, *"Gamma spectrum of activated foil (Ge Spectrometer)"* 2011

[94] A. Weidburg, "*The Versatile Link common project: feasibility report"* JINST **7,** (2012) http://iopscience.iop.org/article/10.1088/1748-0221/7/01/C01075/pdf

[95] CERN, *"AIDA — Result In Brief"* (http://cordis.europa.eu/ /result/rcn/170397_en.htmll) 2016 WWW Document

[96] R. French, *"Ti Activation Foil tests of beam"* 24/11/2011

[97] R. French, *"Image of Scanning Robot (L) and 2009 Low Energy Irradiation Area Layout"* 2010

[98] R. French, *"Upgraded high energy irradiation layout proposal 2012"*

[99] R. French, *"Upgraded cold box and robotic scanning systems"* 2016

[100] R. French, *"ITk Strip Stave Core Design"* 2009

[101] T. Jones, "ATLAS ITk Stave09 Design" 2009

[102] R. French, "Stave core materials radiation length" 2011

[103] R. French, *"200x magnification cross sectional view of 316L weld sample"* 2012

[104] R. French, *"Micro-focus CT x-ray image of 316L tube-tube"* 2012

[105] R. French, "*316L tube welding, X-Ray (a) and images of joint"* 2012

[106] A. Gerradin, *"Micro-hardness profiles of 316L tube weld sample"* 2012

[107] R. French, *"Tensile Test results of 316L tube sample elongation"* 2012

[108] E. Lauid, *"AMS-02 Tracker thermal control system: development of new technologies for manufacturing of two-phase cooling system"* www document, (*www.infn.it/thesis/PDF/getfile.php?filename=5684-Laudi-dottorato.pdf*)

[109]   R. French, *"ITk Stave CP2Ti welded tube joint 3.175mm OD x 220µm WT"* 2013

[110]   R. French, *"500x magnification image of CP2 Ti Oxide layer"* 2012

[111]   R. French, "*Investigation of the TIG orbital welding process on tube-to-tube joints in titanium and stainless steel thin wall tubes",* 68th International Institute of Welding Assembly, Helsinki, Finland, 2015. WWW Document, (http://www.vbcie.com/contentfiles/files/Joints_Paper%232_02%20_2_.pdf)

[112]   R. French, *"High Value Intelligent Aerospace Turbofan Jet Engine Blade Remanufacturing System"* Advances in Ergonomics of manufacturing: Managing the Enterprise of the Future. Springer 2016. Available at: (https://books.google.co.uk/books?isbn=3319416979)

[113]   R. French, "Underpinning UK High-value manufacturing: Development of a robotic remanufacturing system". IEEE ETFA 2016

DOI: 10.1109/ETFA.2016.7733705

[114]   R. French, *"HF etching trial Ti tube sample results"* 2012

[115]   R. French, *"50um image of CP2 Ti tube end view"* 2013

[116]   E. Spencer, *"One quarter section diagram of ITk Faraday Cage"* 2010

[117]   E. Vigeolas, "Diagram of IBL cooling tube electrical isolator" email correspondence 2010

[118]   R. French, *"Evaporator and type I cooling tubes and their connections for the ATLAS Phase-II barrel strip tracker Part I: Requirements and Specifications"* www document, (https://indico.cern.ch/event/363327)

[119]   R. French, *"500x magnification Cp2 Ti brazed with VBC CuSil alloy to Macor"* 2012

[120]   R. French, *"Image of prototype ITk Strip electrical isolator"* 2013

[121]   P. Sutcliffe, *"CAD Rendering showing encapsulated electrical isolator in Stave"* WWW Document (https://twiki.cern.ch/twiki/bin/view/Atlas/ITK)

[122]   P. Sutcliffe, *"Drawing of production version of Strip electrical isolator assembly"* WWW Document, (https://twiki.cern.ch/twiki/bin/view/Atlas/ITK)

[123]   R. French, *"ITk Strip (Barrel) Detector Cooling System Layout"* 2015

[124]   A. Van der Vaart, *"Bernstein-von Mises Theorem"* Asymptotic Statistics, (1998) ISBN 0-521-78450-6.

Reference Publications

A.1   Engineering for the ATLAS SemiConductor Tracker (SCT) End-cap

The ATLAS Collaboration

Journal of Instrumentation, Volume 3 (5), May 2008, Article Number: P05002

http://iopscience.iop.org/article/10.1088/1748-0221/3/05/P05002/meta

A.2   The evaporative cooling system for the ATLAS inner detector

The ATLAS Collaboration

Journal of Instrumentation, Volume 3 (7), July 2008, Article Number: P07003

http://iopscience.iop.org/article/10.1088/1748-0221/3/07/P07003

A.3   The integration and engineering of the ATLAS Semi-Conductor Tracker Barrel

The ATLAS Collaboration

Journal of Instrumentation, Volume 3, October 2008

http://iopscience.iop.org/1748-0221/3/10/P10006

A.4 Combined performance tests before installation of the ATLAS Semiconductor and Transition Radiation Tracking Detectors

The ATLAS Collaboration

A.5 Progress with the single-sided module prototypes for the ATLAS tracker upgrade stave

The ATLAS Collaboration

A.6 Testing of bulk radiation damage of n-in-p silicon sensors for very high radiation environments

The ATLAS Collaboration

A.7   Development of n-on-p silicon sensors for very high radiation environments

The ATLAS Collaboration

https://inspirehep.net/record/918168?ln=en

A.8   A double-sided, shield-less stave prototype for the ATLAS Upgrade Strip Tracker for the High-Luminosity LHC

The ATLAS Collaboration

http://iopscience.iop.org/article/10.1088/1748-0221/9/03/P03012/meta

A.9   Development of n+-in-p large-area silicon microstrip sensors for very high radiation environments – ATLAS12 design and initial results

The ATLAS Collaboration

A.10   The Birmingham Irradiation Facility

P. Dervan, R. French, P. Hodgson, H. Marin-Reyes, and J. Wilson

A.11   Detailed Studies of Full-Size ATLAS12 Sensors

R. French, P. Hodgson, H. Marin-Reyes, P. Dervan, J. Wilson

https://www.researchgate.net/publication/301681530_Detailed_studies_of_full-size_ATLAS12_sensors

A.12   Upgrade to the Birmingham Irradiation Facility

P. Dervan, R. French, P. Hodgson, H. Marín-Reyes, K. Parker, J. Wilson, M. Baca,

https://indico.cern.ch/event/313925/contributions/1687283/attachments/601591/827976/Florence_2014_091014.pdf

A.13   Pre-configured XY-axis Cartesian Robot System for a new ATLAS scanning facility

H. Marin-Reyes, R. French, P. Hodgson, K. Parker, J. Wilson, P. Dervan

Mobile Service Robotics: Proceedings of International Conference on Climbing and Walking Robots – CLAWAR 2014, Poznan, Poland, 21 – 23 July 2014, World Scientific Publishing Co.,pp. 477 – 483, 2014.

Mobile Service Robotics: Proceedings of CLAWAR, World Scientific, ISBN 978-981-4623-34-6